35

FACTORS INFLUENCING THE MOBILITY OF URANIUM, THORIUM AND RARE EARTH ELEMENTS AT THE STEENKAMPSKRAAL MONAZITE MINE, NORTH WESTERN CAPE

By

John Edward Glendinning

(B.Sc. Hons. Geology, Rhodes University)

Submitted in partial fulfilment of the Masters degree in
Environmental Geochemistry, Department of Geological Sciences
University of Cape Town.
Cape Town
Rondebosch
7700

December 1996

Preface

The experimental work described in this thesis was carried out in the Department of Geological Sciences, University of Cape Town, from August to November, 1996, under the supervision of Professor J P Willis of the Department of Geological Sciences.

These studies represent original work by the author and have not been submitted for degree purposes to another university. Where use was made of the work of others it has been acknowledged in the text.

Signed by candidate

Signature Removed

J E Glendinning

Acknowledgements

I would like to express my gratitude to the following persons and institutions which helped to make the completion of this study possible:

The Atomic Energy Board for generous financial support.

Dr Marco Andreoli from the Atomic Energy Board for his involvement at Steenkampskraal.

Dr Neil Jarvis from the Atomic Energy Board for his help both in organising the ICP-MS analyses as well as in coordinating the project.

Mr Robie Louw from Rareco for his help both in the field and the numerous valuable discussions at Somerset west.

Mr Harry Stolz and Mr Sarel Mostert for their help and hospitality at the mine.

Mr Julius Pretorius from the Department of Chemistry for his help with the Th and rare earth element speciation.

Dr John Rogers from the Department of Geological Sciences for help with the particle size analyses.

Dr Chris Harris from the Department of Geological Sciences for his help in the isotope analyses.

Professor David Reid from the Department of Geological Sciences for his assistance in some of the computer programs used in the study.

The Computing Centre for Water Research, for access to the MINTEQA2 software.

Dr Martin Fey, whom I was privileged to have as a co supervisor for this project, for valuable discussion and input.

Finally I would like to thank Professor James Willis, supervisor of the project for his dedication and enthusiasm.

My special thanks go to them.

Abstract

It is well known that the release of long-lived radionuclides to the water path is probably the most relevant radiological risk originating from an underground repository. Transuranic elements (ie. all elements with an atomic number greater than 92 (U)) do not have any non-radioactive isotopes and are very rare in natural materials. The long term geochemical behaviour of these elements must thus be derived from chemical analogues such as the rare earth elements (REE), Th and U. Steenkampskraal monazite mine, situated 350 km north of Cape Town, has been found to be an excellent locality for the study of these elements, due to the high concentration of these elements in the ore as well as the ideal geology, which consists of low permeability rocks with groundwater flow governed by fractures. The ore body consists of a monazite [(REE, Th, U)PO_4], apatite [$Ca_3(PO_4)_2$], chalcopyrite [CuFeS] and magnetite [Fe_3O_4] vein deposit.

Water was sampled from six boreholes in the vicinity of the mine and five windpumps on the surrounding farms, Nabeep and Brandewynskraal. Surface water samples were taken from the slimes dam, an ephemeral stream on the western side of the mine, as well as from the surface of a road shortly after rain, below the tailings. Four water samples were taken from within the underground mine workings (Main shaft, Main shaft extension, Sump on level 3 and Inclined shaft). Colloids were sampled from three of the boreholes and a precipitate was taken from the surface of the main shaft water. Soils were sampled along two transects away from the mine on the eastern and western side of the ore body. Due to the topography of the area, surface contamination could only occur on these two sides.

Stable isotopes of oxygen ($\delta^{18}O$) and hydrogen (δD) indicated the presence of two distinct groups of waters within the vicinity of the mine. One group is composed of unevaporated waters and includes all boreholes and the water sampled in the inclined shaft. The water moving through the inclined shaft is in contact with the ground water. A second group of highly evaporated waters was present in the slimes dam samples as well as the underground water samples not directly in contact with groundwater.

Groundwater contamination by REE-bearing phosphate minerals has resulted in measurable concentrations of U, Th and REE in all mine waters and boreholes in the near vicinity of the mine. The chondrite-normalized REE patterns of the water samples are similar to those displayed by monazite, with a distinctive Eu depletion and an obvious enrichment in LREE with respect to HREE.

Monazite-normalized REE patterns for the selected borehole waters show a marked fractionation between LREE and HREE, with the HREE strongly enriched in the aqueous phase. Heavy REE have been shown to have a greater tendency for complexation and a greater affinity for mineral surfaces. In the present study, the three boreholes in which colloids were found had high concentrations of U, Th and REE. It is likely that colloidal transport of these elements is the dominant mechanism of transport.

The degree of contamination within the waters varied, depending on the proximity to the ore body and the tailings. Phosphate and SO_4^{2-} were generally present in elevated concentrations (up to 4290 and 32600 mg/dm^3, respectively), and were found to be highly dependent on the presence of Fe in the system. Iron significantly decreases the concentrations of PO_4^{3-} and to a lesser extent SO_4^{2-}, in the system, through precipitation reactions.

The contaminated waters generally had high concentrations of chalcophile elements (such as 12500 mg/dm^3 Cu in the slimes dam) due to the weathering of sulphide minerals in the ore body and tailings. Elements such as Al (1420 mg/dm^3 in the slimes dam) are present in high concentrations due to the low pH (2.6) and its presence in many of the minerals associated with the ore body and surrounding country rocks.

The soils in the Steenkampskraal area generally have high concentrations of basic cations with neutral to alkaline pH values (up to pH 8.5), thus creating a relatively high acid buffering capacity. Extreme soil acidification has, however, occurred on the eastern side of the ore body. With increasing distance from the tailings, there is an associated decrease in some anion and element concentrations and an increase in pH from 3.6 to 7.6. The SO_4^{2-} (8980 to 50 mg/dm^3), PO_4^{3-} (212 to 46 mg/dm^3) and F^- (27 to 0.4 mg/dm^3) concentrations decrease, while the HCO_3^- (0 to 255 mg/dm^3) and to some extent the Cl^- (392 to 551 mg/dm^3) concentrations increase away from the tailings dam. Phosphate and, to a lesser degree SO_4^{2-}, are generally immobile, resulting in their rapid decrease in concentration away from the tailings. Chloride is a mobile anion which appears to increase away from the tailings. The increase in Cl^- concentration might indicate the presence of a contamination plume moving outwards away from the tailings material.

The soil concentrations of Cr, Cu, Ni, Pb, U, Th and Y along the transect on the eastern side of the mine are highest close to the tailings. The degree of contamination is initially very high, but drops off rapidly and reaches a fairly stable value approximately 600 meters from the tailings material (eg Th decreases from 27800 to 70 mg/kg).

On the western side, the degree of contamination and acidification of the soils as a result of mining activity is much lower (pH ranges from 7.7 to 8.5) due to the absence of tailings material, resulting in a much smaller volume of material from which contamination can occur as well as a much smaller surface area from which mineral dissolution can take place. Associated with the smaller volumes and surface area of contaminant material on the western side is the steeper gradient which significantly reduces the residence time of water in the vicinity of the mine.

The chondrite-normalized REE patterns along both transects are similar to that of monazite. The soils with a neutral to alkaline pH have developed a Ce depletion, due to the oxidation of Ce^{3+} to Ce^{4+} and subsequent immobilization of Ce as CeO_2. Soils with acidic pH values (i.e. those close to the tailings) have no Ce depletion, presumably due to the inhibition of oxidation of Ce^{3+} to Ce^{4+} at low pH.

Table of Contents

Chapter 3

Chapter 4

Chapter 5

Chapter 6

References

Appendices

List of Figures

List of Tables

Chapter 1

Background and Aims

1.1. Introduction

The release of long lived radionuclides to the water path is probably the most relevant radiological risk originating from a repository in the deep underground (Geckeis et al., 1996). Low permeability rocks in which the groundwater flow is governed by fractures are being considered as potential suitable candidates for the long term storage of radioactive waste at depth. Such rocks are also one of the main sources of the radionuclides derived from the natural decay chains headed by U and Th. This characteristic makes this type of rock very useful in providing natural chemical analogues for the behaviour of radionuclides present in nuclear waste (Ivanovich and Harmon, 1992).

Transuranic elements (ie. all elements with an atomic number greater than 92 (U)) do not have any non-radioactive isotopes and are very rare in natural materials. The long term geochemical behaviour of these elements must thus be derived from chemical analogues such as rare earth elements (REE), Th and U (Krauskopf, 1986). Rare earth elements and the actinides Am and Cm have many common features (eg. same oxidation state, close ionic radii, similar hydrolysis constant) (Lei et al., 1986). Thorium is a fairly satisfactory analogue for Pu and Np in the tetravalent state. A sound knowledge of the geochemical behaviour of the REE, U and Th is, therefore, important in understanding the long term fate of their transuranic counterparts.

Steenkampskraal monazite mine has been found to be an excellent locality for the study of these elements, due to the high concentration of these elements within the ore, as well as the ideal geology, which consists of low permeability rocks with groundwater flow being governed by fractures. Another advantage of using Steenkampskraal as a natural laboratory is the number of boreholes already in place for groundwater sampling.

The Steenkampskraal mine is situated 350 km north of Cape Town in the Namaqua metamorphic complex (Figure 1.1).

The Steenkampskraal mine (Figure 1.2) operated from 1952 to 1963 when it represented the world's leading producer of Th and REE (Kremers, 1958). Thorium and REE were extracted from monazite [(REE, Th, U)PO_4]. During mining of the monazite concentrate it was found to contain an average of 45 wt% REE oxides, 4 wt% ThO_2, 600 ppm U_3O_8, 1.08 wt% Cu, 18 wt% P_2O_5 as well as minor traces of gold (Pike, 1959).

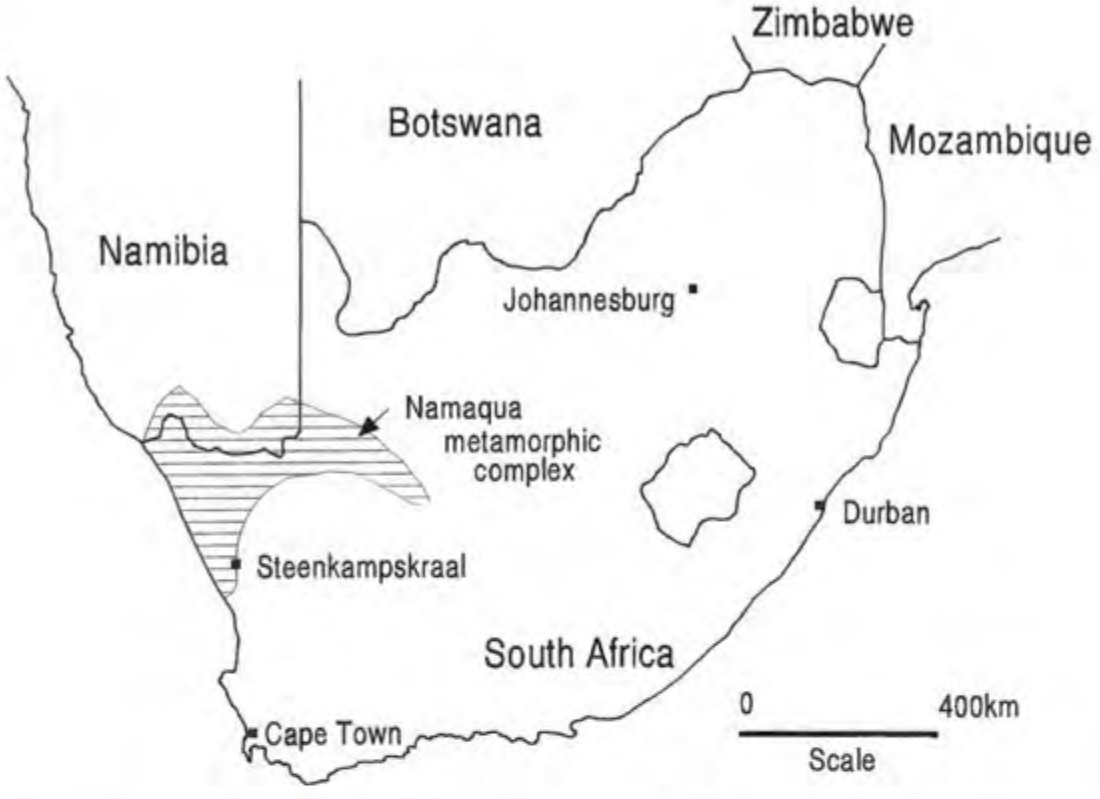

Figure 1.1. Locality map of the Steenkampskraal monazite mine in the Namaqua metamorphic complex (After Andreoli et al., 1994).

Figure 1.2. View of the intrusion hosting the ore body, looking towards the west.

The mine consists of 3 levels and 2 shafts. Initially the main (vertical) shaft was sunk to a depth of 30 m with a drive advancing from north to south to intersect the ore. The second (inclined) shaft was later sunk to a depth of 130 m and the deposit was mined through a series of intermediate levels (Figure 1.3) (Pike, 1959).

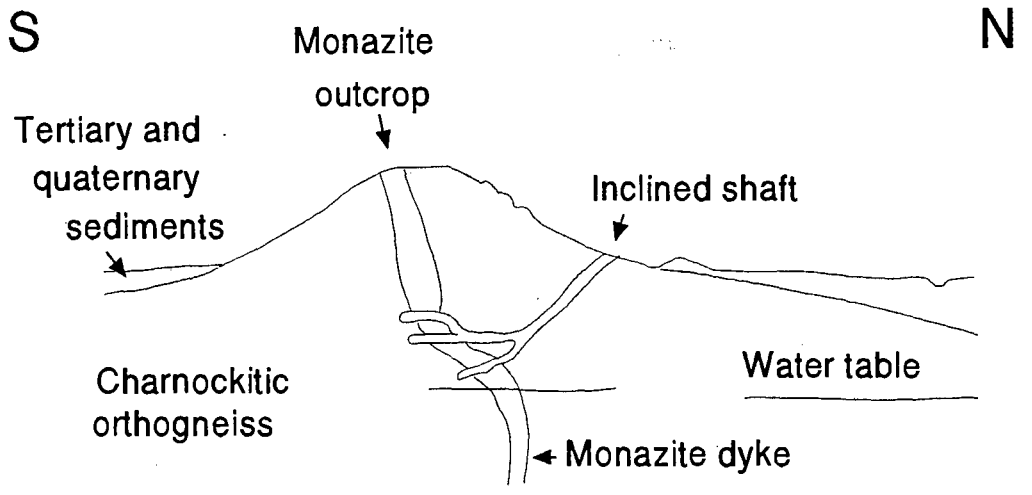

Figure 1.3. Generalised cross-section through the Steenkampskraal monazite mine revealing the ore body (After Pike, 1959).

1.2. Aims and objectives

The objectives of this study were to review the pertinent literature on the geochemical behaviour of Th, REE and U in both surface sediments and ground waters, and to conduct an investigation of the waters and sediments in the Steenkampskraal area to address the following specific questions:

1) What is the extent of contamination and acidification of the ground waters after mining ?

2) If colloidal matter is present in the groundwaters at the site, what is its role in promoting the mobilisation and movement of trace metals ?

3) What is the extent of element (U, Th, Cu, and REE) transport away from the primary ore body and tailings dams under *in situ* conditions ?

1.3. Geology

Up until 1994, the Steenkampskraal monazite deposit was thought to represent a hydrothermal vein deposited within a large fracture of the granitic country rocks. Andreoli et al. (1994) found evidence for the ore body to have intruded under granulite facies conditions (T ~ 800-860°C, P ~ 5-6 kbars).

According to their model, the monazite-enriched charnockitic vein at Steenkampskraal was derived from the crystallization of CO_2-enriched residual magmas. After the emplacement of enriched mafic magmas during granulite facies metamorphism, fractionation of residual fluids led to the formation of charnockite dykes, veins and charnockitized gneisses. Steenkampskraal is the largest of a number of these charnockite dykes, which consists of a monazite [(REE, Th, U)PO_4], apatite [$CaPO_4$], chalcopyrite [CuFeS] and magnetite [Fe_3O_4] vein deposit.

The monazite deposit is characterized by poor exposures, with the area being overlain by younger sedimentary rocks unconformably overlying the high grade basement. The cover is represented by late Proterozoic Nama quartzite, late Paleozoic Dwyka tillite, Cenozoic calcrete and wind-blown Kalahari deposits.

The basement is dominated by orthogneisses and charnockitic rocks with subsidiary granulite facies paragneisses. In addition, small intrusions of anorthosite, leuconorite, enderbite, charnoenderbite, quartz diorite, leucotonalite, and hypersthene are disseminated throughout the monazite deposit. These rocks have recently been referred to as the "Roodewal suite" (Andreoli et al., 1994).

1.4. Mineralogy of the ore body

Monazite at Steenkampskraal is an orthophosphate that preferentially incorporates the light rare earth elements (lanthanum, cerium, praseodymium, neodymium and samarium), thorium and yttrium. The monazite at Steenkampskraal is depleted in the heavier rare earth elements (gadolinium, terbium, dysprosium, holmium, erbium, thulium, ytterbium, and lutetium) (Andreoli et al., 1994). The primary sulphide minerals include pyrite (FeS_2), chalcopyrite (CuFeS), and less commonly galena (PbS) (Pike, 1959). The primary oxide minerals include magnetite, ilmenite and Zn-bearing hercynite ($FeAl_2O_4$).

1.5. Aquifer characteristics

The average rainfall over Steenkampskraal is 70 mm per annum. The water table rests approximately 50 m below ground surface at the mine, with the direction of ground water flow south or south-west.
The water table around Steenkampskraal mine is predicted to rest at an elevation of 325-326 m. This predicted figure is confirmed from the measurement in the flooded 3.5 level of the mine where the water table rests at an elevation of 298 m (Jarvis et al., 1996). Because the deposit is hosted by high grade metamorphic and igneous rocks with low porosity (<3%), the water flow is expected to be controlled by the pattern of fractures (Jarvis et al., 1996).

Chapter 2

Factors influencing REE, U and Th mobility and speciation during weathering. A review of the relevant literature

2.1. Introduction

The REE include all elements in the scandium group (ie. Sc, Y and La) as well as all the lanthanides (ie. Ce-Lu). Although their chemical properties are very similar, the REE are distinguished by a progressive reduction in size of each element from lanthanum through to lutetium. The lanthanide contraction is contrary to the expected trend in the periodic table. It is the result of an increasing positive charge on the nucleus of each rare earth element. This causes a more strongly contracting electron cloud whose size would otherwise remain approximately constant (Potts, 1976). The REE can be divided into the light REE (LREE) (lanthanum, cerium, praseodymium, neodymium and samarium) and the heavy REE (HREE) (gadolinium, terbium, dysprosium, holmium, erbium, thulium, ytterbium, and lutetium). Promethium is a radiogenic element that has long disappeared.

There are very few major elements with ionic radii equivalent to those of the REE. Only Ca^{2+} and Na^{+} have similar radii, which allow HREE to enter the Ca and Na sites in minerals. The substitution of the REE is limited due to a charge balance problem. Only Eu^{2+} (1.2Å) has the same radius and charge as Sr^{2+}, which results in a correlation between Eu and Sr in feldspars. This leads to a Eu depletion in the REE patterns of differentiated rocks resulting from plagioclase fractionation.

The rare earth phosphates exist in nature as the phases, monazite and xenotime. Monazite preferentially incorporates the larger LREE and xenotime (YPO_4) incorporates the smaller HREE. These phases are important accessory minerals in granitoids and rhyolites, and, because of their incorporation of REE and the high distribution coefficients of REE, they can effectively control REE distribution in igneous rocks despite the fact that they usually occur only as an accessory phase (Yunxiang et al., 1995).

Monazite and xenotime are not present in all igneous rocks. In the absence of significant monazite or xenotime, the LREE have been found to be incorporated into phases such as plagioclase, apatite, allanite (Ce-containing aluminosilicate) and orthite (La-containing aluminosilicate). The HREE are incorporated into zircon, garnet, biotite and muscovite (van der Weijen and van der Weijen, 1995) (Figure 2.1).

When the abundances of REE's are plotted against increasing atomic number, a saw-toothed pattern results. This is due to the Oddo-Harkins observation that elements of even atomic number occur in greater abundance than neighbouring elements of odd atomic number. This is due to the extra stability of nuclei containing even numbers of protons and neutrons. It is, therefore, difficult to interpret any trends or fractionation patterns. It has become conventional to normalize REE values relative to chondrite by dividing each REE abundance by the corresponding chondrite abundance (Potts, 1976). Chondrite-normalised plots usually show a smooth variation of REE composition from element to element.

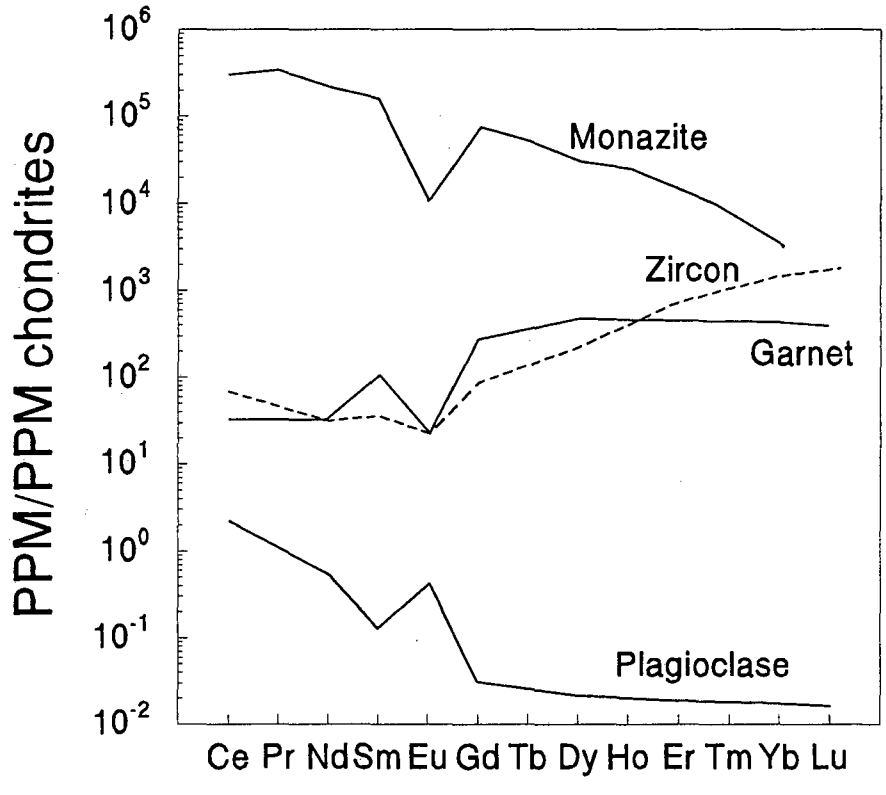

Figure 2.1. Chondrite-normalized REE diagrams of monazite, zircon, garnet and plagioclase (Modified from Taylor and McLennan, 1985).

Uranium and Th belong to a group of elements known as the actinides. None of the actinides have stable nuclei, and only U and Th have sufficiently long half-lives to occur in nature. Thorium as well as U are also incorporated into the monazite structure. Electron microprobe analyses of monazite from Steenkampskraal, as well as other localities, display high ThO_2 contents of up to 8.8 wt% and U up to 600 ppm (Andreoli et al., 1994).

2.2. Chemical processes affecting the mobility of trace elements during weathering

During the weathering process, the chemical behaviour of REE, U and Th depends on several factors such as Eh (especially Ce and U), pH, the presence of organic and inorganic ligands, cation exchange sites on clays, mineralogical distribution of REE, U and Th in the parent material, and especially the nature of the host rock-accessory mineral association (Nesbitt, 1979).

Three main processes are involved in weathering: 1) the breakdown of the parent minerals; 2) the removal in solution of some of the released constituents; and 3) the formation of secondary phases with components from the atmosphere, from the parent rock and shallower levels, and from components transported by the percolating solutions (Nesbitt et al., 1980).

2.3. Mobility and fractionation of REE during weathering

The only two REE in which Eh plays a role in weathering are Ce and Eu. For all the others, pH determines the fractionation and mobility in the soils. Braun and Pagel (1994) found that in a lateritic profile in SW Cameroon, most of the REE were released into the soil during weathering where they were influenced by pedogenic processes. A strong Ce enrichment was found to be present. Positive Ce anomalies are interpreted as the result of oxidation of Ce^{3+} to Ce^{4+} in an oxidizing environment, which results in the deposition of Ce as cerianite (CeO_2). Ce^{4+} would behave as an immobile element due to the limited solubility of cerianite (Middelburg et al., 1988).

Gouveia et al. (1993) found that during the weathering of granitic rocks in Portugal, the REE distribution depended on the different size fraction being analyzed. REE contents were low in the coarser fractions, mainly due to a quartz dilution, with a significant positive Eu anomaly, suggesting that REE are mainly present in "unaltered" plagioclase grains, since Eu^{2+} is preferentially incorporated in feldspar crystals during magmatic processes and is consequently easily liberated and concentrated in residual soils. With decreasing particle size, the REE content increased and the positive Eu anomaly became negative. This can be explained by the increase of REE bearing minerals in the finer fraction, ie. the breakdown of apatite and zircon present as inclusions in biotite, together with plagioclase weathering.

The existence of Ce enrichments only in the finer fractions, and not in the whole sample, indicates that temperate climatic conditions seem not to be influential enough to produce positive Ce enrichments in the whole samples as found in tropical zones (Braun et al. 1990).

van der Weijen and van der Weijen (1995) studied the mobility of some of the REE during the weathering of four granitoids in central Portugal. The granites contain small quantities of monazite and xenotime as well as other REE-bearing minerals such as orthite. The relative losses and gains of the different REE during weathering were not identical. Fractionation of REE during weathering of a parent rock can result in different REE patterns in different parts of the weathering profile (Duddy, 1980). Nesbitt (1980) observed preferential leaching of HREE from extremely weathered materials near the top of a soil profile which had developed on a granodiorite. Mongelli (1993) found that, in a granitic weathering profile in southern Italy the LREE-HREE fractionation was partly due to non-acidic pH environments which favour a greater HREE solubility, and partly to the removal of HREE-rich phases from the residual component. Xenotime may have a lower solubility than monazite (Middelburg et al., 1988).

Middelburg et al. (1988) found that during the weathering of granitic rocks, fractionation of REE results from the initial distribution of the REE in both leachable and residual mineralogical sites. REE concentrated in resistate minerals do not become easily enriched in the residual soils, whereas REE in leachable phases such as plagioclase, K-feldspar and apatite are easily liberated and consequently enriched in the residual soils.

Daux et al. (1994) studied the fate of major elements, REE and Th in basaltic rocks subjected to weathering. The behaviour of Th and REE's was found to be similar during weathering. Mass balance calculations account for Th and REE losses of up to 40%. These losses could be due to the fact that the elements are sorbed onto colloidal matter and transported in the aqueous phase involved in the dissolution. It has been suggested that most of the REE adsorb onto colloidal matter in groundwater, and that colloidal transport could be an important way for REE to leave the host rock (Smedley, 1991).

In first approximation, the relative impoverishment or enrichment in REE can be attributed to the ratios of weathered and weathering resistate minerals and their REE contents (Nesbitt, 1979). When the monazite content exceeds the xenotime content of the parent rock, the LREE may become relatively enriched in the saprolite or vice versa (van der Weijen and van der Weijen, 1995).

Increases and decreases in the REE contents as well as the marked differences of the REE patterns can be caused by inhomogeneities in the parent rocks and/or by differences in susceptibility to weathering of their host minerals in combination with sorption from percolating solutions under different redox conditions and solution chemistry.

2.4. Mobility of redox-sensitive elements (U and Th) during weathering

Middelburg et al. (1988) found that redox conditions have a marked influence on certain elements that are redox sensitive such as uranium. In the parent rock U occurs as U^{4+} or U^{6+}. The solubility of U^{4+} is negligible and U is, therefore, immobile under oxygen-free weathering conditions. Under oxygenated conditions, U is relatively soluble as U^{6+} species, but the uranyl ion (UO_2^{2+}) is strongly adsorbed onto Fe^{3+} oxides and organic matter (van der Weijen et al., 1985). There is no general trend in U behaviour during weathering (Middelburg et al., 1988 ; van der Weijen and van der Weijen, 1995). When trends in redox-sensitive element behaviour are not identical, it implies that there are either variations in the mineral and chemical homogeneity of the parent rocks or that there are variations in the weathering conditions (van der Weijen and van der Weijen, 1995). Differences in weathering conditions may consist of differences in the concentrations of oxygen and of humic and fulvic acids in groundwater, in liquid/solid ratios during water-rock interaction, and in flow direction (vertical and lateral). Braun and Pagel (1994) found that in a lateritic profile in SW Cameroon, U mobility was comparable to that of the most mobile alkaline and alkaline earths, Na, Ca and Mg.

In contrast to U, Th is solubilized under specific conditions (pH > 3 and in the presence of complexing agents) (Langmuir and Hermann, 1980). Thorium is found in nature as a tetravalent cation. Most Th host minerals are highly refractory to weathering and Th has long been considered a very insoluble and immobile element in natural waters. During the initial stages of weathering, Th is immobilized as thorianite (ThO_2) (Braun and Pagel, 1994).

2.5. Complexation of REE, U and Th in natural waters

2.5.1. Rare earth element complexation

The REE occur predominantly in the trivalent state. Cerium and Eu have been found to be the only two redox-sensitive REE (Figure 2.2). For all the other REE and Y, pH and solution chemistry determine the different complexes present. Cerium present as Ce^{3+} in the rock forming and accessory minerals, will be readily converted into Ce^{4+} in oxygenated groundwater. Because the solubility of Ce^{3+} is much higher than that of Ce^{4+}, this redox dependent solubility will result in Ce anomalies. Under reducing conditions Eu^{3+} is converted to Eu^{2+} and under extreme reducing conditions Sm and Yb may occur as divalent species (Wood, 1990).

The dominant factor controlling of REE concentrations in water is pH. At pH values higher than 6, REE concentrations are generally restricted to low levels, whereas at pH values less than 6 REE concentrations are generally higher (Smedley, 1991).

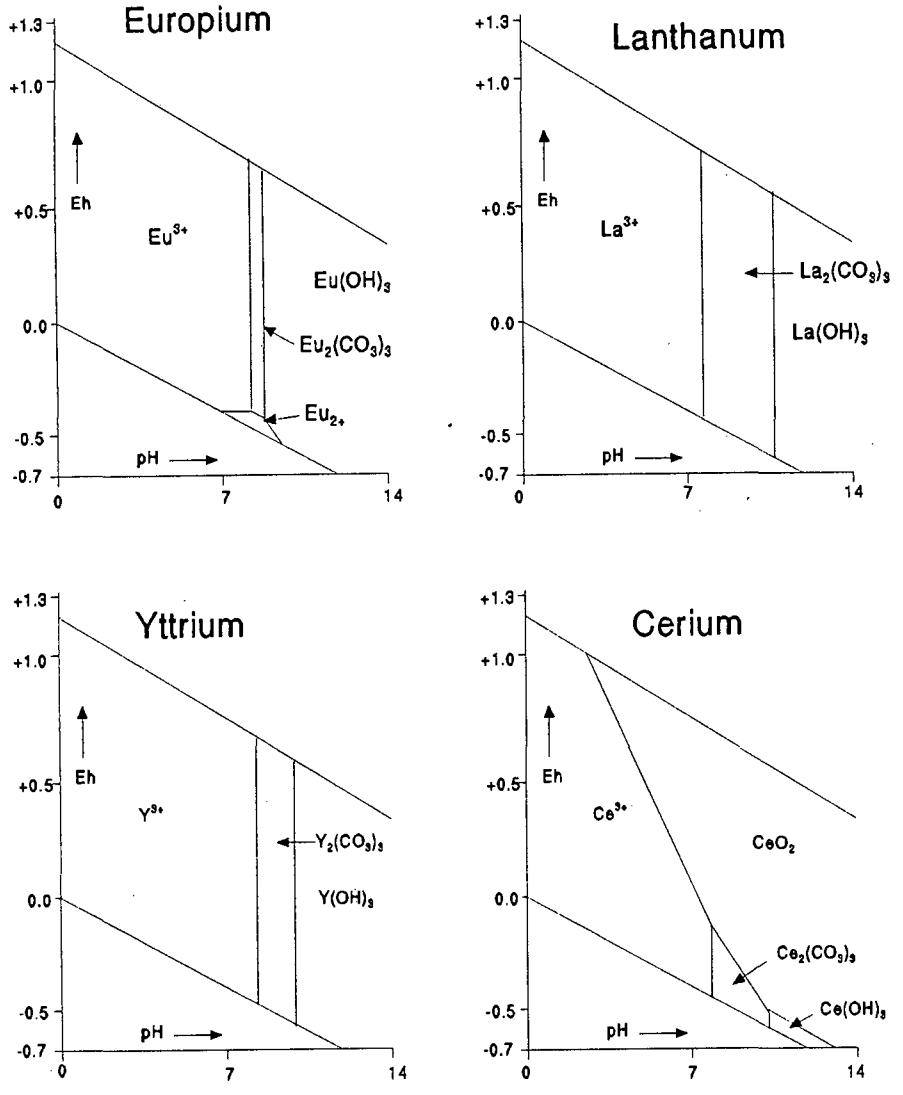

Figure 2.2. Eh-pH diagrams for some of the REE and Y at 25°C and one bar pressure. Activities of M^{2+}, M^{3+}, M^{4+} $=10^{-6}$ M and $\Sigma CO_2 = {}^aH_3CO_3 + {}^aHCO_3^- + CO_3^{2-} = 10^{-3}$ atm. The diagrams for Eu and Ce species involve both Eh and pH as variables while pH is the only variable for the remaining lanthanides (After Brookins, 1983).

The complexation of REE smoothly increases as a function of atomic number and an increase in solubility is expected to follow this trend (Cantrell and Byrne, 1987). The trivalent REE ions complex preferentially with ligands containing highly electronegative donar atoms such as fluoride (F^-), sulphate (SO_4^{2-}), carbonate (CO_3^{2-}), phosphate (PO_4^{3-}) and hydroxides (OH^-). Electrostatic bonds between the REE^{3+} cations and the ligands are formed (Wood, 1990).

Using Eu^{3+} as a representative REE, Wood (1990) calculated the inorganic speciation of Eu^{3+} as a function of pH, using a model groundwater (Table 2.1).

Table 2.1. Model groundwater composition, used in the determination of Eu complexes as a function of pH (After Wood, 1990).

	Molality
ΣEu	10^{-7}
ΣF^-	10^{-6}
ΣCl^-	2×10^{-4}
ΣSO_4^{2-}	10^{-4}
ΣPO_4^{3-}	10^{-6}
ΣCO_3^{2-}	10^{-4}
ΣNO_3^-	10^{-4}

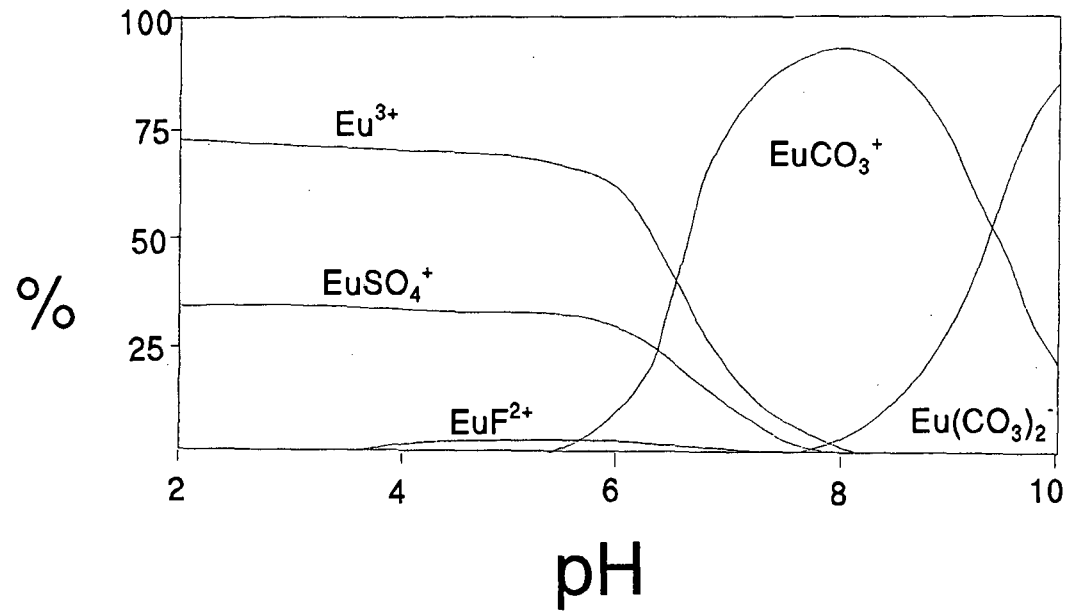

Figure 2.3. The distribution of Eu among various inorganic complexes as a function of pH, composition of water in Table 2.1 (After Wood, 1990). X-axis indicates the percentage complex at the corresponding pH.

Europium (Figure 2.3) exists predominantly as the simple ion Eu^{3+}, and the sulphate complex $EuSO_4^+$ at pH 2 to 6.5. The carbonate complex $EuCO_3^+$ is the dominant species between pH 6.5 to 9.5 and the carbonate complex $Eu(CO_3)_2^-$ at pH greater than 9.5. Thus, only the carbonate and sulphate complexes are sufficiently stable in typical groundwaters to affect REE transport (Wood, 1990).

Based on the available data, the carbonate complexes of the REE are the most important inorganic species in the transport of REE in near neutral to slightly basic groundwaters. Fluorides, sulphates, phosphates, carbonates and hydroxides may, however, be the most important ligands present, where their concentrations are unusually high due to either natural or anthropogenic processes.

It is possible that hydrolysis could play a more important role in the speciation of the REE, if the hydrolysis constants are higher than the ones used in the study. This could be the case as the present knowledge of hydrolysis constants for the REE is poor.

In the publication by Wood (1990), only the speciation of Eu was considered. The speciation calculated for Eu will not change in overall form but only in detail for the other REE. Wood (1990) predicted that both fluoride and carbonate complexes should become dominant at lower ligand concentrations for the HREE and at higher ligand concentrations for the LREE. The REE released during weathering of granitic rocks may well be transported as fluoride complexes due to the elevated content of F^- in groundwaters (Wadepohl, 1978). Oxidation of sulphides during weathering may provide sufficient sulphate to transport the metals.

Solubilities may be changed by complexation of REE by inorganic and organic ligands that are present in the percolating water. Adsorption of REE from these solutions will result in enrichment when the input of REE exceed REE losses. In the absence of ligands the affinity for adsorption increases from the LREE to the HREE, in the presence of ligands the reverse is the case (Braun et al., 1993).

2.5.2. Thorium complexation

Thorium complexation can increase the mobility of dissolved Th by many orders of magnitude below pH 8 relative to the solubility of Th-bearing minerals in pure water. This is exemplified by the solubility of thorianite (ThO_2) above pH 5 which is only 1 x 10^{-5} ppb Th as $Th(OH)_4^0$. With increasing pH, Th in natural waters is usually complexed as sulphate [$Th(SO_4)_2^0$], fluoride [ThF_2^{2+}], phosphate [$Th(PO_4)_2^0$ and $Th(HPO_4)_3^{2-}$] and hydroxide [$Th(OH)_4^0$]. Organic Th complexes greatly predominate over inorganic Th complexes in organic-rich waters. The complexes greatly increase the solubility of Th minerals and the mobility of Th in surface soil and groundwaters (Langmuir and Hermann, 1980).

The solubility of Th is reduced by hydrolysis. This leads to precipitation or sorption, and reduced complexation by other ligands in the waters. The hydrolysis of Th^{4+} can be extensive even in relatively acidic solutions. Studies of Th complexation are limited due to hydrolytic competition (Erten et al., 1994).

Although Th complexing in natural waters increases the solubility of Th-bearing minerals and can lead to desorption of Th, Th concentrations in natural waters (pH 5-9) rarely exceed 1 ppb. These low concentrations reflect a combination of slow solution rates, paucity and insolubility of Th-bearing minerals, and strong adsorption of Th by natural materials in this pH range (Langmuir and Hermann, 1980).

2.5.3. Uranium complexation

The geochemical behaviour of U is strongly affected by its oxidation state. In reduced groundwater conditions, U concentrations are low due to the low solubility of U^{4+} compounds, while in more oxidized conditions, U transport is facilitated by the higher solubility of U^{6+} (Figure 2.4a)(Ahonen, 1994). The uranyl ion (UO_2^{2+}) does not hydrolyse as readily as Th. The alkalinity of the percolating solutions will determine the concentration of the uranyl carbonate complexes and, accordingly, the mobility of the U will be determined by the concentration of the uranyl carbonate complexes (Figure 2.4b) (van der Weijen et al., 1985).

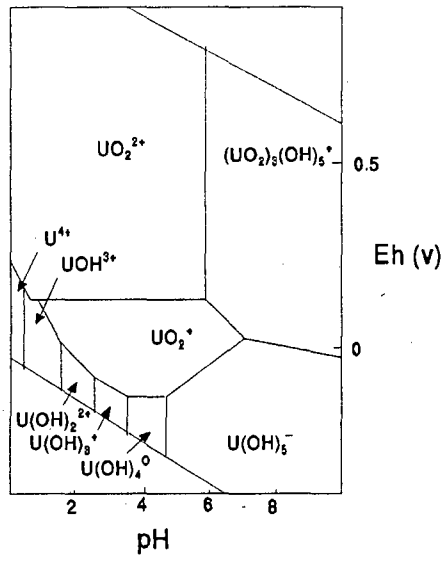

Figure 2.4a

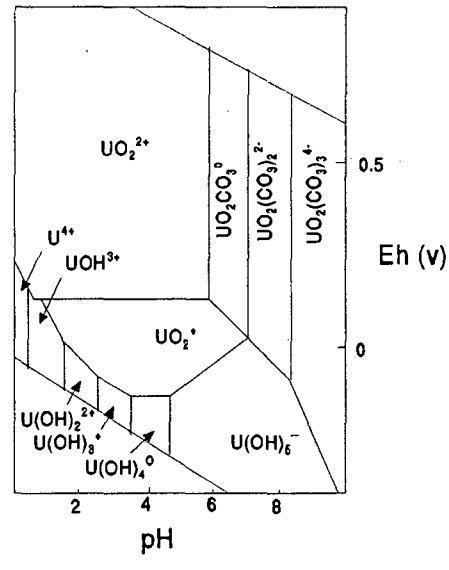

Figure 4b

Figure 2.4. Eh-pH diagrams showing the relative importance of +4, +5 (UO_2^+), and +6 valent uranium species at 25°C; for $\Sigma U = 10^{-6}$ M (Figure 2.4a), and for $\Sigma U = 10^{-6}$ M at a typical groundwater with CO_2 pressure of 10^{-2} atm (Figure 2.4b) (After Langmuir, 1978).

Uranium forms stable complexes with several commonly occurring ligands. The comparative importance of the various uranyl complexes is evident from Figure 2.5. The diagram is drawn from a CO_2 pressure and concentrations of chloride, fluoride, sulphate, phosphate and silica for a uraniferous groundwater (Harshman, 1972).

The plot shows that fluoride complexing would predominate below pH 4. The uranyl silicate complex is relatively unimportant. Between pH 6.6 to 8.3, both phosphate and carbonate complexes can predominate.

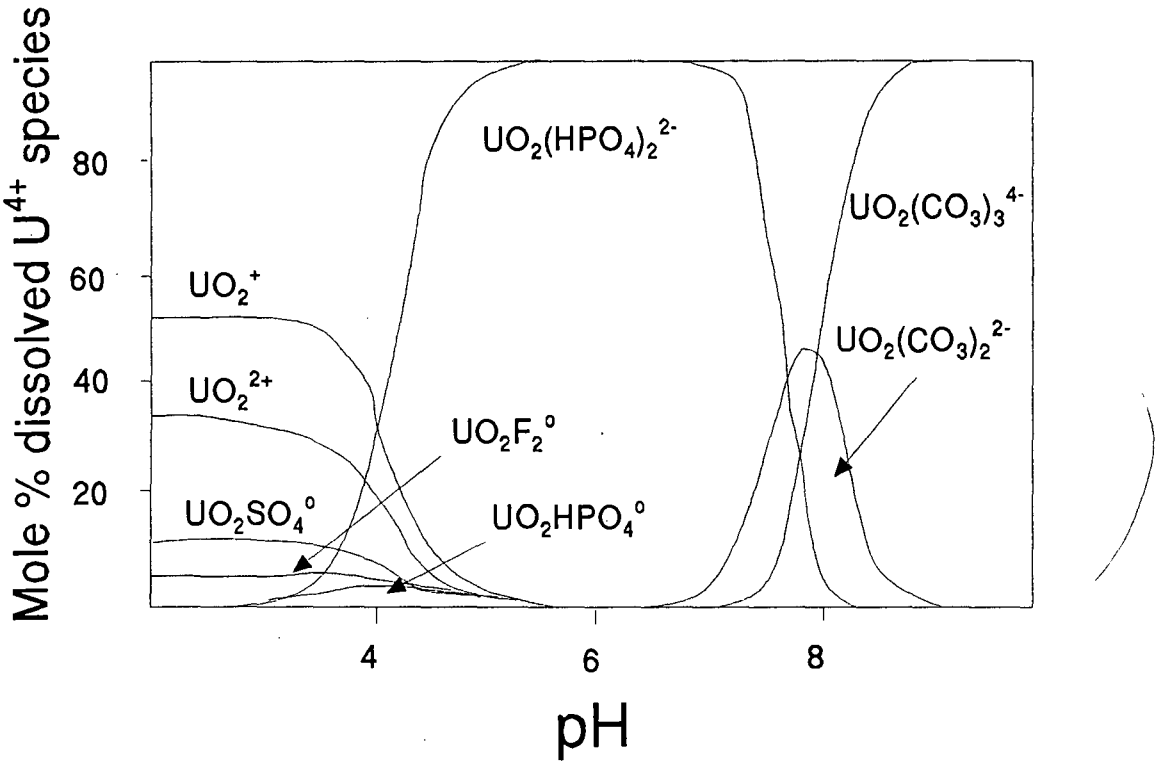

Figure 2.5: Distribution of uranyl complexes with pH for some typical ligand concentrations in groundwaters of the Wind River Formation at 25°C. $PCO_2 = 10^{-2.5}$ atm, $\Sigma F^- = 0.3$ ppm, $\Sigma Cl^- = 10$ ppm, $\Sigma SO_4^{2-} = 100$ ppm, $\Sigma PO_4^{2-} = 0.1$ ppm, $\Sigma SiO_2 = 30$ ppm (After Langmuir 1978).

2.6. Adsorption of REE, U and Th onto colloidal matter

Mobility of released elements is controlled not only by soluble complexes, but also by solid structures, whether crystallized (transformed or newly transformed minerals), amorphous or even colloidal, including oxyhydroxides and iron oxides (Short et al., 1989).

Colloids are solid particles with diameters ranging between 0.01 and 10 μm (clay sized and fine silt-sized) with low water solubility (Sposito, 1989). The chemical composition of these particles may vary from that of a clay mineral or a metal hydrous oxide to that of soil humus or a combination of inorganic and organic species (Sposito, 1989).

A colloidal suspension in which the clay particles are dispersed is said to be stable. The process by which a colloidal suspension becomes unstable and undergoes gravitational settling is coagulation. Particles no longer repel each other as they collide. Flocculation is said to have occurred when an initially turbid solution separates out into a clear solution with coagulated particles in suspension or as bottom sediment (van Olphen, 1977).

van der Waals forces are forces of attraction between particles whose magnitude depends on the size and shape of the particle (van Olphen, 1977). When two particles are brought close together, each induces a dipole moment. This produces an attractive interaction whose energy is inversely proportional to the distance of separation (Sposito, 1989). As particles approach each other more closely, the van der Waals forces can be strong enough to cause particles to flocculate.

In stable solutions, particles remain dispersed as the particle attractive forces are balanced by repulsive forces. As clay particles carry a net negative charge, a repulsive force arises and the tendency of particles to collide and coalesce together is minimized.

Stable colloidal suspensions can be generated in subsurface waters by several mechanisms including movement of colloids from the vadose zone, formation of colloid sized precipitates, dissolution of binding agents and ionic interactions that result in clay dispersion (McCarthy and Zacchara, 1989).

Colloids are widely recognized as an important vector of elemental transport in the geosphere (Yarif and Cross, 1979). This is due to their strong affinity for metallic elements and their well established mobility in underground waters. The presence of colloids may either increase or decrease the mobility of the adsorbed metallic elements. The mobility of elements decreases if they are incorporated on relatively large sized species, which are in addition prone to form aggregates and to be retained in the rock porosity. Mobility increases, however, if the colloids remain in the solution and are able to follow the water stream (Dran et al., 1994). A decrease or increase in mobility could also occur whenever an inversion of electric charge occurs with respect to the original ionic species, which hampers or favours the sorption of the combined species onto the solid phase (Dran et al., 1994).

The presence of colloids can enhance the concentration of contaminants, often by several orders of magnitude over levels found in ultrafiltered solutions. In extreme cases, such as the Gorleben site in Germany, measured solubilities are merely a function of filter size (Kim et al., 1994). Experimental studies have shown little or no transport of actinides and lanthanides in ultra filtered samples (approximately 1nm), whereas uptake onto inorganic (Read et al., 1994) or organic (Kim et al., 1995) colloids led to a breakthrough on timescales comparable to those of "ideal" tracers.

Adsorption of Th onto clays, oxides and organic matter increases with increasing pH and is practically complete at pH 6.5. Adsorption is more complete onto humic organic solids than onto clays. However, inhibition of adsorption and a tendency towards desorption is favoured when strongly complexing organic ligands such as fulvic acid are present (Bondeitti, 1974).

Dran et al. (1994) studied the mechanism of colloid [ceria (CeO_2), thoria (ThO_2) and haematite (Fe_2O_3)] attachment to mineral surfaces. These three types of colloids differ by their chemical composition, their size and their charge variations in the pH range investigated. The retention properties of the colloidal suspensions towards several mineral surfaces were studied as a function of pH (range 3 to 8), ionic strength (0.001 to 0.1M) and concentration.

It was found that the quantity of sorbed colloids strongly increased with concentration (Dran et al., 1994). Increase in pH resulted in an increase in sorption in the case of thoria and ceria. In both cases, the charges of the suspensions and the mineral surfaces are opposite, thus favouring the sorption. A charge inversion occurred with the increase in pH of the hematite colloid, leading to a decrease in colloid sorption. Ionic strength affects the stability of the colloidal suspensions, which results in a tendency to aggregation and flocculation when this parameter was increased. Another important finding was whatever the colloid-surface system, the sorption of colloids was not reversible with respect to solution composition.

Whenever present as true colloids, transuranic elements probably would be bound to mineral surfaces and their mobility would be reduced because of the irreversible character of the sorption process. The strong affinity of the tetravalent actinides to other inorganic colloidal species present in greater abundance makes their occurrence as individual entities unlikely. The carrier colloids will control the transport properties of the heavy elements. Hence, mobility enhancement or retardation of the radiotoxic element may occur, depending on the possible exclusion phenomena of matrix pores or filtration phenomena (Dran et al., 1994).

Previous work has suggested that colloidal mineral surfaces in the environment may be coated to some extent by natural organic matter (NOM) conferring a more negative surface charge to the mineral (Tipping and Cooke, 1982) and influencing colloidal mobility and stability (Amirbahman and Olson, 1993). Fairhurst et al. (1995) studied the effect of pH on Eu mineral interactions in the presence and absence of humic acid. In the absence of humic acid, the adsorption behaviour of Eu showed a strong pH dependence, with Eu adsorption generally increasing with increasing pH.

In all cases Eu was found to adsorb onto the negatively charged mineral surfaces. The adsorption may be explained by electrostatic interactions and by specific site binding between the positively charged Eu species likely to exist (Eu^{3+}, $EuCO_3^+$ and $EuOH_2^+$) and the negative surface.

Around pH 8, negatively charged $Eu(CO_3)_2^-$ species were found to predominate and charge repulsion is thus expected. It therefore appears that the adsorption of Eu is dependent upon the dissolved form of the metal and/or the surface properties of the adsorbent.

Thorium is known to adsorb strongly onto colloidal particles (Santschi, 1994). It is, therefore, important to have quantitative information about sorption processes that affect the migration of Th in natural waters, in order to understand the behaviour of Th in these environments. Silica, in the form of colloidal particles, is abundant in many natural aquatic environments. Its ability to sorb metal ions is well known (Schindler et al., 1975). Östhols (1995) found that although the pH region where Th is predominantly sorbed on the silica surface will to some extent depend on the ratio of Th concentration to silica surface, it is clear that Th sorbed on silica will rarely be present above pH 5 to 6. It is more likely that in the neutral to alkaline pH range, Fe and Mn will be the main sorbents of Th (Hunter et al., 1988). Thorium has been found to have a strong association with Fe oxides in granitic groundwaters (Landström and Tullborg, 1990).

2.7. Conclusions

The chemical behaviour of REE, U and Th depends on several factors such as Eh (especially Ce, Eu and U), pH, the presence of organic and inorganic ligands, cation exchange sites on clays, mineralogical distribution of REE, U and Th in the parent material, and especially the nature of the host rock accessory mineral association (Nesbitt, 1979).

The only two REE for which Eh plays a role in weathering are Ce and Eu. For all the others, pH determines the fractionation and mobility in soils. Fractionation of REE during weathering of a parent rock can result in different REE patterns in different parts of the weathering profile. Losses of REE during weathering could be due to the fact that the elements are sorbed onto colloidal matter and transported in the aqueous phase involved in the dissolution.

Uranium is sensitive to redox conditions. In the parent rock, U occurs as U^{4+} or U^{6+}. Solubility of U^{4+} is negligible and is, therefore, immobile under oxygen free weathering conditions. Under oxygenated conditions, U is relatively soluble as the U^{6+} species (UO_2^{2+}). In contrast to U, most Th host minerals are highly resistant to weathering and Th has long been considered a very insoluble and immobile element in natural waters. During the initial stages of weathering, Th is immobilized as thorianite (ThO_2).

The REE occur predominantly in the trivalent state. The trivalent REE, U and Th ions complex preferentially with ligands containing highly electronegative donar atoms such as fluoride (F^-), sulphate (SO_4^{3-}), carbonate (CO_3^{2-}), phosphate (PO_4^{3-}) and hydroxides (OH^-).

The mobility of the released elements is controlled not only by soluble complexes, but also by solid structures, whether crystallized, amorphous or even colloidal, including oxyhydroxides and iron oxides.

Colloids are widely recognized as an important vector of elemental transport in the geosphere, due to their strong affinity for metallic elements and their well established mobility in underground waters. Colloids may decrease the mobility of the adsorbed metallic elements, if the elements are adsorbed on relatively large sized species, which are in addition prone to form aggregates and to be retained in the rock porosity. Mobility would increase if the colloids remain in the solution and are able to migrate in the water stream. The presence of colloids (0.01 to 10μm) can enhance the concentration of contaminants, often by several orders of magnitude, over levels found in ultrafiltered solutions (<1nm).

Chapter 3

Sampling and analysis

3.1. Sample collection and preparation

A total of nineteen water samples, thirty three soil samples, three colloidal samples and one precipitate were collected during three field trips to the Steenkampskraal Monazite Mine. The surface sample positions were determined using a geographical positioning system (GPS). The latitude and longitude co-ordinates determined by the GPS were converted into X-Y coordinates to remain consistent with the maps obtained on the mine. Samples were collected during 3 field trips in August and September.

Locality maps of all surface sample positions can be found in Figures 3.1 and 3.2. A brief description of all samples, including both latitude and longitude coordinates as well as X-Y coordinates, can be found in Appendix 1.

Water was sampled from six boreholes in the near vicinity of the mine (BH 1-6). During initial sampling the boreholes were unpurged. On the third field trip boreholes were purged using bailers. During purging it was found that BH 4 contained very little water and purging was, therefore, not possible. Water was also sampled from five windpumps on the farms, Nabeep and Brandewynskraal (MOS 1-4 and BRAND 1) (Figure 3.2). These boreholes were being used for watering livestock and purging was therefore unnecessary.

Water was sampled on both the first and second field trips from the same place in the slimes dam (SD 1 and SD 2). This was done because it had rained in between the two visits, and the stable isotope signature of the slimes dam was of interest in determining the origin of the water in BH 6 as it was initially suspected that the water in BH 6 may have originated from the slimes dam. Water was also sampled in the stream along the soil transect 1 (Stream water) on the second field trip after the rain, as well as from a road (Road water) below the slimes dam on the third field trip shortly after rain. Four water samples were taken from within the underground mine workings (Main shaft, Main shaft extension, Sump on level 3 and Inclined shaft). Four bottles were used at each water sampling location, where 2 acidified and 2 unacidified water samples were taken. Samples were acidification immediately after collection, with all water samples sealed to limit the interaction with the atmosphere. Unacidified samples were filtered using a 0.2μm milipore filter, at the laboratory (approximately 1 to 2 days after sampling).

Colloids were sampled from three boreholes during the purging process (BH 1, BH 2 and BH 6). A surface precipitate was sampled from the surface of the main shaft water.

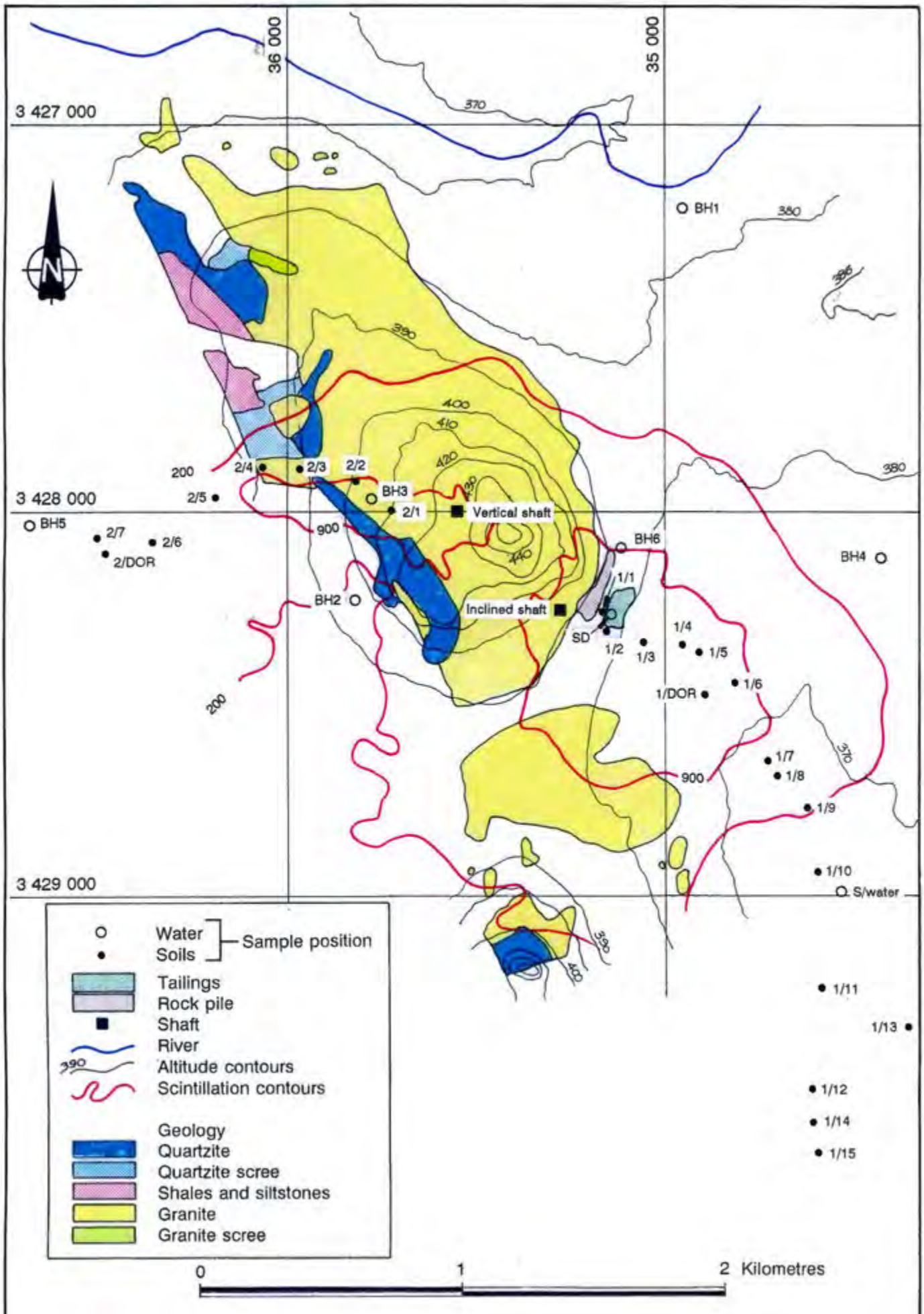

Figure 3.1. Locality map of samples from the Steenkampskraal monazite mine.

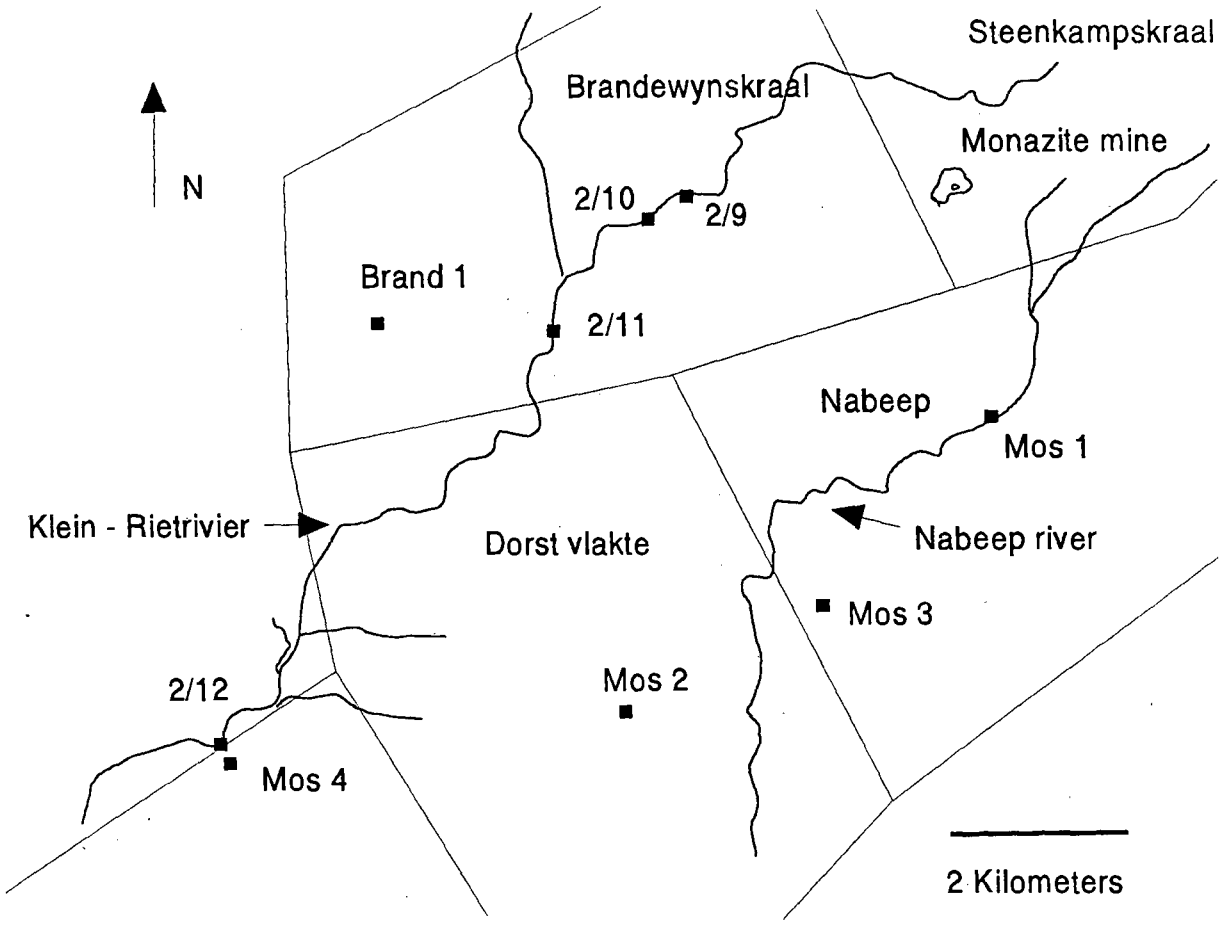

Figure 3.2. Map of the general Steenkampskraal area, showing the farms Nabeep and Brandewynskraal. Samples not included in Figure 3.1 have been placed in Figure 3.2.

Soils were sampled along two transects away from the mine. Transect 1 started below the rock pile on the eastern side of the ore body and extended out towards the south east (1/1 - 1/15) (Figure 3.1). Transect 2 was sampled from below the main shaft, extending out towards the south west (2/1 - 2/12) (Figure 3.1 and 3.2). A sample of dorbank was taken on both transects (1/DOR and 2/DOR). The final soil sample was sampled in the river bed near BH 1 (2/BH 1). This soil sample was presumed to have received no contamination from monazite mining at Steenkampskraal.

The two transects followed the dominant drainage patterns on either side of the mine. All samples are regarded as soils, with the mechanism of element transport believed to be similar for all samples. Five or six grab samples of approximately equal mass (1kg) were taken at each locality. Sampling depth extended to the dorbank, at a depth ranging from 10 to 30cm. Bulk samples were thoroughly mixed and split, of which 1 subsample (1.5kg) was taken back to the laboratory where they were air dried and sieved through a 2mm sieve to remove the coarse fraction. All soil sample analyses were performed on the fraction finer than 2mm.

Duplicate samples were not taken, mainly due to budget and time constraints. An attempt was made to make sure the final sample taken was representative of the area in which it was sampled.

3.2. Solution analysis

Numerous analytical techniques were used in determining the chemical properties of both the water samples and the saturated paste extracts from ten soil samples (1/2A, 1/2B, 1/4A, 1/4B, 1/6, 1/8, 2/1, 2/3, 2/5, 2/7).

3.2.1. pH measurement

The pH measurements for both saturated paste extracts and water samples were measured using a CRISON Micro pH 2001 instrument. Precision and accuracy for the measurement of pH can be found in Appendix 2.

3.2.2. Electrical conductivity (EC)

The electrical conductivity was measured on all water and soil extract samples using a CRISON micro CM 2201. The conductivity meter values have been reported in $mS.cm^{-1}$. The procedure details were taken from the Standard Methods for the Examination of Water and Waste Water (1985).

3.2.3. Alkalinity

The total alkalinity (end point pH = 4.5) of the unfiltered water samples was determined using an automatic potentiometric titrator (Radiometer Copenhagen DTS800 multi-titrator system). This involved titrating a 10 ml aliquot of sample against 0.025M HCl. Procedure details for the measurement of alkalinity can be found Appendix 2.

3.2.4. Acidity

Acidity was determined by titrating a 10 ml aliquot of sample against a known concentration of Titrisol NaOH to reach an end point of pH 8.3. The titration was used to determine the acidity of all water samples and extracts with a pH < 4.5.

3.2.5. Determination of ionic and elemental concentrations in solution

High Performance Ion Chromatography (HPIC) was used to determine the anions Cl^-, SO_4^{2-}, NO_3^-, PO_4^{3-}, F^- and Br^- and the cations Ca^{2+}, Mg^{2+}, Na^+, K^+ and NH_4^+. Analyses were made on filtered (0.2μm), unacidified water samples. Deionised water (Milli-Q) was used to dilute the samples to an EC of less than 0.1 $mS.cm^{-1}$ prior to the analysis. In certain cases, further dilutions were necessary.

Inductively Coupled Plasma-Atomic Emission Spectrometry (ICP-AES) was used to determine the total concentration of the elements Ca, Mg, Na, K, Fe, Al, Cu, Cr, Mn, Ni, Si, Co, Pb, Zn, As and Cd. These elements were determined in the Department of Chemistry at the University of Cape Town on unfiltered acidified water samples. Inductively Coupled Plasma-Mass Spectrometry (ICP-MS) was used to analyze for Th, U and REE. These elements were determined in the Anglo American Research Laboratories in Johannesburg on unfiltered acidified samples. Principles of HPIC, ICP-AES and ICP-MS can be found in Appendix 2.

The phosphorus (P) concentration was determined by the Murphy and Riley (1962) method, due to PO_4^{3-} dilution to below detection limits on the HPIC analyses. The phosphorus concentrations were then converted to PO_4^{3-}. Procedure details can be found in Appendix 2.

Fluoride analyses by HPIC were similar to those of phosphate in that dilution resulted in concentrations at or near the detection limits of the HPIC. Fluoride concentration was therefore determined using an ion selective electrode. Procedure details can be found in Appendix 2.

3.2.6. Stable isotopes of oxygen ($^{18}O/^{16}O$) and hydrogen (D/H)

Samples were prepared in the stable isotope laboratory in the Department of Geological Sciences, and analyzed in a Mass Spectrometer (Finnigan MAT-252) in the Archaeology Department, both departments being at the University of Cape Town. Details of the preparation of oxygen and hydrogen isotopes for analysis by the mass spectrometer can be found in Appendix 2.

3.2.7. Saturated paste extract

In order to measure the dissolvable inorganic solutes of the soils, saturated paste extracts were prepared. Soil samples were saturated with water, as it is often not practical for routine analysis of soil samples that contain usual field water contents. Because the absolute and relative amounts of various solutes are influenced by the soil/water ratio at which the extract is made (Reitemeier, 1946), the soil/water ratio must be standardized to obtain results that can be applied and interpreted universally (Rhoades, 1982).

The soil/water ratio used for the saturated paste extract is the lowest reproducible ratio for which enough extract for analysis can be readily removed from the soil with a vacuum (Rhoades, 1982). The results obtained from the analysis of the saturated paste extracts give relative comparisons only, since the soils are adjusted to unnaturally high water contents during extraction (Rhoades, 1982).

The saturated paste extracts were used in the analysis of both cations, anions and trace metals by HPIC, ICP-AES and ICP-MS as well as for various other chemical analyses such as phosphorous determination, alkalinity, acidity, pH and EC.

The saturated paste extracts were extracted using a 0.45μm filter and then further filtered through a 0.2μm filter to remove any additional colloidal particles. A subsample of the saturated paste was acidified for the determination of elements by ICP-AES and ICP-MS. Procedure details for the preparation of the saturated paste extracts are found in Appendix 2.

3.2.8. Prediction of chemical speciation and saturation indices

The geochemical equilibrium speciation model for dilute aqueous systems, MINTEQA2, was used to determine ionic speciation in both the water samples and saturated paste extracts. MINTEQA2 is able to calculate saturation indices (SI) for minerals likely to occur under the prevailing conditions.

The MINTEQA2 model is based on the assumption of thermodynamic equilibrium between phases, with the thermodynamic equilibrium constant defined as follows.

$$aA + bB \rightleftharpoons A_aB_b$$

$$K^0 = \frac{A_aB_b}{A^aB^b}$$

where A and B are chemical entities that react to form the reaction product A_aB_b, having a thermodynamic equilibrium constant K^0. The various chemical reactions that are modelled are quantified by the Davies equation which is an extension of the Debye-Hukel equation in which the ion-size-dependant parameters are the same for each charged ion (MINTEQA2/PRODEFA2, 1991).

3.3. Soil and colloid analysis

Numerous analytical techniques were used in determining the chemical and physical properties of the soil samples, colloid samples and main shaft precipitate.

3.3.1. X-ray fluorescence spectrometry (XRF)

Both major and trace element analyses were conducted on the soils and main shaft precipitate using XRF in the Department of Geological sciences at the University of Cape town.

Due to the high concentrations of Th in the soil samples, it was necessary to calculate the mass adsorption coefficients (MAC's) for Th at a wavelength at which errors in the analytical results are eliminated. The presence of major or minor element absorption edges between the analyte wavelength and the wavelength at which the mass absorption coefficient is calculated, eg ThL_{III} abs between MoKαC and $ThL\alpha_1$, can introduce serious errors in the analytical results (Willis and Duncan, 1996). In order to use the mass absorption coefficients (MAC's), estimated by the Compton peak method, for the determination of high concentrations of Th, it was necessary to calculate the MAC's for Th at a suitable wavelength (eg RbKα) (Figure 3.3).

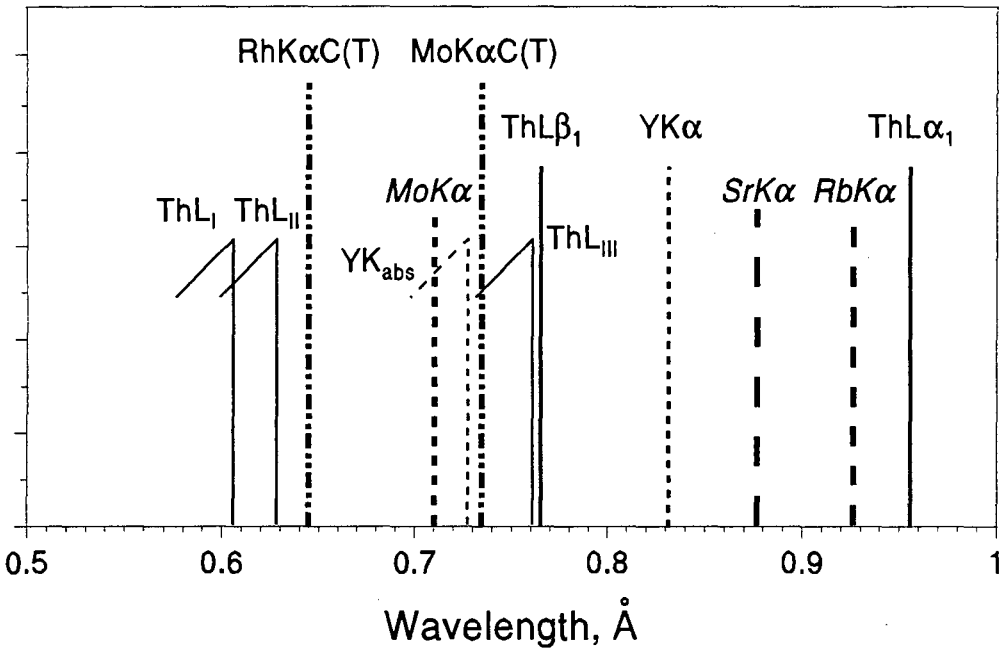

Figure 3.3. The relation between the Rh and Mo tube Compton peak wavelengths, analyte peak wavelengths (YK_α, $ThL_{\alpha l}$) and Th and Y absorption edges.

Nesbitt et al. (1976) described a method for estimating MAC's on the long wavelength side of intervening major or minor element absorption edges from MAC's known or determined on the short wavelength side of the absorption edges.

In Figure 3.4 element X is present in a sample at a) trace element concentrations and b) major or minor element concentrations, but only at trace element levels in a standard, and γ is the wavelength at which the MAC's were determined [RhKαC(T)] and λ_i is the analyte wavelength. r_λ is the ratio of sample and standard MAC's on the short wavelength side of the X_{abs}, and $r_{\lambda i}$ is the ratio of the sample and standard MAC's at the analyte wavelength, ie on the long wavelength side of the X_{abs} edge.

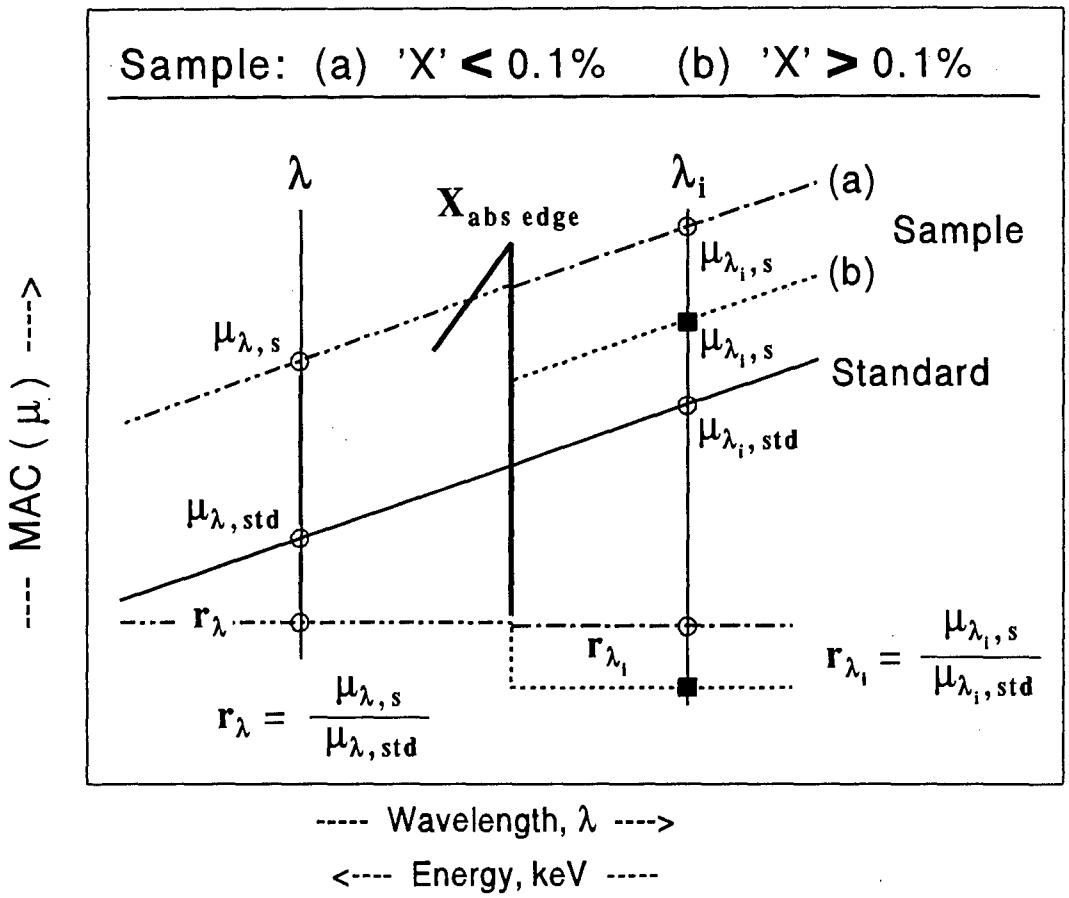

Figure 3.4. Ratios (r_λ or $r_{\lambda i}$) of mass absorption coefficients on either side of (a) a trace element absorption edge and (b) a major or minor element absorption edge (After Willis and Duncan, 1996).

When X is present at concentrations < ~ 0.1%, the ratio r_λ of the MAC's of sample and standard on the short wavelength side of the X_{abs} edge is not significantly different from the ratio $r_{\lambda i}$ at the analyte wavelength on the opposite side of X_{abs}. The use of either r_λ or $r_{\lambda i}$ in the equation:

$$C_s = C_{std} \times I_s/I_{std} \times (\mu/p_s)/(\mu/p_{std})$$

will give the same concentration for C_s. When X is present at concentrations > ~ 0.1%, the ratio $r_{\lambda i}$ at the analyte wavelength is very different from r_λ on the opposite side of the X_{abs}. Using $r_{\lambda i}$ in the above equation will give the correct concentration of X in the sample. Using the Compton peak MAC's (r_λ) would give an incorrect concentration for element X. The amount of bias would depend on the concentration of X.

The Nesbitt method for obtaining the correct value of $\mu_{\lambda i,s}$ from $\mu_{\lambda,s}$, when X is present at concentrations >0.1%, is described below. The difference in magnitude between r_λ and $r_{\lambda i}$, the ratio $\mu_{\lambda,s}/\mu_{\lambda i,s}$ and the analyte peak intensity at λ_i are all proportional to the concentration of X. Plotting $\mu_{\lambda,s}/\mu_{\lambda i,s}$ against the peak intensity R_i for a number of standards with different concentrations of X yields a straight line (Figure 3.4).

Figure 3.5 illustrates a plot, in which the intensity of the ThLα_1 line is plotted against various MAC ratios. By selecting the equation of the straight line of the plot of MC/Rb vs Th (cps), it was possible to calculate the MAC's at the RbKα wavelength knowing the MAC at the measured MoKαC wavelength. This allowed the original data to be reprocessed with MAC's that were calculated on the long wavelength side of the Th absorption edge, and which would give actual concentrations for all monazite concentrations longer than the ThL_{III} abs edge, eg Y, Sr, U, Rb, Th, Pb, Zn, Cu and Ni. In order to calculate MAC's across the Th absorption edge, 10%, 5%, 2.5%, 1.25%, 0.625% and 0.315% ThO_2 standards were made up in pure SiO_2.

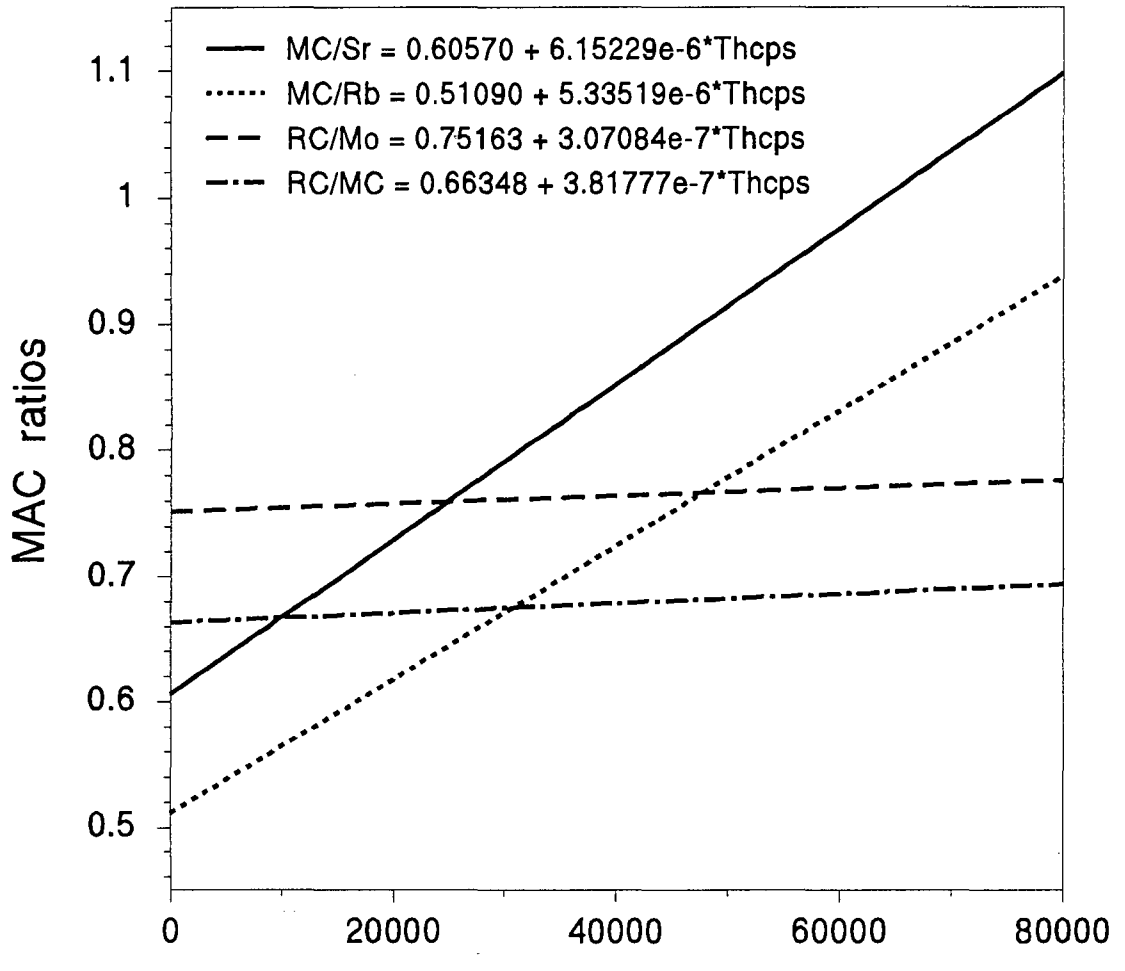

Figure 3.5. Plot of MAC ratios against ThLα_1 counts per second. Mc = MAC at MoKαC / Rc = MAC at RhKαC / Sr = MAC at SrKα / Rb = MAC at RbKα / Mo = MAC at MoKα (See Figure 3.3).

Table 3.1. Thorium concentrations of samples using the MAC's at the MoKα wavelength and the RbKα wavelength.

Sample	Th (mg/kg) using UMoKαC	Th (mg/kg) using URb
1/1	311	314
1/2A	31380	27783
1/3A	27652	24667
1/4A	9457	8865
1/5	4903	4711
1/6	497	500
1/7	76	77
1/8	68	69
1/9	93	95
1/10	64	65
1/11	67	68
1/12	943	942
1/13	23	23
1/14	105	106
1/15	17	17

As can be seen from Table 3.1 noticeable differences in Th concentration occur above about 2000 mg/kg. Principles of XRF can be found in Appendix 2.

3.3.2. Particle size analysis

Prior to the removal of the coarse fraction (>2 mm), a known mass of soil samples 1/4A and 2/3 were split into 7 size fractions (>2 mm, 2-1 mm, 1-0.5 mm, 0.5-0.25 mm, 0.25-0.125 mm, 0.125-0.065 mm and < 0.065 mm). This was done using a series of stainless steel sieves attached to a mechanical shaker. The mass of each fraction was weighed after separation, and the concentrations of various elements were determined using XRF.

3.3.3. Organic carbon: Walkley-Black Method (1935)

Organic carbon was determined on the ten selected soil samples along transects 1 and 2 (1/2A, 1/2B, 1/4A, 1/4B, 1/6, 1/8, 2/1, 2/3, 2/5, 2/7). The Walkley-Black method of determining organic carbon percentage is based on the oxidation of organic material in the soil with a mixture of $K_2Cr_2O_7$ (potassium dichromate) and H_2SO_4.

The reaction may be represented by the equation:

$$2Cr_2O_7^{2-} + 3C + 16H^+ = 4Cr^{3+} + 3CO_2 + 8H_2O$$

The excess dichromate is titrated with iron (II) ammonium sulphate hexahydrate. As the endpoint is approached, the solution colour changes from brown to dark violet brown initially, and then abruptly to green as the endpoint is reached. Procedural details for the determination of organic carbon by the Walkley-Black method can be found in Appendix 2.

3.3.4. Sample preparation for mineralogical analysis

3.3.4.1. Saturation of exchange complexes

Since expandable phyllosilicates may retain different amounts of interlayer water depending upon the nature of interlayer exchangeable cations, it is essential that the fraction prepared for diffraction analysis be homoionic to ensure that the expansion as a result of hydration will be uniform within all crystals of a species (Whittig and Allardice, 1986). Clay samples are also commonly analyzed after drying in air, so it is advisable to exchange saturate the clay with a cation that will minimize changes in interlayer water adsorption due to fluctuations in relative humidity (Whittig and Allardice, 1986).The colloid samples were saturated with Mg to ensure that the expansion was uniform within all crystals of a species. Procedure details for the principles of saturation of exchange complexes can be found in Appendix 2.

3.3.4.2. Dissolution of noncrystalline hydrous oxides

The main shaft precipitate was treated with acid ammonium oxalate in the dark (Jackson et al., 1986). This allows for the dissolution of noncrystalline materials. Procedural details can be found in Appendix 2.

3.3.4.3. X-ray diffraction (XRD)

Colloids from three boreholes were identified using XRD. The colloid samples were carefully prepared in a dispersed state on a glass slide for analysis. Procedural details of the XRD method can be found in Appendix 2.

3.3.5. Carbonate content

The presence of carbonate was initially established by placing HCl onto the ten selected soil samples as well as the colloid samples. Effervescence indicated the presence of carbonate. Only colloid sample BH 6 showed effervescence. The carbonate content of BH 6 was then determined quantitatively using the "Karbonat-bombe" method described by Birch (1981). Procedural details for the determination of the carbonate content can be found in Appendix 2.

3.3.6. Scanning electron microscopy (SEM)

SEM was used for both qualitative and quantitative identification of the mineralogy present in the Main shaft precipitate. Settings used on the SEM can be found in Appendix 2.

Chapter 4

Water chemistry

4.1. Introduction

This study on U, Th and REE mobility in the ground waters within the Steenkampskraal area follows a pilot study that was launched in January 1995, in which high concentrations of actinide and lanthanide elements were found to be present in solution, together with pronounced fractionation, between the HREE and LREE (Anderson et at., 1995). The object of this study was to answer some of the questions that arose from the pilot study. In particular the objective was: to determine the origin of elevated concentrations of elements and ions in solution; to establish the presence of colloidal matter, and to evaluate its role in promoting the mobilization of trace metals; and finally, to study the effects of acidification after evacuation of the mine.

4.2. Stable isotope study

Stable isotopes of oxygen ($^{18}O/^{16}O$) and hydrogen (D/H) were used in an attempt to determine the origin of the present-day groundwater flow regime. By having a clear understanding of the origin of the Steenkampskraal waters, an attempt could be made to assess the extent of ground water acidification after mining, as well as to assess the role of colloids in promoting the mobilization or retardation of the actinides in the system. The positions of the boreholes and the slimes dam whose waters were analyzed in the study are shown plotted in Figure 4.1.

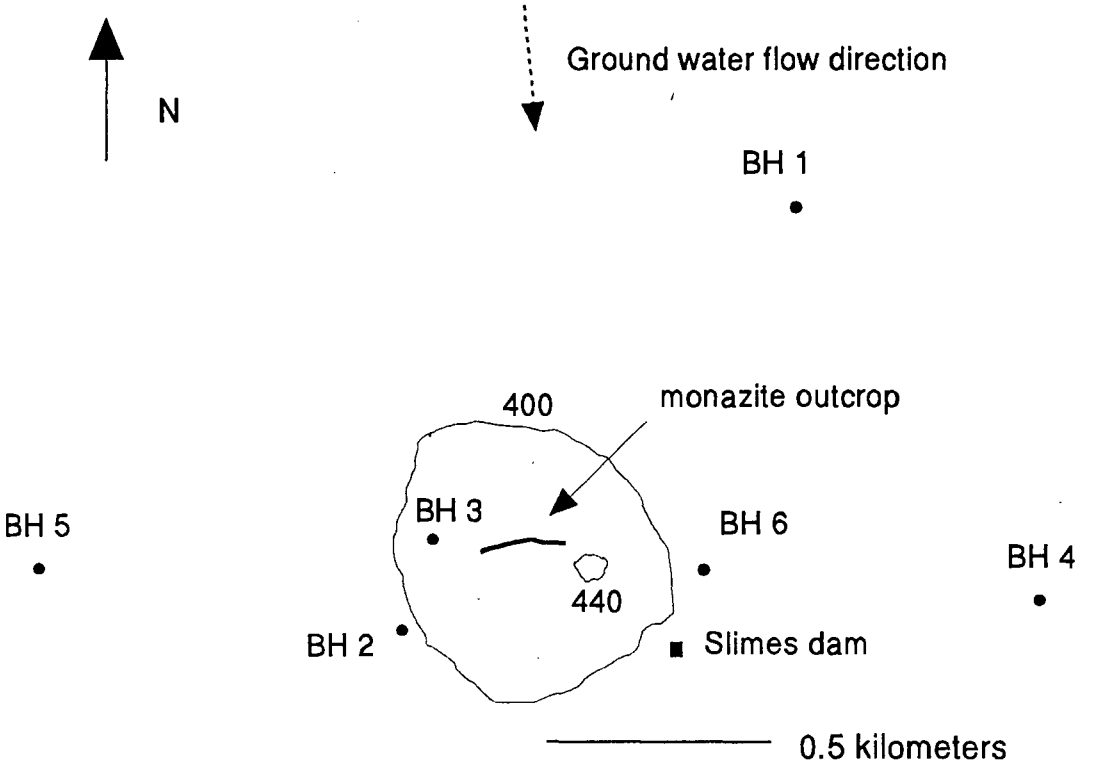

Figure 4.1. Locality of the slimes dam and boreholes, with the 400 and 440 m elevation contours.

Two distinct groups of values were obtained (Table 4.1). One group comprises unevaporated waters, present in all boreholes (BH 1 to BH 6) as well as the water sampled in the inclined shaft (Reference numbers 6 - 11, Table 4.1), where all $\delta^{18}O$ and δD values were negative and δ refers to the difference in thousands of the ratios in the sample and the standard (SMOW - standard mean ocean water). A second distinct group of highly evaporated water was found to be present in both slimes dam samples as well as the underground water samples from the main shaft, main shaft extension and the sump on level 3 (Reference numbers 1 - 5, Table 4.1), where all $\delta^{18}O$ and δD values were positive. The isotopic signature of the sump on level 3 is, however, less "evaporated" than the main shaft and main shaft extension water samples.

Table 4.1. Stable isotope data for waters sampled in the Steenkampskraal area. Reference number refers to Figure 4.2. All $\delta^{18}O$ and δD values are relative to SMOW.

SAMPLE	$\delta\ ^{18}O$	δ D	Reference number
Slimes dam 1	+5.5	+15	1
Slimes dam 2	+4.3	+17	2
Main shaft extension	+3.6	+20	3
Main shaft	+2.7	+15	4
Sump on level 3	+1.5	+6	5
Inclined shaft	-3.4	-23	8
BH 1	-4.0	-24	9
BH 2 (SKP 35)	-5.5	-25	11
BH 3 (SKP 37)	-3.6	-18	6
BH 4 (SKP 34)	-4.5	-27	12
BH 5 (BPK 1)	-4.8	-24	10
BH 6 (STK 25)	-5.1	-20	7

The equations corresponding to the two lines in Figure 4.2 represent the southern African meteoric water line ($\delta D = 6\delta^{18}O + 5$) (I.A.E.A., 1981) and the water line defined by the Steenkampskraal data ($\delta D = 4.6\delta^{18}O - 2.3$. The isotopic signature of the two slimes dam samples (1 and 2) are strongly positive. The $\delta^{18}O$ value is more reliable than the δD value in these samples due to the very high concentration of dissolved metals in these waters.

During the initial preparation of the δD samples various reactions were believed to be taking place with the hydrogen gas, which induced significant fractionation. The samples were eventually prepared via distillation. Distillation improves the accuracy of the δD value by removing the metals. Fractionation during the distillation process may, however, still occur, but will only increase error slightly.

With slightly higher δD values for the slimes dams samples, the Steenkampskraal meteoric water line would conform closer to the southern African meteoric water line ($\delta D = 6\delta^{18}O + 5$). The $\delta^{18}O$ value for SD 1 indicates it is more highly evaporated that SD 2. This would be expected from the history of the two water samples in that dilution from rain-fall occurred between the time of sampling of SD 1 and SD 2. The δD values suggest the opposite. This is presumed to be due to a small error in the analysis.

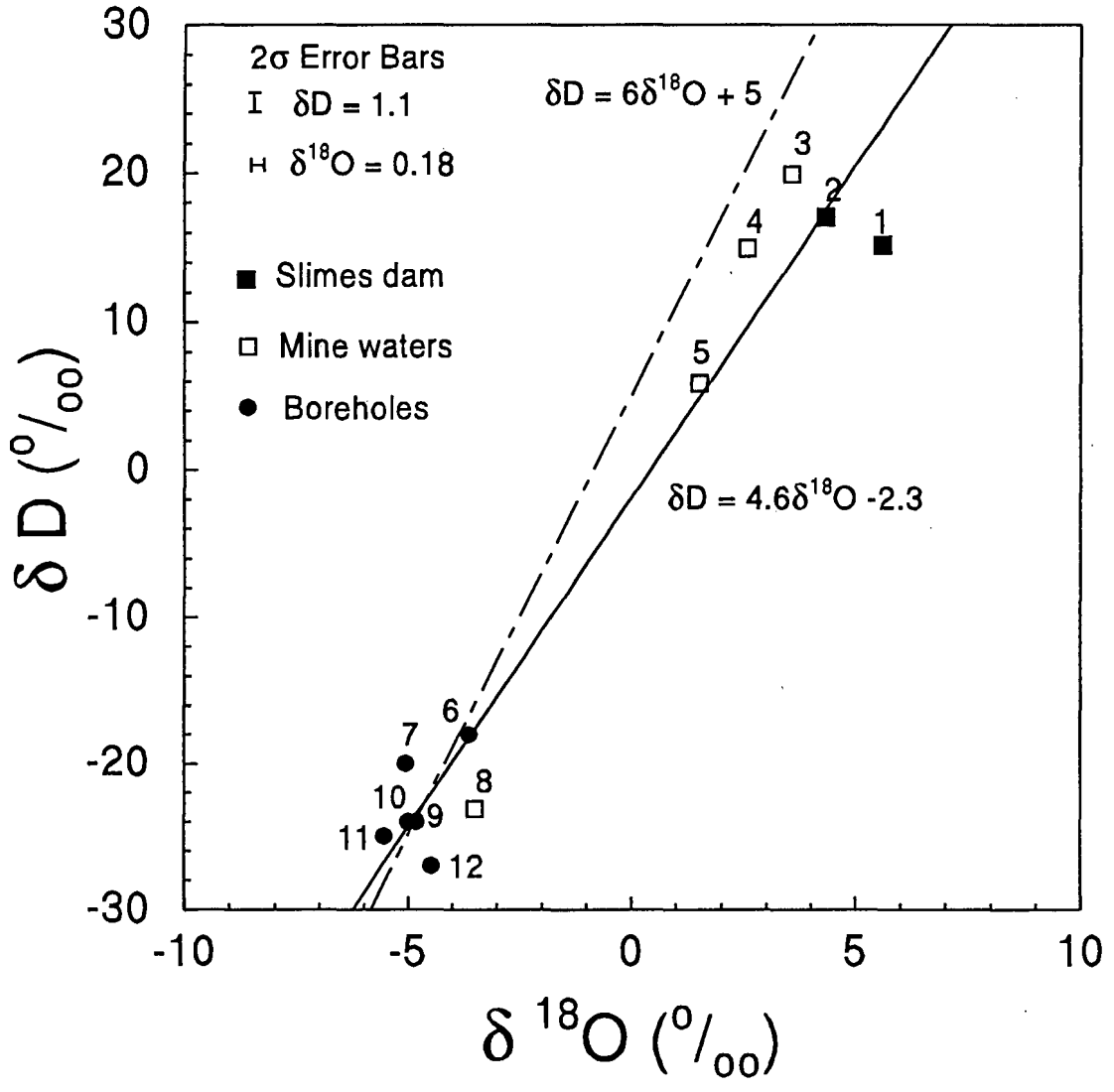

Figure 4.2. Plot of $\delta^{18}O$ vs δD for waters from the Steenkampskraal area. Error bars were determined from multiple analyses of water samples during the same time period as the analysis of the Steenkampskraal samples.

From the results in Table 4.1 and Figure 4.2, it can be seen that all boreholes at Steenkampskraal as well as the water in the inclined shaft fall into a single group. These waters are believed to have stable isotopic signatures similar to the surrounding ground water.

The water moving through the inclined shaft is believed to be in contact with the ground water (Jarvis et al., 1996). This was confirmed by an extensive dewatering test conducted on the inclined shaft in 1991, where water was pumped uninterruptedly for a month (24 h / 24 h) at a rate of 15 m^3/h. The water level in the mine dropped by 2 m on the first day of pumping, and then remained constant for the rest of the month. At the end of the experiment the water level rose by 1.5 m and now sits at a constant height of 328 m.a.m.s.l, (Jarvis et al., 1996; Louw. pers.comm., 1996).

The source of the water sampled in BH 6 was of interest due to the high concentration of actinides and lanthanides found in the waters on a previous study by Jarvis et al. (1996) at Steenkampskraal. Because of its unusual chemistry numerous theories for the origin of this water have been proposed. It has been suggested that the origin of the water is either an unconnected, free flowing aquifer, or that it represents the result of infiltration into the borehole of nearby slimes dam water. The latter was considered possible due to the ponds filled with green Cu-sulphate rich water close to the collar of BH 6 (Figures 4.1 and 4.3) (Jarvis et al., 1996). A third suggestion was that the water represented downward vertical infiltration into the borehole from surface of unevaporated rainwater.

Figure 4.3. Photograph of copper sulphate rich slimes dam.

The isotopic signature of BH 6 was found to be consistent with that of the general ground water and, therefore, could not be from the infiltration of the highly evaporated slimes dam water (SD 1 and SD 2). Its unusual chemistry - high F^-, U and LREE as well as neutral pH and very high alkalinity (expressed as HCO_3^-) (Table 4.9) - indicate that the water is likely to have been in contact with the tailings material, with infiltration occurring before significant evaporation had occurred, followed by neutralization as the water moved through a carbonate-rich host. The suggestion that the water belongs to an unconnected, free flowing aquifer in contact with the ore body can be disputed as water was only found to be present in the borehole after rain. This indicates that the water in BH 6 is moving rapidly, not in contact with any aquifer. There has, however, been no evidence for the presence of carbonate rocks in the near vicinity of BH 6. It has been suggested that although the dorbank (common feature of soil in semi-arid climates, consisting of a hard subsurface horizon cemented by silica, calcium carbonate and iron oxides) in the area tends to be siliceous, patches of carbonate may occur.

Although no rain water was sampled at Steenkampskraal, Diamond and Harris (1996) found that the isotopic signature of Citrusdal rain water during August in 1995 had a $\delta^{18}O$ value of -5.4 and a δD value of -19. The isotopic signature of Steenkampskraal would be expected to be similar to Citrusdal due to the close proximity and similar altitudes of the two locations. The unevaporated ground waters in the Steenkampskraal area are all similar to the Citrusdal rainwater for August.

In an attempt to purge the water in BH 4 it was found that there was approximately 0.4 m of water in the hole, with no refill after it had been removed. It is likely that the water present in BH 4 is ground water and not rain water sitting at the bottom of the hole due to the characteristic high EC of the water. It is presumed that ground water refill in BH 4 is very slow.

The waters in the main shaft (Reference numbers 3 and 4, Table 4.1) as well as in the sump on level 3 (Reference number 5, Table 4.1) are believed to be stagnant (Louw, R. pers.comm., 1996). The isotope signature of the sump on level 3 has possibly resulted from a lower degree of evaporation than the main shaft water, rather than from the mixing of evaporated mine water with unevaporated groundwater. This is possibly due to the presence of the ventilation fans near the main shaft which would cause evaporation.

4.3. Surface water

Table 4.2. Analytical results for all surface water samples collected at Steenkampskraal.

Analyte	Samples			
	Slimes dam 1	Slimes dam 2	Road water	Stream water
pH	2.60	2.86	2.77	5.52
EC: mS/cm	18.60	13.78	14.99	1.03
Acidity: mol/dm^3	0.559	0.377	0.492	nd
Anions:*		mg/dm^3		
Cl^-	35	37	264	149
SO_4^{2-}	32600	18600	24400	272
PO_4^{3-}	4291	2897	1233	3.4
F^-	137	86	65	0.46
HCO_{3-}	nd	nd	nd	3.8
NO_3^-	bdl	bdl	bdl	4.0
Cations:*		mg/dm^3		
Ca^{2+}	442	286	298	52
Mg^{2+}	235	188	186	29
Na^+	146	130	162	101
K^+	73	52	4.1	11
NH_4^+	8.6	8.0	bdl	bdl
Trace metals:$		mg/dm^3		
Fe	66	56	392	0.85
Al	1420	917	965	0.70
Cu	12500	8480	9980	37
Cr	4.8	3.6	5.6	<0.1
Mn	30	21	19	3.1
Ni	226	147	132	1.9
Si	11	6.5	5.2	3.6
Co	23	17	15	0.98
Pb	25	19	21	<1.0
Zn	120	79	91	0.57
As	2.8	1.7	1.8	<0.5
Cd	1.6	1.2	0.42	<0.06

bdl - below detection limits / nd - not determined / * HPIC / $ ICP-AES

Table 4.2 (cont.). Analytical results of ICP-MS data for U, Th and REE, for all surface water sample. All values in mg/dm^3.

Trace metal	Slimes dam 1	Slimes dam 2	Road water	Stream water
U	323	212	6.7	0.02
Th	22	12	1.1	0.01
Ce	98	65	3.9	0.07
Pr	18	11	4.6	0.01
Nd	89	56	27	0.06
Sm	22	14	20	0.01
Eu	<0.005	0.56	1.1	<0.005
Gd	26	17	4.5	0.02
Tb	5	3.1	0.69	0.005
Dy	27	18	3.2	0.03
Ho	4	2.8	0.27	0.005
Er	9	6	1.5	0.009
Tm	<0.005	0.57	0.22	<0.005
Yb	4	2.7	1.6	<0.005
Lu	<0.005	0.29	0.72	<0.005

4.3.1. Slimes dam and road water

Both slimes dam water samples and the road sample are very acidic with extremely low pH values. These three water samples have extremely high concentrations of SO_4^{2-} (Wetzel, 1996), PO_4^{3-} (Hounsome, 1994), F^- (McCaffrey, pers comm. 1996), Cu (Johnson and Thornton, 1986), U, Th (Chapman, 1992; Hardy and Duerden, 1989) and REE (Smedley, 1991). The concentrations of all the other ions and elements can be regarded as high.

Acidification through mine drainage is a major water pollution problem in most regions with a history of mining for sulphide-bearing ore deposits (Bigham et al., 1992). The acidic nature of the surface and ground waters associated with the Steenkampskraal mine is due the exposure and oxidation of sulphide minerals in the tailings, storage ore dump and ore body, as well as the input of large concentrations of acidic metals such as Fe, Al and Cu (McBride, 1994).

The oxidation of sulphide minerals exposed in mines and tailings material is clearly a complex geochemical process (Nordstrom, 1992). The general stoichiometry is, however, commonly represented by a single incongruent reaction:

$$FeS_2 + 3.75O_2 + 3.5H_2O \rightarrow Fe(OH)_3(s) + 2H_2SO_4$$

in which Fe sulphide (including pyrite, chalcopyrite and other mixed-metal sulphides) decomposes in the presence of water and oxygen to yield sulphuric acid and an insoluble hydrolysis product of ferric iron (Bigham et al., 1992).

The PO_4^{3-} concentrations in the waters are high according to Hounsome (1994). The PO_4 would be present due to the weathering of monazite and apatite in both the tailings and the ore pile. As explained below, PO_4^{3-} is strongly adsorbed by Fe between pH 3 and 6. The concentration of Fe in the slimes dam is low relative to the concentration of PO_4^{3-}, thus resulting in the unusually high dissolved PO_4^{3-} concentration. Fluoride is present in extremely high concentrations (McCaffrey, pers. comm. 1996), and is probably present due to the large concentration of fluoride- bearing minerals (fluorite and fluorapatite) associated with the ore body and surrounding country rocks and later exposed on the rock pile and tailings.

The high concentration of chalcophile elements (Cu, Fe, Co, Ni, Pb, Zn, As and Cd) would have been derived from the weathering of the sulphide minerals (pyrite, chalcopyrite and galena) as well as from the weathering of the oxide minerals (magnetite, ilmenite and Zn-bearing hercynite). The dominant cation in all three water samples is Cu [giving rise to the deep blue colour (Figure 4.3)]. Copper is present in the unweathered ore body in concentrations of approximately 1.1% (Pike, 1959).

The remaining metals (Al, Cr, Mn and Si) would be present in many of the minerals associated with the ore body and surrounding country rocks. The very high Al concentrations have resulted due to the high concentration of Al in the ore body and very low pH resulting in increased dissolution, solubility and mobility.

The concentrations of REE, U and Th in both slimes dam samples are extremely high (Chapman, 1992; Hardy and Duerden, 1989), due to the high concentration of these elements in monazite. The concentration of these elements in solution is not only dependent upon the absolute concentration in the system, but also on the pH at which they become mobile. The acidic nature of these solutions, originally derived from the oxidation of the sulphide minerals, would result in an increase in the solubility of certain metals and thus increase the concentration of these metals in solution. The increase in the solubility of hydrolysable metals such as Fe, Al and Cu further increases the acidity.

The higher Al:Fe ratio in the slimes dam samples may not be due solely to the fact the Al is more abundant in the system, although it often is, but could be due to the higher pH in which Al becomes soluble compared to the lower pH at which Fe becomes soluble.

Both slimes dam samples display the same chondrite-normalized REE pattern (Figure 4.4). Rare earth elements were normalized to chondrite values to remain consistent with the monazite normalization. Average concentrations of REE in chondrites were taken from Sun and McDonough (1989). As expected, the actual concentrations of REE, Th and U are higher in SD 1, due to the dilution with rain water in slimes dam 2. The chondrite-normalized REE pattern is similar to that displayed by monazite (Taylor and McLennan, 1985) (Figure 2.1), with a distinctive Eu depletion and an obvious enrichment in LREE with respect to HREE. It is expected that ground waters circulating through fractured bedrock, and in this case the samples from the slimes dam, would inherit the REE characteristics of their hosts provided no major fractionation occurred either during or after the dissolution of REE-bearing mineral phases (Smedley, 1991). Because monazite is present in the associated country rock; and the REE pattern of monazite can effectively contol the REE pattern of the host rock; the average REE pattern of the surrounding country rock would be similar to that of monazite (Figure 2.1).

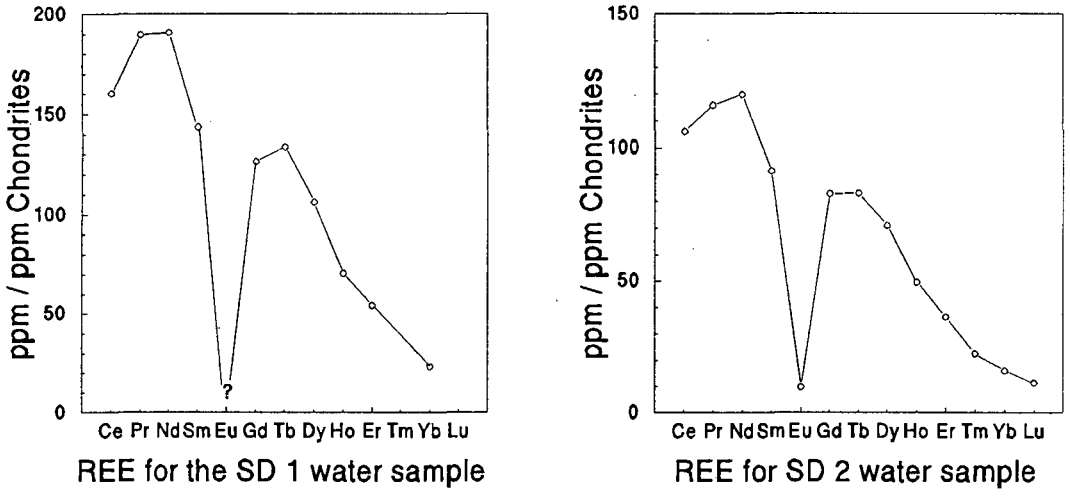

Figure 4.4. Chondrite-normalized REE data for both slimes dam (SD 1 and 2) water samples.

Lanthanum was not determined in the water samples. Tetravalent Ce is highly insoluble, and hence under oxidising conditions at neutral to high pH dissolved Ce concentrations should be low (Figure 2.2), with open ocean waters having a well developed Ce depletion as a response to oxidative removal of Ce in its tetravalent state (Smedley, 1991).

Both plots in Figure 4.4 show that the chondrite-normalized Ce concentrations are lower than those of the other LREE (Pr and Nd). This could indicate that a small proportion of the Ce, derived from the monazite as Ce^{3+}, has oxidized to Ce^{4+} and has precipitated out of solution as cerianite (CeO_2). However, from Figure 2.2, it can be seen that Ce^{4+} is unlikely to exist below pH 4, with Ce^{3+} being the dominant form. The very low pH of the solutions in the slimes dam would have limited the oxidation of Ce^{3+} to Ce^{4+} even though the redox conditions of the slimes dam are expected to be of an oxic nature. A Ce depletion would best be determined in the presence of La data. Because the ratio of Ce^{3+}/ Ce^{4+} is not known, only thermodynamic data for Ce^{3+} was used in an attempt to carry out speciation modelling (Table 4.16).

4.3.2. Stream water

The stream water sample taken along soil transect 1 has much lower concentrations of dissolved metals than the other three samples (Table 4.2). This is due to the fact that the water was sampled further away from the tailings, shortly after rain. The pH of the water is, however, low considering the expected pH range for natural waters in South Africa is between 6 and 5 (Dallas and Day, 1993). Although the concentrations of Cu are much lower than the other three surface water samples, the concentration of Cu is still orders of magnitude higher than the recommended concentration ranges for livestock (Table 4.3) (DWAF, volume 5, 1996).

It is presumed that during the rainy season, ponds that form in the stream would act as potential sources of livestock drinking water. The high concentrations of Cu would be due to the movement of tailings water and material downstream during the rainy season and subsequent evaporation. Contamination of the stream water by Cu, Ni and possibly Pb (detection limits of Pb were 1 mg/dm^3) could be a serious threat to livestock in the area and steps should be taken to prevent such contamination (DWAF, volume 5, 1996).

Table 4.3. Recommended levels of dissolved metals in livestock (sheep) and human drinking water (Department of Water Affairs and Forestry, volumes 1 and 5, 1996).

	Stream water	Livestock consumption	Human consumption
Anion	mg/dm^3		
Cl^-	149	<3000	<100
SO_4^{2-}	272	<1000	<200
F^-	0.5	<2	<1
NO_3^-	4.0	<100	<6
Trace metals	mg/dm^3		
Ca	52	<1000	<32
Mg	29	<500	<100
Na	101	<2000	<600
K	11	-----	<100
Fe	0.85	<10	<10
Al	0.70	<5	<0.15
Cu	37	<0.5	<30
Cr	<0.2	<1	<0.05
Mn	3.1	<10	<14
Ni	1.9	<1	------
Co	0.98	<1	------
Pb	<1.0	<0.1	<0.01
Zn	0.57	<20	<10
As	<0.5	<1	<0.001
Cd	<0.06	<0.01	<0.005

4.4. Underground water

The four water samples collected underground (Table 4.4) display 3 different types of chemistry. The two samples from the main shaft and main shaft extension show very similar concentrations of cations, anions and trace metals. The chemistry of these waters are different from the chemistry of the sump on level 3 and in turn different from the chemistry of the water from the inclined shaft.

Table 4.4. Analytical results for all water samples collected from the underground mine shafts at Steenkampskraal.

Analyte	Sample			
	Main Shaft	Main Shaft extension	Sump on level 3	Inclined Shaft
pH	3.47	3.88	3.58	7.15
EC: mS/cm	10.93	11.07	11.25	6.15
Acidity: mol/dm^3	0.012	0.012	0.007	----
Anion:*			mg/dm^3	
Cl^-	2714	2241	1850	1814
SO_4^{2-}	3179	2955	9664	486
F^-	6.2	4.6	137	2.1
NO_3^-	bdl	bdl	91	bdl
PO_4^{3-}	1.7	2.0	2.7	24
HCO_3^-	nd	nd	nd	84
Cation:*		mg/dm^3		
Ca^{2+}	634	550	595	147
Mg^{2+}	311	293	470	154
Na^+	1730	1569	959	1130
K^+	107	104	67	47
NH_4^+	54	48	43	bdl
Trace metals:$		mg/dm^3		
Fe	241	234	20	0.66
Al	13	9.8	389	0.30
Cu	6.8	4.4	2020	0.62
Cr	0.26	0.59	0.31	<0.1
Mn	47	49	87	0.32
Ni	6.2	4.5	114	0.33
Si	18	19	49	1.4
Co	2.4	2.5	14	<0.1
Pb	1.7	3.1	8.2	<1.0
Zn	7.9	7.2	65	<0.1
As	<0.5	<0.5	nd	<0.5
Cd	0.2	0.35	1.0	<0.06

bdl - below detection limits / nd - not determined / * HPIC / $ ICP-AES

Table 4.4 (cont.). Analytical results of ICP-MS data for U, Th and REE for water samples collected from the underground within the mine. All values in mg/dm^3.

	Main shaft	Main shaft extension	Sump on level 3	Inclined shaft
U	0.32	0.36	<0.005	0.31
Th	0.31	0.11	<0.005	0.32
Ce	3.7	3.8	<0.005	0.17
Pr	0.51	0.51	<0.005	0.18
Nd	2.1	2	<0.005	0.89
Sm	0.46	0.43	<0.005	0.85
Eu	0.02	0.02	<0.005	0.48
Gd	0.72	0.66	<0.005	0.9
Tb	0.12	0.12	<0.005	0.17
Dy	0.72	0.66	<0.005	0.53
Ho	0.11	0.1	<0.005	0.27
Er	0.23	0.21	<0.005	0.52
Tm	0.02	0.02	<0.005	0.16
Yb	0.07	0.06	<0.005	0.36
Lu	<0.005	<0.005	<0.005	0.12

4.4.1. Main shaft and main shaft extension

The main shaft and main shaft extension show very similar concentrations of cations, anions and elements. Both samples display almost exactly the same chondrite-normalized REE pattern (Figure 4.5). The REE normalized plots for the main shaft and main shaft extension do not have Ce normalized concentrations lower than those of the other LREE (Pr and Nd), in contrast to the slimes dam samples (Figure 4.4). This could be due to the fact that both waters have a pH below 4, thus preventing the oxidation of Ce^{3+} to Ce^{4+}, with redox conditions less oxic than the slimes dam water samples. This again can explain the presence of the high concentrations of Ce in these waters.

The concentrations of Th are, however, different with main shaft being considerably higher than the main shaft extension. The reason for the differences Th concentrations between the two samples is not known and could be due to analytical error. The similar chemistry between the two samples is expected as both locations are part of an interconnected water body. The chemistry of the two water samples is very acidic, again with high concentrations of dissolved metals (Johnson and Thornton, 1986). The concentrations of the metals are not as high as the slimes dam and road water samples due to the lower surface area, compared to the ore/tailings dumps, in which mineral dissolution can occur, as well as a lower degree of oxidation, resulting in a slightly higher pH.

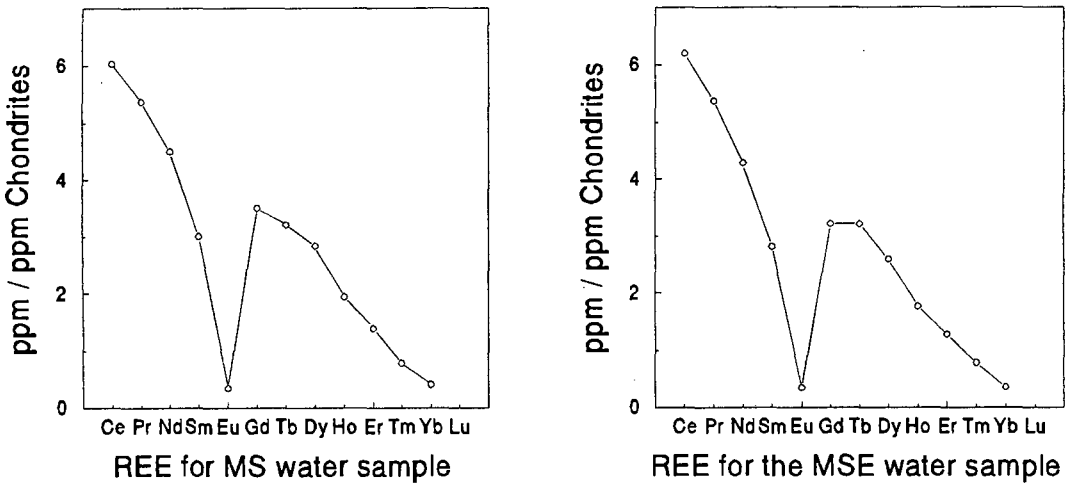

Figure 4.5. Chondrite-normalized REE data for the main shaft (MS) and main shaft extension (MSE) water samples.

In order to predict the fate of SO_4^{2-} and associated pollutants, (eg in acid mine waters and in soils), a knowledge of the chemical speciation in solution and the processes occurring at the mineral-water interface is required (Rauret et al., 1987). It is important to establish whether a particular anion adsorbs in an inner- or outer- sphere mode. This is important because where the anions reside will determine much of their chemical behaviour at the interface (Persson and Lövgren, 1996). An inner-sphere surface complex is formed when there is a direct chemical bond between the adsorbing anion and the metal ion at the surface. In outer-sphere complexes hydroxyl groups or water molecules separate the adsorbing anion and the surface metal ion centres (Kooner et al., 1995).

Sulphate adsorption was likely to occur in these waters, as numerous iron sulphate minerals had precipitated in the main shaft. A sample of precipitate (Table 4.5) contained approximately 13% SO_3. The extremely high concentrations of SO_4^{2-} in these waters are not likely to be affected significantly by the formation of Fe sulphate precipitates due to the relatively small volumes of precipitate.

The concentrations of PO_4^{3-} in the main shaft and main shaft extension are relatively low compared with the slimes dam and road water samples, considering the relatively high concentrations of REE, U and Th and the probable dissolution of monazite and apatite. It has been found that the presence of Fe, and to some degree Al, in a system is possibly the most important influence on PO_4^{3-} availability (Borggaard et al., 1990). Phosphate can become extremely strongly adsorbed onto iron hydroxide particles.

Table 4.5. XRF major element analysis of the main shaft precipitate. Units in percentages.

Oxide/Element	Main shaft precipitate
Fe_2O_3	66
TiO_2	0.052
BaO	0.009
CaO	4.1
K_2O	0.63
Cl	2.6
SO_3	13
P_2O_5	0.35
SiO_2	4.8
Al_2O_3	1.4
MgO	0.94
Na_2O	2.2
Y_2O_3	0.032
ThO_2	0.21
Ce_2O_3	0.22
Nd_2O_3	0.074
La_2O_3	0.10
Total	97 %

Sposito (1989) describes the reaction as taking place when a hydroxyl group in the mineral goethite is protonated to form a Lewis acid site. It can then be exchanged to allow the formation of an inner-sphere complex with the ligand HPO_4^{2-}. The surface complex is detailed in the reaction:

$$Fe\text{-}OH_2 + HPO_4^{2-} \Rightarrow FeOPO_2OH + H_2O \quad \text{(from Mott, 1989)}$$

Phosphate is bound through its oxygen pairs to a pair of adjacent Fe^{3+} cations forming a binuclear complex (Sposito, 1989). Phosphorous sorption onto Fe and Al hydroxide surfaces will predominate under acidic pH conditions, and the stability of the complexes decreases as pH increases to a point where Ca-phosphate minerals are more stable (Tisdale et al., 1985). The low concentration of PO_4^{3-} in the main shaft and main shaft extension is probably a result of PO_4^{3-} removal from solution by the iron phosphate precipitation. The XRF analysis of the main shaft precipitate (Table 4.5) indicates the presence of 0.35% P_2O_5.

Compared with the slimes dam water samples, the Al concentrations are also relatively low. Although aluminium phosphate minerals were not identified in the main shaft precipitate, it is possible that they are present. The low Al concentrations may however also be due to the lack of Al-bearing minerals in the ore body, but this is unlikely due to the high concentration of Al in the sample from the sump on level 3.

The pH of the solution is another factor controlling the sorption of PO_4^{3-} out of solution (Mott, 1989). Wild (1988) notes that PO_4^{3-} sorption is greatest at pH 3-5, consistent with the pH's of the main shaft and main shaft precipitate. As pH is increased, the valence of the phosphate state, through speciation, becomes increasingly negative and adsorption declines steeply (Mott, 1989). The comparison of the calculated MINTEQA2 phosphate speciation for the main shaft and the inclined shaft, where in the main shaft phosphate is bound predominantly as $FeH_2PO_4^{2+}$ (88%) with the remainder (12%) bound as $H_2PO_4^-$. In the inclined shaft, only 21.7% is bound as $H_2PO_4^-$ and the remainder as single or unprotonated Ca and Mg phosphates. The relatively high PO_4^{3-} concentration in the water from the inclined shaft is, therefore, likely to be due to the higher pH and lower concentration of Fe in the system even if the total PO_4^{3-} concentration in the system is lower.

The main shaft precipitate was intensively studied in order to obtain a better understanding of the processes controlling the concentrations of certain elements, with respect to removal from solution via precipitation or adsorption.

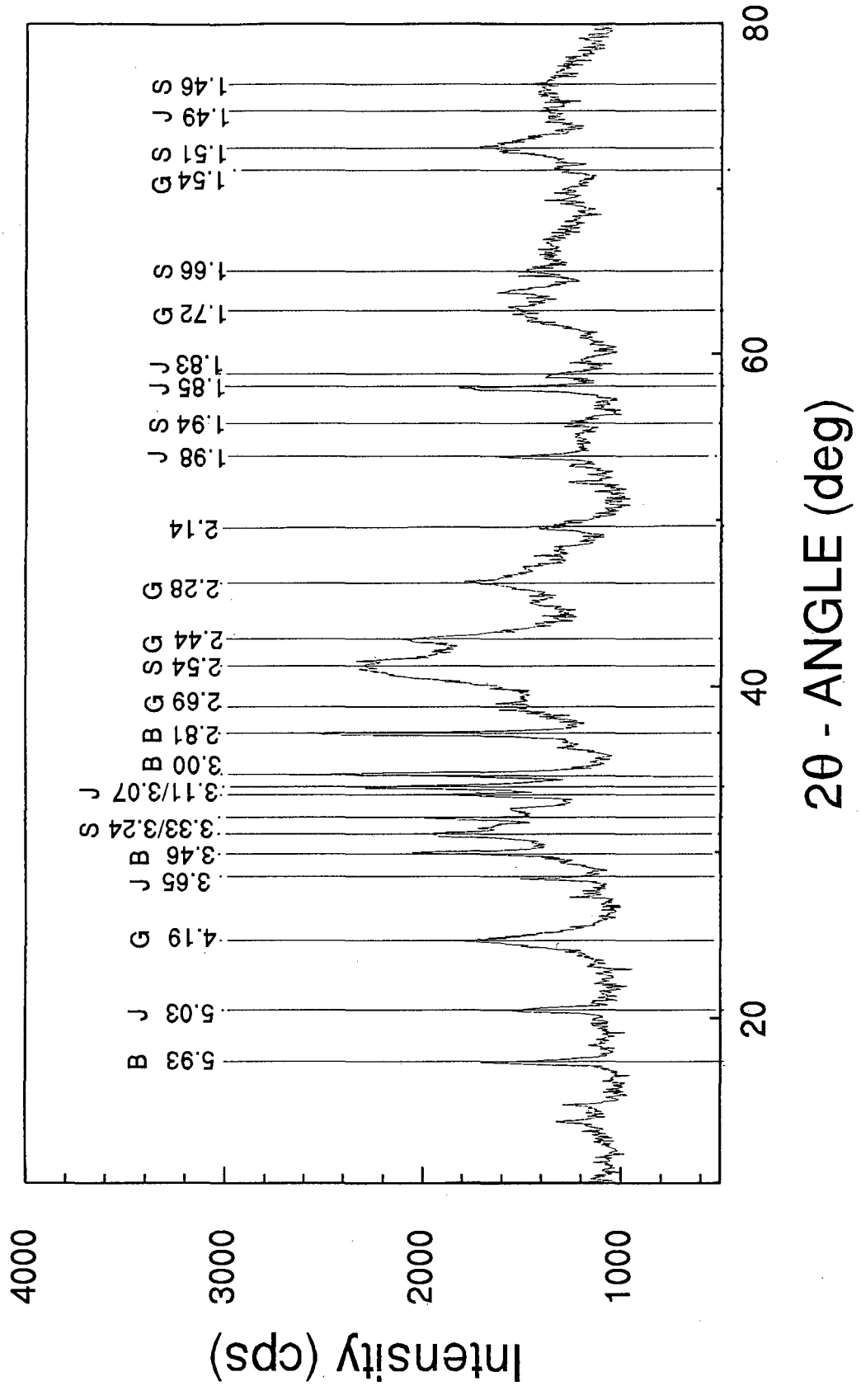

Figure 4.6. X-ray diffraction scan of the iron precipitate found in the main shaft. Lines define mineral peaks, with the corresponding d-spacings and mineral abbreviations above. Peaks associated with specific minerals are listed in Table 4.6.

Table 4.6. List of minerals identified in the main shaft precipitate, with their corresponding d- spacings. d-spacings obtained from JCPDS (1980).

Mineral	Mineral formula	d-spacing (Å)
Jarosite	$(K, Na, H_3O)Fe_3OH_6(SO_4)_2$	5.03 / 3.65 / 3.11 / 3.07 / 2.28 / 1.98 / 1.85 / 1.83 / 1.49
Goethite	α-FeOOH	4.19 / 2.69 / 2.44 / 2.28 / 1.72 / 1.54
Schwertmannite	$Fe_8O_8OH_6SO_4 \leftrightarrow Fe_8O_8OH_{4.8}(SO_4)_{1.6}$	3.33 / 3.24 / 2.54 / 1.51 / 1.46
Bassanite	$CaSO_4.1/2H_2O$	5.93 / 3.46 / 3.00 / 2.81

The d-spacing of 2.14 is unidentified.

Because schwertmannite is a relatively recently described mineral, further confirmation was necessary. Schwertmannite is known to dissolve with treatment by acid ammonium oxalate. The main shaft precipitate was treated with acid ammonium oxalate in the dark (Jackson et al., 1986), and reanalysed by XRD (Figure 4.7). The dominant schwertmannite peak at 2.54 decreased in size relative to the goethite peak at 2.25. Goethite has a higher degree of crystal structure than schwertmannite and is, therefore, not affected by the treatment with acid ammonium oxalate. The increase in the intensity of the goethite peak at 2.45 from about 2000 cps in the untreated sample to about 2800 cps in the treated sample is due to the enrichment of goethite in the treated sample,as a result of the removal of bassanite and schwertmannite. Bassanite was also removed in the treatment, where the peaks at 3.00 and 2.81 were completely removed. The Ca oxalate mineral, whewellite, formed during the treatment of the precipitate with acid ammonium oxalate.

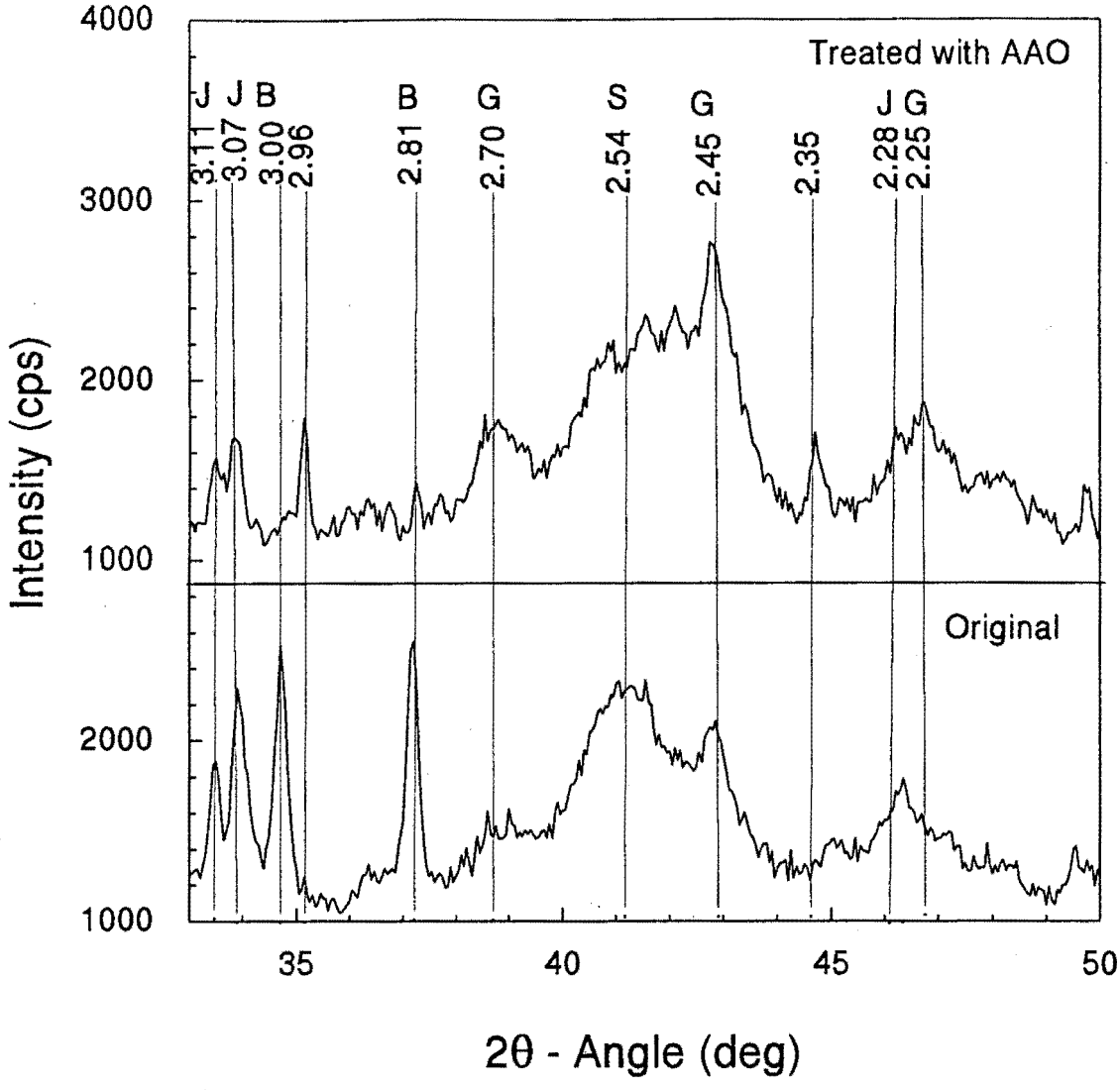

Figure 4.7. X-ray diffraction scan of the untreated original iron sample (below), with the diffraction scan after treatment with acid ammonium oxalate (AAO) (above) over a 2Θ range of 33 -50°. Lines define mineral peaks, with the corresponding d-spacings and mineral abbreviations above. Peaks associated with specific minerals are listed in Table 4.7.

Table 4.7. List of minerals identified in the main shaft precipitate, with their corresponding d- spacings. d-spacings obtained from JCPDS (1980).

Mineral	d-spacing (Å)
Jarosite	3.11 / 3.07 / 2.28
Goethite	2.70 / 2.45 / 2.25
Schwertmannite	2.54
Bassanite	3.00 / 2.81
Whewellite (Ca oxalate)	2.96

The d-spacing of 2.35 in the treated diffractogram is from the aluminium holder.

Ochreous precipitates often form voluminous blankets (Bigham et al., 1992), as in the case of the precipitate found on the surface of the main shaft water (Figures 4.8 and 4.9).

Figure 4.8. Photograph of main shaft water, with precipitate covering the surface.

Figure 4.9. Photograph of main shaft precipitate.

The presence of sulphate as the dominant anion has been found to be important in the formation of ochreous precipitates in at least two respects. It has been reported that SO_4 is required in a metabolic sense for the oxidation of Fe^{2+} by acidophilic chemolithotrophic bacteria such as *Thiobacillus ferrooxidans* (Lazaroff, 1963). Chemolithotrophic bacteria use a chemical energy source and CO_2 as the principal carbon source. Energy is obtained from the oxidation of reduced inorganic elements such as sulphur or iron. These organisms can grow in strictly mineral media in the absence of light (Stanier et al., 1986). Sulphate also appears to exert a major influence on the thermodynamics and kinetics of the mineral formation (Bigham et al., 1992). In a study of ochreous precipitates from sulphitic mine drainage, Bigham et al. (1992) classified the mineralogy present in the precipitate according to effluent pH (Figure 4.10).

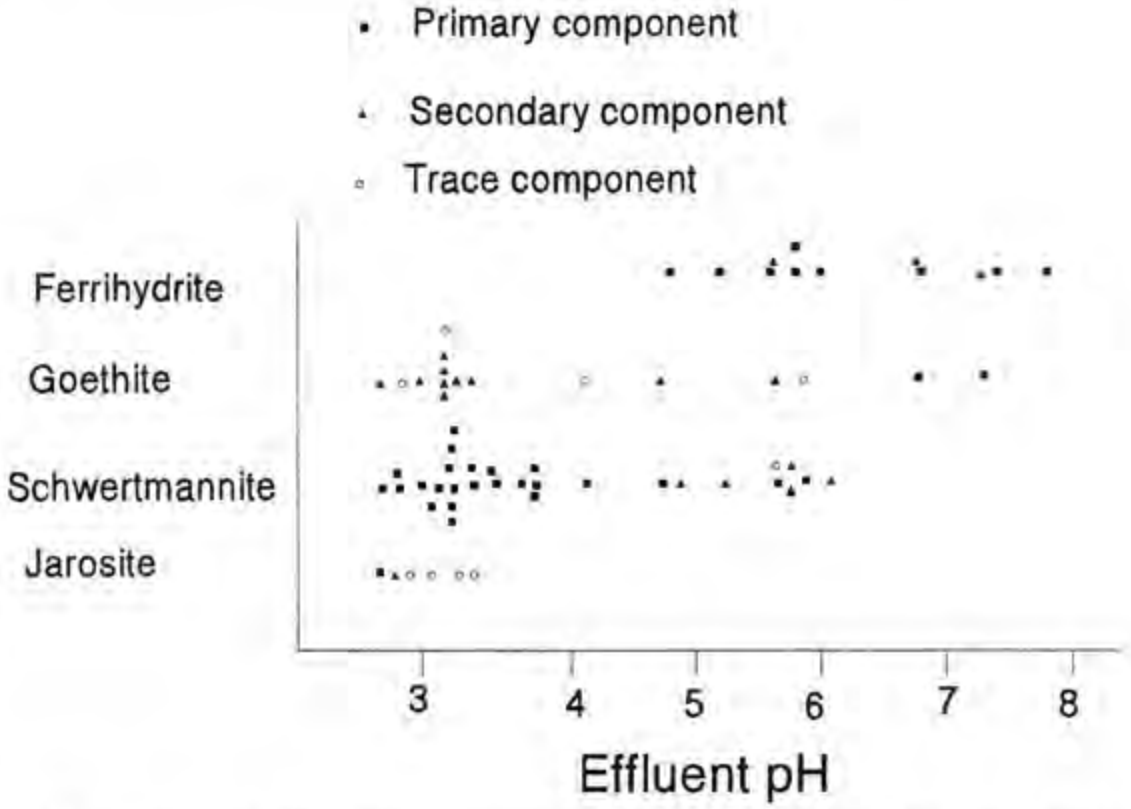

Figure 4.10. Occurrence of mine drainage minerals as a function of solution pH (After Bigham et al., 1992).

The precipitate sampled on the surface of the water at the base of the main shaft was analyzed using XRF, XRD and SEM. The minerals identified using XRD and SEM include goethite, jarosite, bassanite and schwertmannite. This is similar to the results of the studies by Bigham et al. (1992) (Figure 4.10) and Bigham et al. (1996), where it was found that above pH 6.5, precipitates were composed of a mixture of ferrihydrite and goethite, whereas those precipitates from waters with a pH between 2.8 and 4.5 were dominated by schwertmannite with minor amounts of goethite.

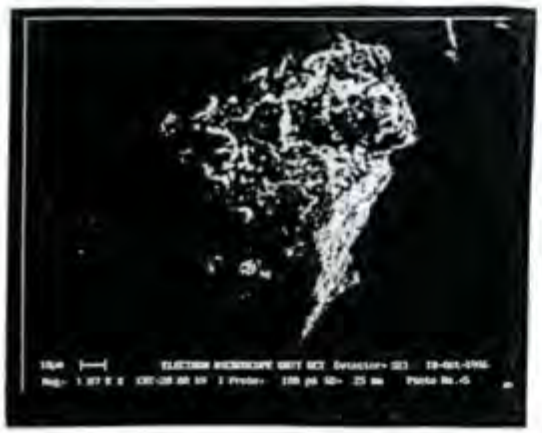

A. Botryoidal Jarosite

B. Goethite

C. Schwertmannite

D. Bassanite

E. Bassanite

Figure 4.11. Scanning electron micrograph images of various minerals within the main shaft precipitate.

Goethite (α-FeOOH) is a stable mineral commonly observed in mine drainage precipitates. Goethite has a typical yellow brown colour. Brady et al. (1986) found that although well crystallized goethite commonly displays fibrous or lath-like morphologies, those occurring in mine drainage precipitates usually form short rod-like particles. From Figure 4.11, this is consistent with the goethite present in the main shaft precipitate. Goethite appeared to represent the dominant mineral phase present in the precipitate. MINTEQA2 calculated that the water in the main shaft was supersaturated with respect to goethite (Table 4.8), with goethite having a saturation index of 5.1.

Table 4.8. Calculated saturation indices for selected minerals in the main shaft water sample.

	Main shaft
Anhydrite ($CaSO_4$)	-0.02
Gypsum ($CaSO_4.H_2O$)	0.19
$Fe(OH)_{2.7}Cl_{0.3}$	7.22
Ferrihydrite ($Fe_5(O_4H_3)_3$)	0.7
Goethite (α - FeO.OH)	5.09
Hematite (α - Fe_2O_3)	15.20
Jarosite H ($HFe_3(OH)_6(SO_4)_2$)	10.61
Lepidocrocite (γ - FeO.OH)	4.22
Maghemite (γ - Fe_2O_3)	4.80
Quartz (SiO_2)	0.30
Strengite ($Fe(PO_4).2H_2O$)	3.04

Jarosite [$(H_3O,K,Na)Fe_3OH_6(SO_4)_2$] is a common mineral in acid, high sulphate environments. Pseudocubic, tabular (Doner and Lynn, 1989) and botryoidal (Lazaroff et al., 1985) crystals have been found under the electron microscope. Jarosite was easily identified from its characteristic XRD pattern (Figure 4.6), but K-bearing jarosite was found to be rare under the SEM. The K- bearing jarosite crystal photographed under the SEM was botryoidal in shape (Figure 4.11). It is probable that the jarosite present in the precipitate is in the form of hydronium jarosite [$(H_3O)Fe_3OH_6(SO_4)_2$], a common form of jarosite in sulphide-rich mine tailings (Jambor, 1994). The saturation index of hydronium jarosite was calculated by MINTEQA2 to be 10.1.

Schwertmannite was originally described by Bigham et al. (1990), where it was referred to as MDM (mine drainage mineral). Schwertmannite seems to be a common mineral associated with precipitates from acid sulphate waters, but it appears that it has not previously been described in South Africa. Schwertmannite was identified both by its XRD pattern (Figures 4.6 and 4.7) as well as its presence under the SEM (Figure 4.11).

Schwertmannite is a very poorly crystallized mineral with rapid solubility in acid ammonium oxalate in the dark. The precipitate was treated with an acid ammonium oxalate solution and the dominant schwertmannite peak (d-spacing = 2.54) was found to be reduced significantly (Figure 4.7). Natural specimens of schwertmannite contain 10 to 15 wt% SO_4, which translates to an Fe/S mole ratio ranging from 5 to 8 and a structural formula varying between $Fe_8O_8OH_6SO_4$ and $Fe_8O_8OH_{4.8}(SO_4)_{1.6}$ (Bigham, 1994). The spot analysis of both the goethite and schwertmannite under the SEM were found to have chloride present in the analysis. It is not known whether the chloride is present within the structure of these minerals, or if it is present as an adsorbed ion on the surface of these minerals.

Singer and Stumm (1970) observed that the direct oxidation of Fe sulphides by air was too slow to generate the amount of acidity in most mine drainage, and suggested that acidophilic bacteria must act as catalysts for the reaction by oxidising aqueous Fe^{2+} whenever the pH of the waters drop below 4.5. Otherwise the abiotic oxidation rate for Fe^{2+} would be negligible. The importance of a rapid conversion of Fe^{2+} to Fe^{3+} under strongly acidic conditions lies in the fact that the activity of Fe^{3+} in solution becomes significant at low pH and as a result Fe^{3+} replaces O_2 as the primary oxidant of pyrite. Any Fe^{2+} or (Fe^{3+}) that "escapes" the pyrite decomposition cycle is ultimately oxidised, hydrolysed and precipitated as an insoluble mineral phase (Bigham et al., 1992). Although bacteria actively participate in the oxidation of Fe^{2+} under acid conditions, it appears unlikely that the type of mineral produced is under any type of physiological control by the organism. The mineralization process is extracellular and geochemical parameters such as pH and SO_4 concentration determine the mineralogical fate of Fe once it has been oxidised (Bigham et al., 1992).

The final mineral identified in the main shaft precipitate was bassanite ($CaSO_4.1/2H_2O$) (Figures 4.6 and 4.11). Bassanite is an intermediate form between gypsum ($CaSO_4.2H_2O$) and anhydrite ($CaSO_4$). Bassanite has been found to be a common secondary mineral in sulphatic mine wastes, where it is found to form from the dehydration of gypsum (Jambor, 1994). MINTEQA2 did not predict that bassanite would be supersaturated in the main shaft solution. This is probably due to a lack of thermodynamic data in the database. The main shaft water was calculated by MINTEQA2 to be supersaturated with respect to gypsum and slightly undersaturated with respect to anhydrite (Table 4.8).

The presence of these sulphate mine waste precipitates has been found to be important in the colloidal transport of noxious chemical species through adsorption and coprecipitation reactions. This is particularly important in the Steenkampskraal mine as the ochreous precipitates are present underground, with definite evidence of ground water movement through the mine.

4.4.2. Sump on level 3

The water sample from the sump on level 3 (Table 4.4) has a chemical composition that is different from all the other water samples taken from Steenkampskraal. The water from the sump on level 3 has a very high concentration of Cu and Al compared with the water from the main shaft and main shaft extension. The concentration of PO_4^{3-} is, however, similar to that of the main shaft and main shaft extension. The concentrations of Th, U and all the REE are below detection limits unlike that of the main shaft and main shaft extension. The water is most likely not in contact with the monazite ore body. Although the water has a low concentration of Fe, the other chalcophile elements such as Cu, Ni, Co, Pb, Zn and Cd are present in very high concentrations compared with the water from the main shaft and main shaft extension. It is likely that the water in the sump on level 3 is in contact with a predominantly sulphide-rich part of the ore body. Phosphate entering the system could have also been removed by the precipitation of Fe and Al phosphates similar to the main shaft and main shaft extension. The water has the characteristic blue Cu colour of the surface samples. The water sample from the sump on level 3 was also found to have a relatively high concentration of NO_3^- and NH_4 (Wetzel, 1996), which has probably resulted from droppings from the large population of bats living above the water.

4.4.3. Inclined shaft

The final underground sample (Inclined shaft) has a neutral pH with relatively low concentrations of dissolved metals compared with the other mine waters. The water has been found to have a similar chemistry to the typical surrounding ground water (BH 2, BH 3 and BH 5) (Table 4.9), with a similar isotopic signature as the general ground water. The water from the inclined shaft has a much higher PO_4^{3-} concentration than the other waters in the mine, which, as explained above, is probably due to the low Fe concentration and neutral pH.

The concentrations of the U and Th and REE are very high for ground waters (Smedley, 1991 and Chapman et al., 1992). It is expected that the water in the inclined shaft is or has already been in contact with a monazite rich section of the ore body. The stable isotopic signature as well as the pumping experiments established the water in the inclined shaft as being normal ground water. This is important as it is not known how much, if any, of the other mine waters actually enter the local ground water. The fact that the water in the inclined shaft is rich in REE, U and Th and that the inclined shaft is part of the local ground water system indicates that movement of these elements away from the ore body is occurring. The chondrite-normalized REE pattern of the inclined shaft does not produce a normal pattern. It is believed that the REE analysis of the inclined shaft is incorrect due to the inconsistent pattern. Unfortunately this sample could not be reanalysed.

4.5. Borehole water

Differences between the purged and unpurged borehole waters were found. The most noticeable difference was the fact that the concentrations of REE, U and Th were much lower (usually below detection limits) in the unpurged samples. The analytical results of the unpurged borehole samples have been included in Appendix 4. The significantly lower concentrations of REE in the unpurged samples can not be easily explained. It is possible that the REE, U and Th are present in these waters attached to colloidal particles. The water taken from the unpurged boreholes would have been sampled from the top section of the water column, where little ground water movement would occur due to the potentiometric surface of the aquifer. Colloidal particles containing the REE, U and Th may, therefore, have not been present at the water surface and therefore not detected in the analysis. On purging, colloidal particles would have been sampled, with the release of these elements after acidification, prior to analysis.

Table 4.9. Analytical results of purged water samples from BH 1, 2, 3, 5 and 6 as well as the analytical results from BH 4.

Analyte	Samples					
	BH 1	BH 2	BH 3	BH 4	BH 5	BH 6
pH	4.67	7.11	7.28	7.66	7.15	7.68
EC: mS/cm	4.09	4.09	1.02	7.19	6.14	6.24
Acidity: mol/dm^3	0.0091	-----	-----	-----	-----	-----
Anions:*		mg/dm^3				
Cl^-	1456	1129	168	1095	1812	1371
SO_4^{2-}	76	151	309	302	253	509
PO_4^{3-}	1.6	98	27	3.7	33	12
HCO_3^-	nd	549	30	343	710	1256
F^-	0.70	1.8	0.36	0.10	1.7	3.7
NO_3^-	2.4	bdl	bdl	bdl	bdl	bdl
Cations:*		mg/dm^3				
Ca^{2+}	92	118	32	65	105	216
Mg^{2+}	76	151	53	61	158	49
Na^+	622	564	162	738	987	1170
K^+	21	28	15	24	54	50
NH_4^+	bdl	23	4.1	bdl	bdl	bdl
Trace metals:$		mg/dm^3				
Fe	206	5.7	3.7	0.56	0.70	0.80
Al	0.3	1.8	1.8	0.14	3.9	1.8
Cu	4.2	<0.2	<0.2	<0.2	<0.2	<0.2
Cr	0.11	<0.1	<0.1	<0.1	<0.1	<0.1
Mn	7.1	1.6	<0.04	<0.04	2.5	1.0
Ni	0.30	0.31	0.30	0.31	<0.2	0.34
Si	4.3	17	26	16	12	13
Co	0.63	0.65	0.63	0.64	<0.1	0.65
Pb	<1.0	<1.0	<1.0	<1.0	<1.0	<1.0
Zn	0.64	0.90	0.69	0.63	<0.1	1.3
Cd	<0.06	<0.06	<0.06	<0.06	<0.06	<0.06

bdl- below detection limits / nd- not determined / * HPIC / $ ICP-AES

Table 4.9 cont. Analytical results of ICP-MS data for U, Th and REE for the purged water samples from BH 1, 2, 3, 5 and 6. All values in mg/dm^3.

	BH 1	BH 2	BH 3	BH 5	BH 6
U	0.50	0.54	0.03	0.01	0.01
Th	0.12	0.29	0.02	0.01	0.11
Ce	0.25	0.13	0.02	0.04	0.02
Pr	0.04	0.02	<0.005	0.005	<0.005
Nd	0.17	0.09	0.01	0.02	0.007
Sm	0.04	0.02	<0.005	0.005	<0.005
Eu	<0.005	<0.005	<0.005	<0.005	<0.005
Gd	0.05	0.03	<0.005	0.006	<0.005
Tb	<0.005	0.005	<0.005	<0.005	<0.005
Dy	0.05	0.03	<0.005	0.005	<0.005
Ho	<0.005	0.005	<0.005	<0.005	<0.005
Er	0.01	0.009	<0.005	<0.005	<0.005
Tm	<0.005	<0.005	<0.005	<0.005	<0.005
Yb	<0.005	<0.005	<0.005	<0.005	<0.005
Lu	<0.005	<0.005	<0.005	<0.005	<0.005

4.5.1. Borehole 1

BH 1 is situated upstream of the mine along the general ground water flow path (Figure 4.1). The water chemistry of BH 1 is highly unusual, due to the lower pH and higher Fe, Cu, Mn, REE and Th concentrations than the other ground water samples. BH 1 has a low concentration of PO_4^{3-}, which is atypical of water that has come into contact with the monazite/ apatite ore body.

The chondrite-normalized REE pattern of the purged sample from BH 1 is similar to that of the other samples (Figure 4.12). The pattern shows the HREE are highly depleted with Tm, Yb and Lu, being below detection limits (0.005 mg/dm^3). Europium was also found to be below detection limits, thus producing a strong Eu depletion. Rare earth element concentrations have been normalized to a Steenkampskraal monazite (Andreoli et al., 1994) for BH 1 and BH 2 (Figure 4.12). The pattern obtained by normalizing REE concentrations to the general REE signature of the surrounding country rock has been found to indicate the mechanism of transport in the ground water (Read et al., 1987).

Normalizing REE concentrations to a Steenkampskraal monazite was originally investigated by Andersen et al. (1995), where, with similar results to this study, a marked fractionation between LREE and HREE was found, with the HREE strongly enriched in the aqueous phase. Read et al. (1987) found the HREE to show a greater tendency for complexation and a greater affinity for mineral surfaces. Although the presence of colloids in these 3 boreholes does not prove that they are a vehicle for transportof REE, U, and Th, it is possible that colloidal transport of these elements is the dominant mechanism of transport.

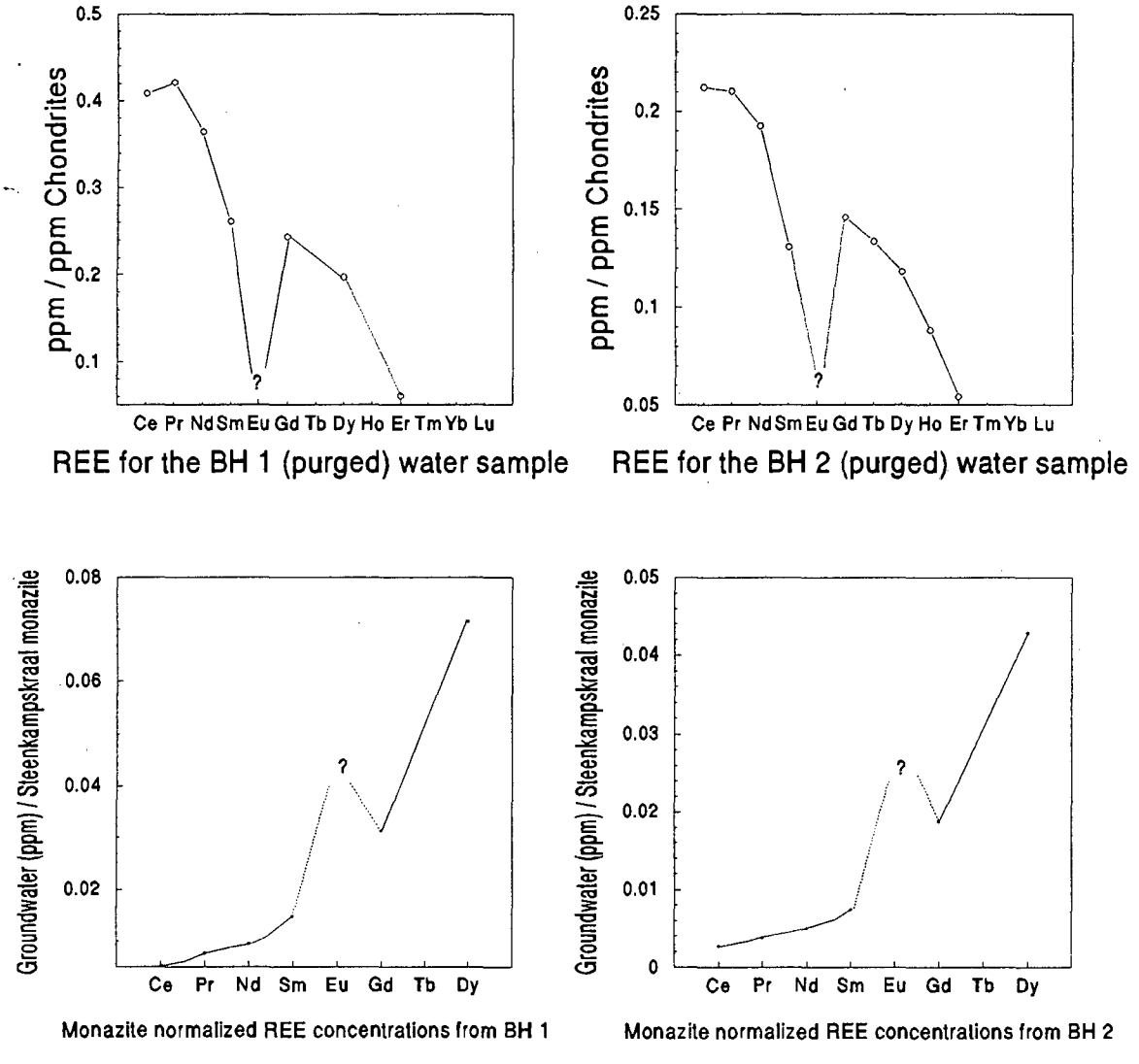

Figure 4.12. Chondrite-normalized and monazite-normalized REE data for BH 1 and BH 2 water samples.

Abundant colloids were found to be present within BH 1, with the colloidal fraction dominated by lepidocrocite. Quartz and feldspar were subsidiary phases (Table 4.10, Figure 4.13). Colloids in groundwater can arise from various sources and may be dispersed and stabilized by hydrogeochemical mechanisms (Degueldre et al., 1996). Although the primary generation of colloidal material is from the erosion and mechanical resuspension of non-cemented small grain size particles, changes in groundwater geochemical conditions can induce supersaturation and precipitation as well as coprecipitation of various phases (Degueldre et al., 1996). The colloidal fraction of BH 1 would result from a compositional change in water chemistry, resulting in an equilibrium of the water with the primary minerals (quartz and feldspar) and the formation of secondary mineral precipitates (lepidocrocite). The presence of lepidocrocite is consistent with the high concentration of Fe in the water and low pH. Calculations using MINTEQA2 assuming all dissolved Fe to be Fe^{3+}, indicated that lepidocrocite would have a saturation index of 6.374. Lepidocrocite has been found to form as a secondary mineral in sulphide-rich tailings (Jambor, 1994). The water in BH 1 was calculated to be supersaturated with respect to numerous other Fe rich minerals (Table 4.11). None of these were, however, identified in the colloidal fraction. Feldspar and quartz are common minerals associated with the surrounding country rock. These minerals would be present as primary minerals, rather than from precipitation out of solution. The water in BH 1 was calculated to be slightly undersaturated with respect to quartz (-0.336).

It is difficult to explain the origin of the iron in the water at BH 1, as the borehole lies approximately 300 m up the groundwater flow direction from the mine. Since BH 1 lies upgradient of the mine with respect to the ground water flow direction, as well as the fact that the water has developed a monazite-like chondrite-normalized REE pattern, it is possible that the water in BH 1 has been in contact with a separate monazite, sulphide-rich ore body similar to that of the Steenkampskraal ore body. The low PO_4^{3-} concentration could be explained by the low pH and high Fe concentration resulting in increased adsorption in a similar mechanism to the way PO_4^{3-} may be removed from the main shaft and main shaft extension water.

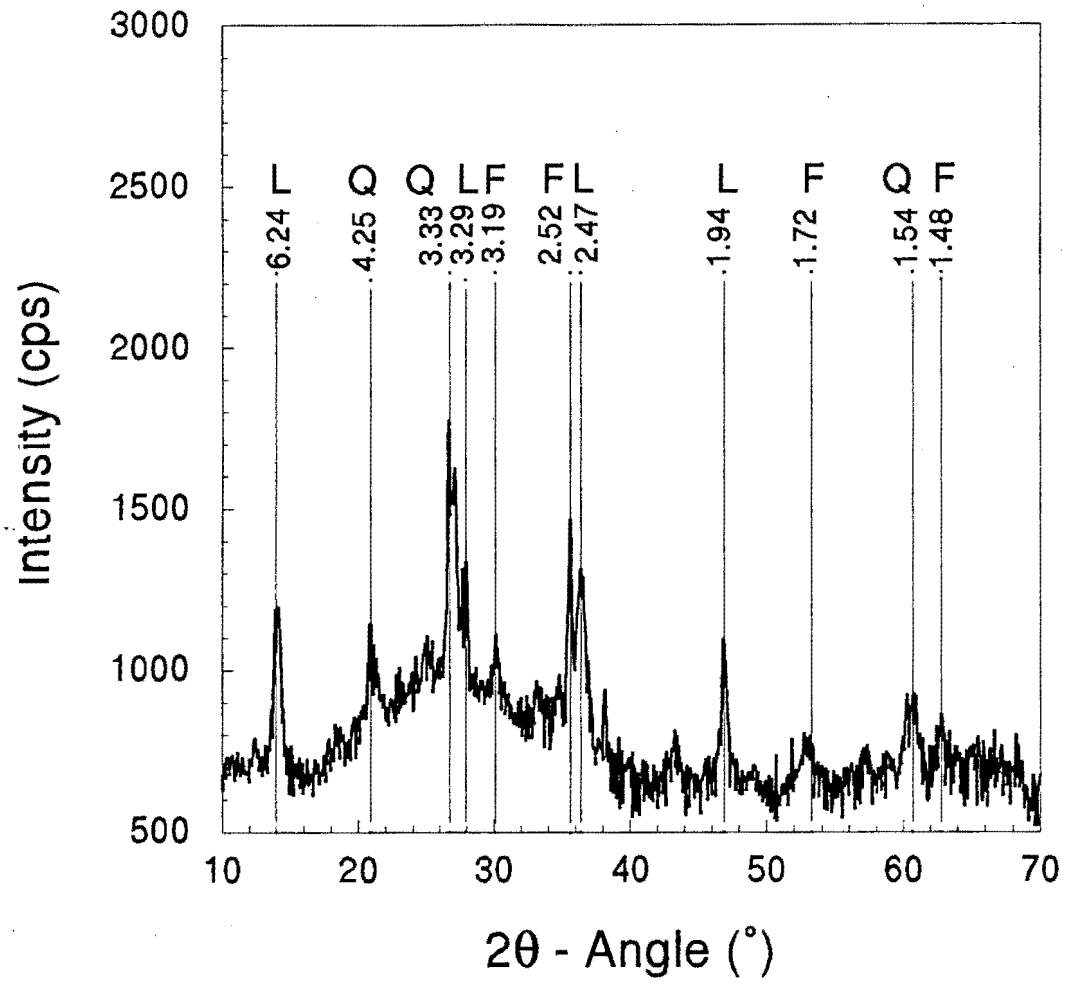

Figure 4.13. X-ray diffraction scan of colloid sample from BH 1. Lines define mineral peaks, with the corresponding d-spacings and mineral abbreviations above. Peaks associated with specific minerals are listed in Table 4.10.

Table 4.10. List of minerals identified in the colloidal fraction of BH 1, with their corresponding d-spacings. d-spacings obtained from JCPDS (1980).

Mineral	Mineral formula	d-spacing (Å)
Lepidocrocite	γ-FeOOHO	6.24 / 3.29 / 2.47 / 1.94
Feldspar	$(K,Na)AlSi_3O_8$ / $CaAl_2Si_2O_8$	3.19 / 2.52 / 1.72 / 1.48
Quartz	SiO_2	4.25 / 3.33 / 1.54

Table 4.11. Calculated saturation indices for selected minerals in BH 1.

	BH 1
$Fe(OH)_{2.7}CL.3$	8.937
Ferrihydrite ($Fe_5(O_4H_3)_3$)	2.854
Goethite (α - FeO.OH)	7.245
Hematite (α- Fe_2O_3)	19.499
Jarosite H ($HFe_3(OH)_6(SO_4)_2$)	9.556
Lepidocrocite (γ - FeO.OH)	6.374
Maghemite (γ - Fe_2O_3)	9.105
Strengite ($Fe(PO_4).2H_2O$)	4.934
Quartz (SiO_2)	-0.336

4.5.2. Borehole 2

The water sample BH 2 has a high PO_4^{3-} concentration (Table 4.9), associated with very high concentrations of Th (Langmuir and Herman, 1980), U (Ahonen et al., 1994), and REE. BH 2 is located on the south-western side of the ore body (Figure 4.1). It is possible that the water sampled in BH 2 has flowed across the ore body from further north. The chondrite-normalized REE distribution of BH 2 is similar to the other water samples (Figure 4.12). The high PO_4^{3-} concentration can again be explained by an initial large input into the groundwater from the weathering of apatite and monazite associated with a neutral pH and relatively low concentration of Fe and Al, resulting in limited adsorption.

The chondrite-normalized REE patterns for BH 1 and BH 2 (Figure 4.12) have similar patterns to both slimes dam samples. The low pH of the water in BH 1 has resulted in Ce being present as Ce^{3+}, ie the prevention of Ce oxidation to Ce^{4+} and removal by precipitation as CeO_2. It is assumed that Ce oxidation has not occured in BH2 as well, even though the it has a neutral pH. This is possible in waters experiencing reducing conditions (Brookings, 1983). The redox potential of the water could not be accurately determined. The exact boundaries defining the different fields of Ce in Figure 2.2 are also dependent on the concentration of CO_3 in the system (Brookings, 1983). Trivalent Ce was again used in the prediction of speciation modelling in BH 2 and 6 (Table 4.16). The relatively high concentrations of REE, U and Th could be due to colloidal transport. The colloidal fraction in BH 2 (Figure 4.14) is dominated by quartz and feldspar with subsidiary muscovite and kaolinite (Table 4.13). MINTEQA2 was used to predict the saturation indices of certain mineral phases that may be present in the system (Table 4.12).

The water in BH 2 was found to be supersaturated with respect to quartz, kaolinite and feldspar (anorthite, albite and microcline). It is expected that quartz and feldspars are present in the form of primary minerals, with kaolinite formed from the weathering of the feldspars. The higher alkalinity of BH 2 than the other borehole waters, excluding BH 6, has resulted in positive saturation indices for calcite, aragonite and dolomite, with magnesite being slightly undersaturated. These carbonates were not identified in the XRD analysis, but could be present in small quantities.

Table 4.12. Calculated saturation indices for selected minerals in BH 2 and BH 6.

	BH 2	BH 6
Anorthite ($CaAl_2Si_2O_8$)	2.126	1.034
Low albite ($NaAlSi_3O_8$)	3.716	3.09
Microcline ($KAlSi_3O_8$)	4.157	3.466
Aragonite ($CaCO_3$)	0.255	0.717
Calcite ($CaCO_3$)	0.394	0.856
Dolomite ($CaMg(CO_3)_2$)	0.863	1.737
Magnesite ($MgCO_3$)	-0.316	0.111
Kaolinite ($Al_2Si_2O_5(OH)_4$)	10.25	8.513
Quartz (SiO_2)	0.462	0.144

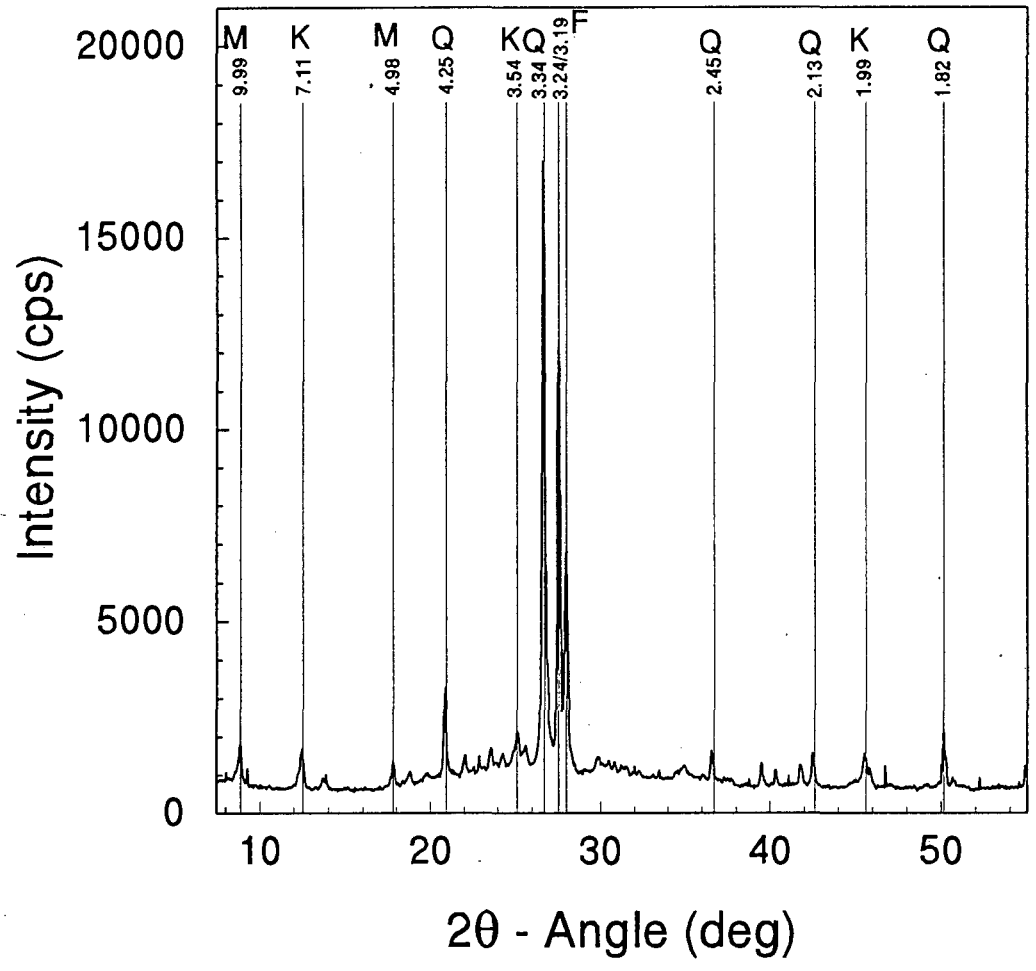

Figure 4.14. X-ray diffraction scan of colloid sample from BH 2. Lines define mineral peaks, with the corresponding d-spacings and mineral abbreviations above. Peaks associated with specific minerals are listed in Table 4.13.

Table 4.13. List of minerals identified in the colloidal fraction of BH 2, with their corresponding d-spacings. d-spacings obtained from JCPDS (1980).

Mineral	Mineral formula	d-spacing (Å)
Mica: chlorite muscovite	$(Mg,Al,Fe)_{12}[(Si,Al)_8O_{20}](OH)_{16}$ $K_2Al_4[Si_6Al_2O_{20}](OH,F)_4$	9.99 / 4.98
Kaolinite	$Al_4[Si_4O_{10}](OH)_8$	7.11 / 3.54 / 1.99
Feldspar	$(K,Na)AlSi_3O_8$ / $CaAl_2Si_2O_8$	3.24 / 3.19
Quartz	SiO_2	4.25 / 3.34 / 2.45 / 2.13 / 1.82

4.5.3. Borehole 3

BH 3 has an unusual chemistry in that it has a much lower EC than all the other waters sampled during the study, with associated low concentrations of dissolved elements. Colloids were also not found in the water. The concentrations of REE are lower than in the other borehole waters, with only Ce and Nd having concentrations above detection limits (0.005 mg/dm^3). BH 3 is located at the top of the hill close to the main shaft, and although accurate surface elevation data for the different boreholes have not been supplied, the vertical depth to the water is only 49 m (Appendix 1, Table A1.1). The borehole is inclined towards the south in the direction of the Nama quartzites running parallel to the monazite ore body. It is possible that the water in this borehole is rain water that has entered an elevated aquifer within the quartzites, thus giving rise to the low concentrations of dissolved elements and ions.

The PO_4^{3-} and Th concentrations present in BH 3, although lower than the surrounding boreholes (BH 6 and BH 2) are, however, higher than those expected from an uncontaminated site (Langmuir and Herman, 1980 and Smedley, 1991), especially in waters derived from a quartzite aquifer within quartzites. The EC, although low, is also higher than that of rain water (Drever, 1988). The water in BH 3 is, therefore, separated from the general ground water. The extent of the aquifer and the degree of mixing with waters in contact with the ore body is not known. The unpurged BH 3 water sample was found to contain NO_3^-. This disappeared with purging.

4.5.4. Borehole 4 and 5

As mentioned in section 4.2. BH 4 has been interpreted as being groundwater similar to the general Steenkampskraal area. Recharge into the borehole is very slow. BH 5 has (Table 4.9) concentrations of dissolved elements and ions typical of the general background samples (Table 4.15), with the exception of PO_4^{3-} and Th. Thorium was not detected in any of the waters sampled from the windpumps on the farms Nabeep (MOS 1-4) or Brandewynskraal (Brand 1). An attempt to sample colloids in BH 5 was made. The borehole was relatively new, and it was presumed that the large proportion of mud taken out of the borehole was present from the original drilling operation.

4.5.5. Borehole 6

One of the interesting aspects of the chemistry of BH 6 is the very high alkalinity (Drever, 1988). The pH of most natural waters is controlled by reactions involving the carbonate system. Buffer intensity controls the magnitude of shifts in the pH of solutions, and the role of the dissolved or homogenous carbonate system in affecting buffer action in natural waters is unquestionably significant (Stumm and Morgan, 1981).

When CO_2 gas is brought into contact with water, the CO_2 will dissolve until equilibrium is reached. At equilibrium the activity of dissolved CO_2 will be proportional to the fugacity of CO_2 in the gas phase.

$$CO_2 + H_2O \rightleftarrows H_2CO_3$$

An equilibrium constant can be written for the reaction:

$$K_H = H_2CO_3 / P_{CO2} = 10^{-1.41} \text{ at } 25°C$$

Dissolved CO_2 is usually referred to as carbonic acid (H_2CO_3) (Drever, 1988), which will tend to dissociate into hydrogen and bicarbonate ions:

$$H_2CO_3 \rightleftarrows H^+ + HCO_3^-$$

An equilibrium constant can be written for the reaction:

$$K_1 = H^+ + HCO_3^- / H_2CO_3 = 10^{-6.35} \text{ at } 25°C$$

with bicarbonate itself able to dissociate into carbonate:

$$HCO_3^- \rightleftarrows H^+ + CO_3^{2-}$$

An equilibrium constant can be written for the reaction:

$$K_2 = H^+ + CO_3^- / HCO_3^- = 10^{-10.33} \text{ at } 25°C$$

The ratios of H_2CO_3 / HCO_3^- and HCO_3^- / CO_3^{2-} depend on the pH of the solution (Figure 4.13).

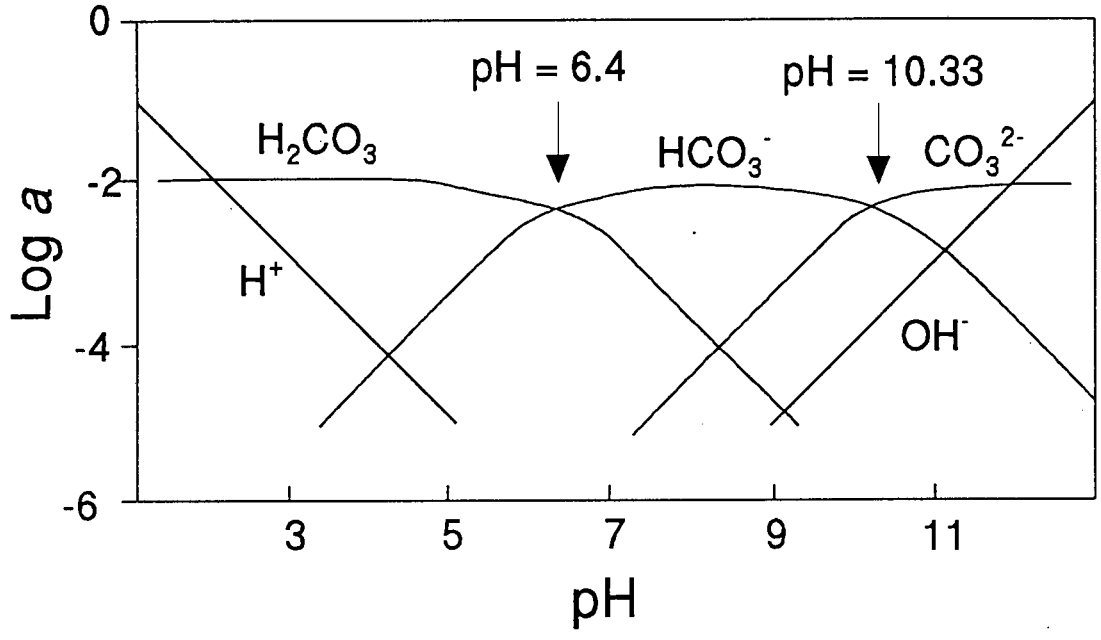

Figure 4.15. Activities of different species in the carbonate system as a function of pH, assuming the $\sum CO_2 = 10^{-2}$ atm, temperature = 25°C (After Drever, 1988).

The greater the concentration of CO_2, therefore, in equilibrium with the water, the lower the pH of the solution. The dominant colloid species found in the water from BH 6 was calcite ($CaCO_3$). The solubility of $CaCO_3$ can be understood by adding one more equation to the equations for the carbonate system. With the solubility products of calcite defined by the equation:

$$CaCO_3\ (s) \rightleftharpoons Ca^{2+} + CO_3^{2-}$$

$$K_{cal} = Ca^{2+} + CO_3^{2-} = 10^{-8.48} \text{ at } 25°C$$

This previous equation predicts that the groundwater in BH 6 should have a pH value near 8.3. However, its actual pH is around 7.6. This may be due to the relatively high SO_4^{2-} concentration indicating some interaction with the surface tailings. This is also supported by the relatively high F^- and U concentrations in the water compared with some of the uncontaminated waters.

The PO_4^{3-} concentration of BH 6 is lower than that of BH 2, 3, 5 and 6. This is expected as PO_4^{3-} is strongly adsorbed to Ca in solutions of neutral pH. The chemical speciation calculated by MINTEQA2 indicates that PO_4^{3-} exists as HPO_4^{3-} (54%), $CaHPO_4$(aq) (20%), $MgHPO_4$(aq) (10%), with the remaining PO_4 present as $CaPO_4^-$, $MgPO_4^-$, $NaHPO_4^-$ and $H_2PO_4^-$.

The colloidal fraction from BH 6 has been found to be dominated by calcite, quartz and feldspar (Figure 4.16, Table 4.14). The percentage of calcite determined in the colloidal fraction of BH 6 was 42.8%. This high concentration of calcite is consistent with the high alkalinity and neutral pH of the water. As suggested previously it is possible that the water present in the borehole has been derived from rain seepage through the tailings dam with neutralization through a carbonate dorbank.

MINTEQA2 was used to calculate the saturation indices of minerals likely to be present in the system. As expected the saturation index of calcite was found to be positive (Table 4.12). Aragonite, dolomite and magnesite are also calculated to be supersaturated. Although the water in BH 6 is calculated to be supersaturated with respect to feldspar (anorthite, albite and microcline) (Table 4.12), it is expected that the presence of these minerals, together with quartz in the colloid fraction are from the weathering of primary minerals and not from precipitation from solution.

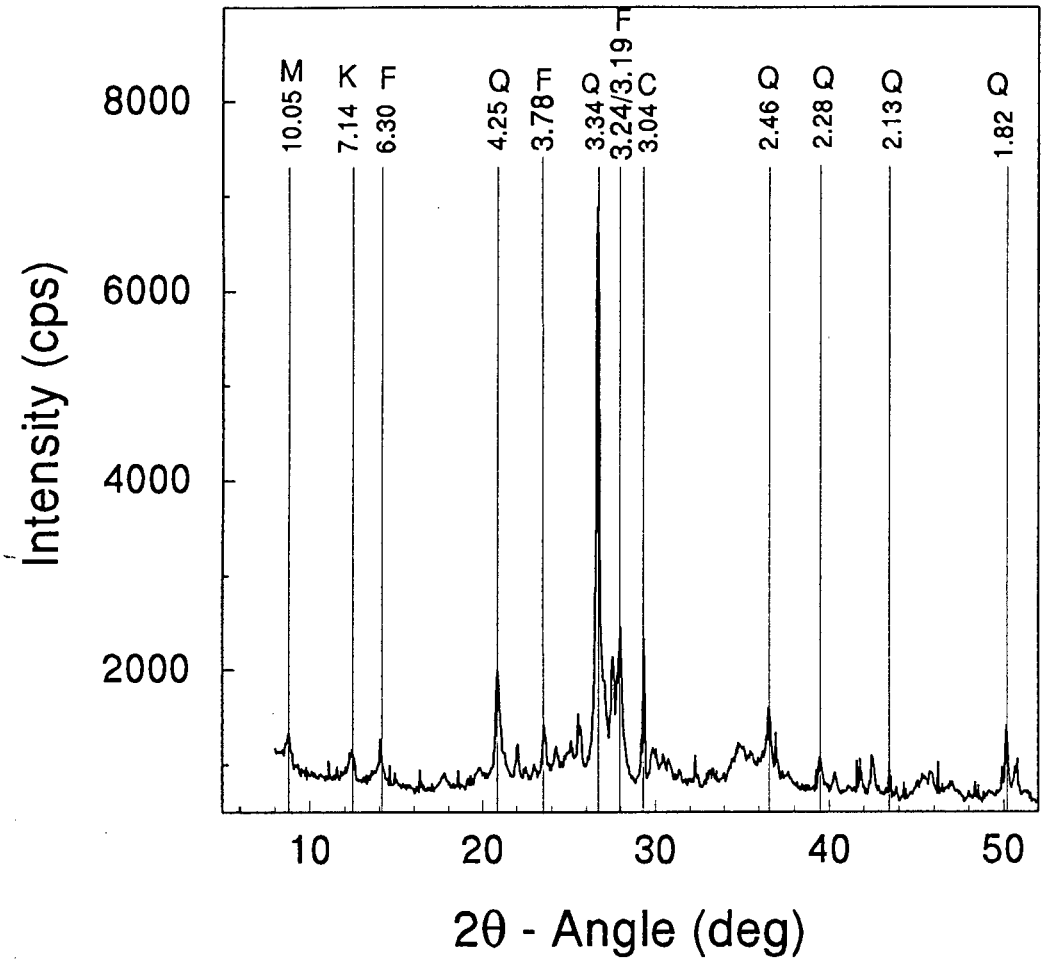

Figure 4.16. X-ray diffraction scan of colloid samples from BH 6. Lines define mineral peaks, with the corresponding d-spacings and mineral abbreviations above. Peaks associated with specific minerals are listed in Table 4.14.

Table 4.14. List of minerals identified in the colloidal fraction of BH 6, with their corresponding d-spacings. d-spacings obtained from JCPDS (1980).

Mineral	Mineral formula	d-spacing (Å)
Calcite	$CaCO_3$	3.04
Mica: chlorite muscovite	$(Mg,Al,Fe)_{12}[(Si,Al)_8O_{20}](OH)_{16}$ $K_2Al_4[Si_6Al_2O_{20}](OH,F)_4$	10.05
Kaolinite	$Al_4[Si_4O_{10}](OH)_8$	7.14
Feldspar	$(K,Na)AlSi_3O_8$ / $CaAl_2Si_2O_8$	6.30 / 3.78 / 3.24 / 3.19
Quartz	SiO_2	4.25 / 3.34 / 2.46 / 2.28 / 2.13 / 1.82

4.6. Water from the farms Nabeep and Brandewynskraal

The water chemistries of borehole water MOS 1 - 4 and BRAND 1 (Figure 3.2: locality map, Table 4.15) are similar to each other, with neutral pH values and similar electrical conductivities. It is assumed that these waters have ion concentrations typical of the local ground water. These samples all have high concentrations of basic cations (Ca, Mg, Na and K) (Wetzels, 1996) characteristic of all ground water samples in the Steenkampskraal area, with the exception of BH 3 (Table 4.9). The high concentrations of Ca, Mg, Na and K are present as a result of mineral weathering from the granite gneiss country rock of the Namaqua metamorphic complex. Compared with the water samples closer to the mine, the farm waters have low concentrations of PO_4^{3-}, SO_4^{2-} and dissolved metals, including U, Th and REE.

The Fe concentrations are naturally high, with the concentrations of Ni and Co following the same trend. These high concentrations are expected, considering the mafic nature of the country rock.

The concentrations of U in some of these waters (especially Mos 1 and Mos 4) are on the high side of ground waters in uncontaminated sites (Smedley, 1991). The U present in these waters is presumed to be from the weathering of the surrounding country rock and not from the long-distance transport of the actinides in the groundwater from the Steenkampskraal mine. In all 4 water samples, Th and all REE were found to be present in concentrations below detection limits.

Table 4.15. Analytical results for water samples from the farms Nabeep (MOS 1-4) and Brandewynskraal (BRAND 1).

Analyte	Samples				
	Mos 1	Mos 2	Mos 3	Mos 4	Brand 1
pH	7.62	7.24	7.51	7.12	7.37
EC (mS/cm)	4.38	6.59	7.65	5.04	4.44
Anions:*		mg/dm^3			
Cl^-	1368	2252	2511	1414	1396
SO_4^{2-}	339	425	477	317	299
HCO_3^-	149	122	165	279	344
F^-	2.9	0.84	1.3	1.4	1.3
PO_4^{3-}	1.9	1.3	1.2	2.1	1.4
Cations:*		mg/dm^3			
Ca^{2+}	67	211	224	81	142
Mg^{2+}	91	212	231	102	144
Na^+	97	1044	1257	879	704
K^+	38	22	70	35	59
NH_4^+	bdl	bdl	bdl	bdl	bdl
Trace metals:$		mg/dm^3			
Fe	2.6	1.9	13	7.5	0.50
Al	<0.5	<0.5	<0.5	<0.5	<0.5
Cu	<0.2	<0.2	<0.2	<0.2	<0.2
Cr	<0.1	<0.1	<0.1	<0.1	<0.1
Mn	<0.04	<0.04	<0.04	<0.04	<0.04
Ni	0.21	0.30	0.35	0.30	0.24
Si	11	19	15	13	14
Co	0.61	0.64	0.66	0.64	0.62
Pb	<1.0	<1.0	<1.0	<1.0	<1.0
Zn	0.74	2.4	3.1	3.1	11
As	<0.5	nd	nd	nd	nd
Cd	bdl	bdl	bdl	bdl	bdl
Th#	<0.005	<0.005	<0.005	<0.005	<0.005
U	0.03	<0.005	0.006	0.02	<0.005

bdl - below detection limits / nd - not determined / * HPIC / $ ICP-AES / # ICP-MS

4.7. Classification of all water samples at Steenkampskraal

A modified version of the Piper plot has been used in an attempt to group all the waters samples within the Steenkampskraal area. Due to the presence of high concentrations of PO_4^{3-} in some of the waters, PO_4^{3-} was added to SO_4^{2-} in the construction of the Piper plot (Figure 4.17, reference numbers in Table 4.16). Although a definite trend could be seen on the combined cation/ anion graph, no distinct separation could be seen between the mine and background waters.

This is expected as SO_4^{2-} and PO_4^{3-} are added to Cl^-, thus limiting separation of the highly contaminated mine waters from the Cl^- rich waters usually present in the area. The presence of alkalinity in the farm waters (Mos 1-4 and Brand 1), BH 2 to 6, and the inclined shaft has resulted in these waters plotting away from the 100% $SO_4^{2-}+PO_4^{3-}+Cl^-$ line. This is better seen on the anion plot (Figure 4.18, reference numbers in Table 4.16), from which two distinct groups of waters have been identified.

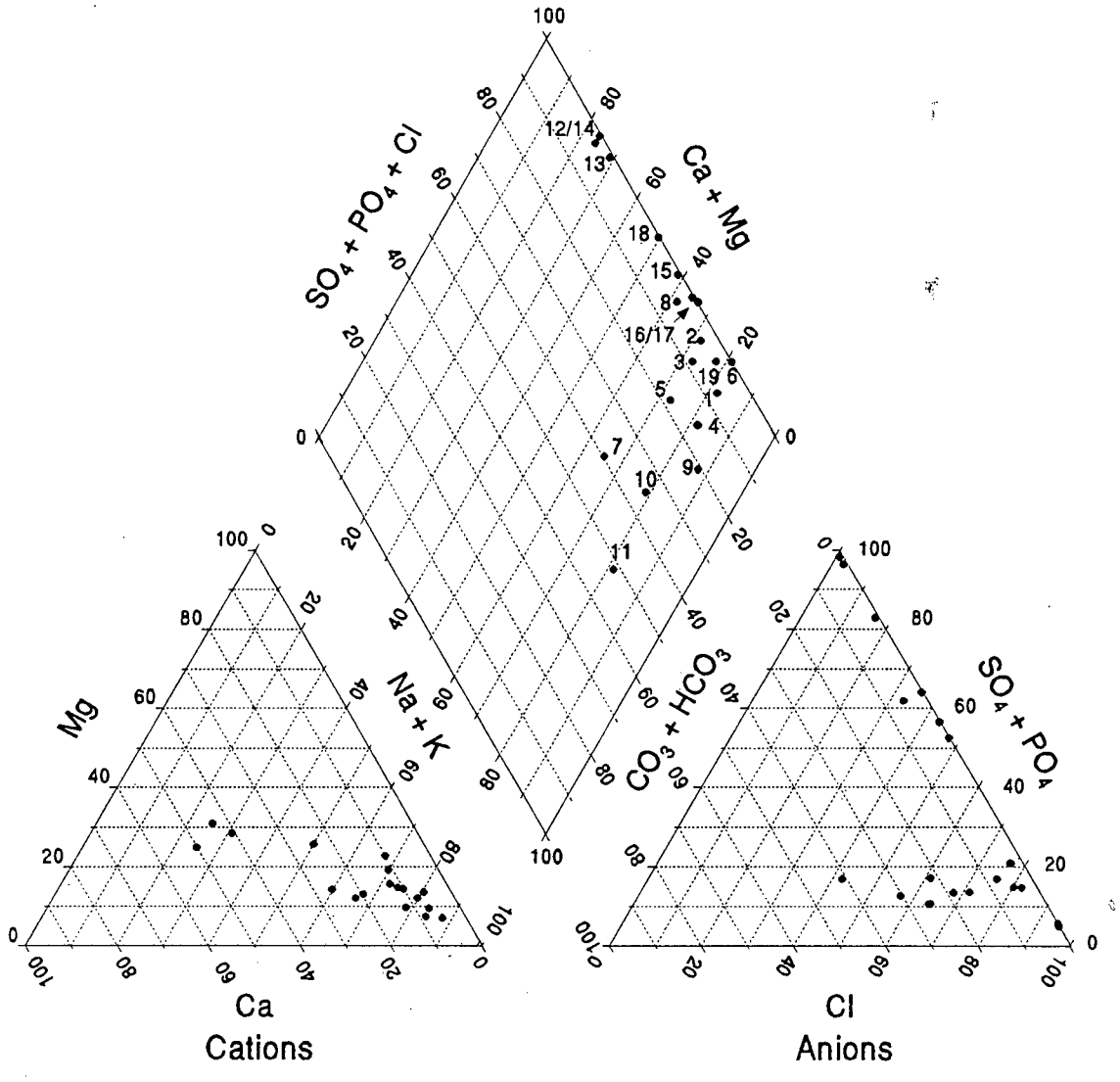

Figure 4.17. Modified Piper plot of all water samples at Steenkampskraal. Corresponding reference number in Table 4.16.

Table 4.16. Water samples with corresponding reference numbers for Figures 4.17 and 4.18.

SAMPLE	Reference number
Mos 1	1
Mos 2	2
Mos 3	3
Mos 4	4
Brand 1	5
BH 1	6
BH 2	7
BH 3	8
BH 4	9
BH 5	10
BH 6	11
Slimes dam 1	12
Slimes dam 2	13
Road water	14
Stream water	15
Main shaft extension	16
Main shaft	17
Sump on level 3	18
Inclined shaft	19

All the farm water samples (Mos 1 to 4 and Brand 1), the inclined shaft and boreholes 1, 2, 4, 5 and 6 fall within group 1. These waters are dominated by Cl^- with varying HCO_3^- percentages. All the surface water samples (SD 1 and 2, Road water and Stream water), the acidic mine water samples (Main shaft, Main shaft extension and the Sump on level 3), and borehole 3 fall within group 2. These samples are dominated by SO_4^{2-} and PO_4^{3-}, due to the contamination from mining activities. The presence of BH 3 in group 2 is interesting, as although it has low concentrations of elements and ions, the anion ratios indicate that contamination from the mine has occurred.

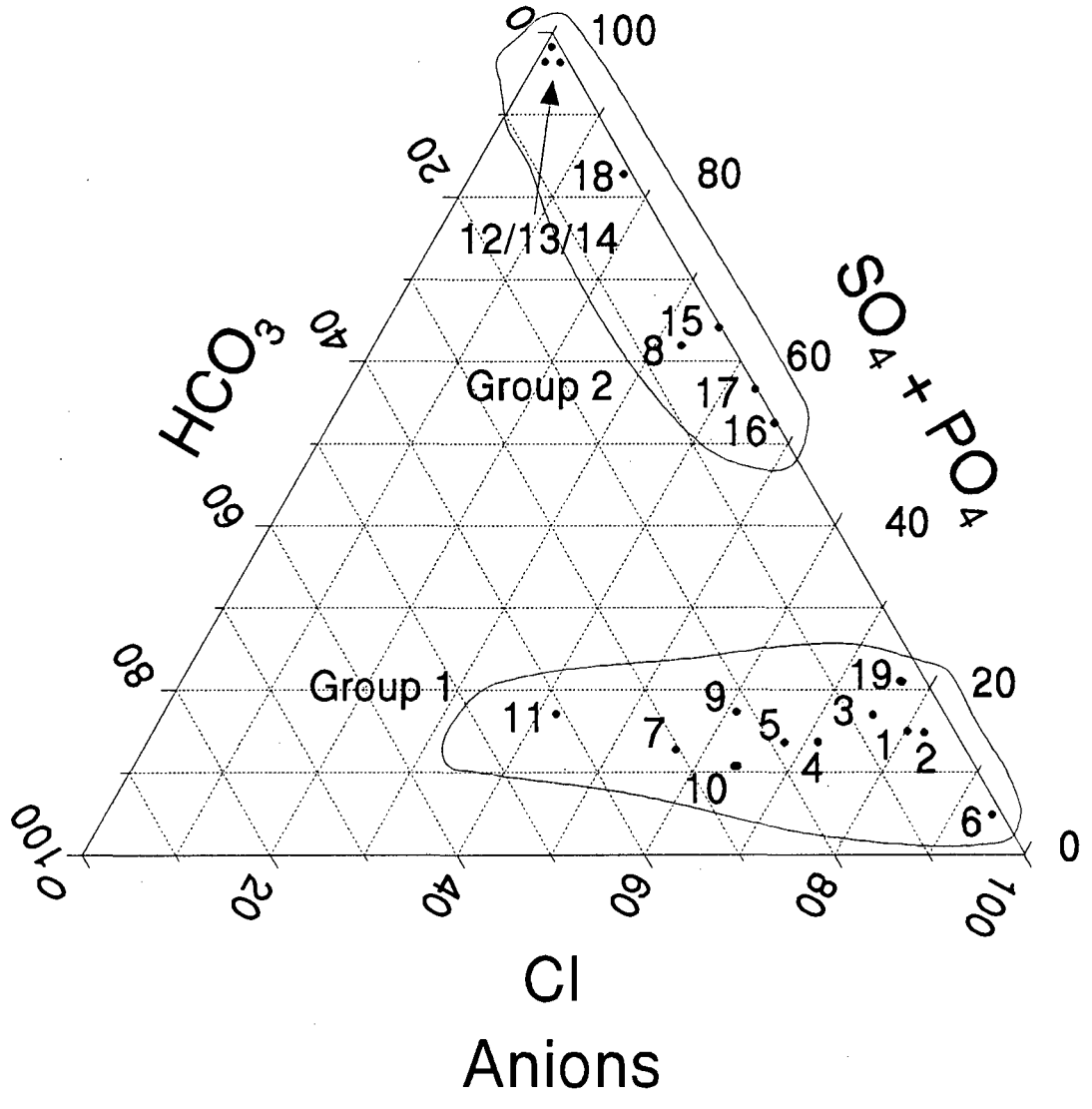

Figure 4.18. Anion section of modified piper plot of all water samples at Steenkampskraal. Corresponding reference number in Table 4.16.

4.8. Uranium, Th and REE speciation within the Steenkampskraal waters

Chemical speciation is an important aspect of any geochemical project involving elemental mobility via colloidal particles. The charge of a particular element due to complexation is an important factor in understanding the extent to which adsorption occurs. As pH increases, the adsorption of metal cations from solution is enhanced (McBride, 1994). This effect is principally the result of increases in the net negative charge on the material surface, caused by the dissociation of acidic functional groups, which in turn increases the electrostatic attraction of the surface for metal cations. The amount of metal cation adsorbed will increase with pH, unless ligands in the solution compete overwhelmingly with the surface functional groups for the metal (Sposito, 1989).

Speciation and ionic strength can greatly affect cation adsorption phenomena. Anionic ligand competition for the adsorbing cation, and competition effects for adsorption sites between different cationic species, can result in significant decreases in metal cation adsorption (Bourg, 1988).

Many geochemical models have been developed to solve problems involving chemical equilibria (speciation). As mentioned in chapter 3, MINTEQA2 was used for the speciation modelling. Although the MINTEQA2 package includes an extensive database comprising thermodynamic data for soluble complexes, no Th or REE data were present. Stability constants for some of the REE (Ce, Pr, Nd, Sm, Gd, Dy and Yb) and Th were collected from the database JESS as well as from Wood (1990), Langmuir and Herman (1980), and Vieillard and Tardy (1984).

The accuracy of speciation predictions is limited by the extent and quality of the database. The author attempted as far as possible to compile a complete database. The Th speciation (Table 4.17) calculated by MINTEQA2 is similar to the study by Langmuir and Herman (1980), where it was found that with increasing pH, Th was complexed as sulphate, fluoride, phosphate and hydroxide. The two highly acidic samples, slimes dam 1 and the main shaft, have Th complexed with sulphate. Sample BH 1 has a pH of 4.59 and was found to have all the Th complexed with F^-. BH 2 and BH 6 have Th predominantly complexed to F^-, with a minor quantity in the form of CO_3^{2-}. This is due to the high alkalinity of the two samples. Langmuir and Herman (1980) found that Th phosphate complexes would dominate between pH 4.5 to 7. This was not found to occur in samples BH 2 and BH 6. The dominant complex is dependent on the relative concentrations of the other anions as well as the concentration of the metal. The high alkalinity of these samples, not included in the study by Langmuir and Herman (1980), would also play a role in determining the speciation.

MINTEQA2 contained U thermodynamic data, which was used for the speciation. Langmuir (1978) showed that uranyl complexes with hydroxyl, carbonate, fluoride, sulphate or phosphate could predominate in oxidized surface and ground waters. The $UO_2H(PO_4)_2^{3-}$ complex dominates in water samples BH 1, BH 2, BH 6 and SD 1 (Table 4.17). Langmuir (1978) and Dongarra and Langmuir (1980) computed that uranium phosphate complexes were the dominant species in natural waters with pH 4-7.5. The very high alkalinity of BH 6, results in a change in complex with the carbonate species becoming important. The sample from the main shaft is again different, with SO_4^{2-} complexes dominating, which is most likely due to the much higher SO_4^{2-}/PO_4^{3-} ratio than the other water samples.

Table 4.17. Calculated U, Th, and REE speciation proportions (%) in the aqueous phase using MINTEQA2 for 5 selected water samples from Steenkampskraal.

	BH 1	BH 2	BH 6	MS	SD 1
Th^{4+}	77 ThF_2^{2+} 13 ThF^{3+} 10 ThF_3^{+}	35 ThF_2^{2+} 56 ThF_3^{+} 6 ThF_4 4 $ThCO_3^{2+}$	16 ThF_2^{2+} 56 ThF_3^{+} 17 ThF_4 2 $ThCO_3^{2+}$	11 $Th(SO_4)_3^{2-}$ 85 $Th(SO_4)_2$ 2 $ThSO_4^{2-}$ 1 ThF^{3-}	45 $Th(SO_4)_3^{2-}$ 54 $Th(SO_4)_2$
UO_2^{2+}	99 UO_2^{2+} $UO_2H(PO_4)_2^{3-}$	100 UO_2^{2+} $UO_2H(PO_4)_2^{3-}$	3 $UO_2(CO_3)_2^{2-}$ 43 $UO_2(CO_3)_3^{4-}$ 54 $UO_2H(PO_4)_2^{2-}$	36 UO_2^{2+} 1 UO_2F^{+} 1 UO_2Cl^{+} 35 UO_2SO_4 AQ 23 $UO_2(SO_4)_2^{2-}$ 3 $UO_2H(PO_4)_2^{3-}$	100 $UO_2H(PO_4)_2^{3-}$
Ce^{3+}	82 Ce^{3+} 2 CeF^{2+} 14 $CeSO_4^{+}$ 3 $CeCl^{2+}$	68 Ce^{3+} 13 CeF^{2+} 18 $CeSO_4^{+}$ 2 $CeCl^{2+}$	42 Ce^{3+} 20 CeF^{2+} 37 $CeSO_4^{+}$ 1 $CeCl^{2+}$	36 Ce^{3+} 63 $CeSO_4^{+}$ 1 $CeCl^{2+}$	14 Ce^{3+} 85 $CeSO_4^{+}$
Pr^{3+}	100 $PrCl^{2+}$	99 $PrCl^{2+}$		99 $PrCl^{2+}$	9 Pr^{3+} 23 $PrCl^{2+}$ 68 $PrSO_4^{+}$
Nd^{3+}	85 Nd^{3+} 13 $NdSO_4^{+}$ 2 $NdCl_2^{+}$	79 Nd^{3+} 18 $NdSO_4^{+}$ 1 $NdCl_2^{+}$	53 Nd^{3+} 41 $NdSO_4^{+}$ 4 $Nd(SO_4)_2^{-}$ 2 NdF^{2+}	32 Nd^{3+} 49 $NdSO_4^{+}$ 18 $Nd(SO_4)_2^{-}$	6 Nd^{3+} 32 $NdSO_4^{+}$ 62 $Nd(SO_4)_2^{-}$
Sm^{3+}	84 Sm^{3+} 16 $SmSO_4^{+}$	76 Sm^{3+} 18 $SmSO_4^{+}$ 2 SmF^{2+}		34 Sm^{3+} 66 $SmSO_4^{+}$	13 Sm^{3+} 87 $SmSO_4^{+}$
Gd^{3+}	83 Gd^{3+} 14 $GdSO_4^{+}$ 3 $GdCl_2^{+}$	62 Gd^{3+} 16 $GdSO_4^{+}$ 22 GdF^{+2}		36 Gd^{3+} 64 $GdSO_4^{+}$	14 Gd^{3+} 86 $GdSO_4^{+}$
Dy^{3+}	86 Dy^{3+} 13 $DySO_4^{+}$	76 Dy^{3+} 6 DyF^{2+} 18 $DySO_4^{+}$		40 Dy^{3+} 61 $DySO_4^{+}$	15 Dy^{3+} 85 $DySO_4^{+}$
Yb^{3+}				45 Yb^{3+} 55 $YbSO_4^{+}$	19 Yb^{3+} 81 $YbSO_4^{+}$

The extent of the thermodynamic data input into MINTEQA2 varied with the different REE. Carbonate stability constants for the different REE were generally lacking. The unspeciated ion and the SO_4^{2-} complex (Figure 4.17) was found to dominate in all 5 samples for all the REE. This is consistent with a study by Wood (1990), who used Eu^{3+} as a representative REE (Figure 2.3) and found that below pH 6.5, the Eu^{3+} ion and the $EuSO_4^{+}$ complex dominated. Carbonate species were found to dominate above pH 6.5. This may have been the case for BH 6 and BH 2 if carbonate stability constants had been available.

The solubility products of the REE phosphates are sufficiently small ($K_{sp}^{\circ} < 10^{-24.4}$) (Jonasson et al., 1985) that even picomolar concentrations of REE can produce saturation and supersaturation (Byrne et al., 1996). Due to the close similarities in ionic radii and chemical properties, the entire suite of REE in the presence of PO_4^{3-} should form coprecipitates of variable composition, 1993), with the process of coprecipitation resulting maintaining the saw-tooth REE pattern present in natural solutions while reducing the overall REE solution concentration (Byrne et al., 1996). The absence of REE phosphate complexes in Table 4.17 is expected due to the small solubility products of the REE phosphates.

One of the reasons for attempting to establish the Th, U and REE speciation in the Steenkampskraal waters is to get a better understanding of the mechanisms involved in the mobility of these elements in the waters. As mentioned above, chemical speciation is an important aspect of any geochemical project involving elemental mobility via colloidal particles.

4.9. Conclusions

Stable isotopes of oxygen ($\delta^{18}O$) and hydrogen (δD) indicate the presence of two distinct groups of water within the vicinity of the Steenkampskraal mine. A group of unevaporated waters comprises all boreholes and the water sampled in the inclined shaft. The water moving through the inclined shaft is in contact with the ground water. A second group of highly evaporated water was found to be present in both slimes dam samples as well as the underground water samples not directly in contact with the ground water.

Groundwater contamination by REE-bearing phosphate minerals has occurred at the Steenkampskraal monazite mine. This has resulted in high concentrations of REE, U and Th in all the mine waters and boreholes that extend below the local groundwater surface. The chondrite-normalized REE patterns of the water samples are similar to that displayed by monazite, with a distinctive Eu depletion and an obvious enrichment in LREE with respect to HREE.

The degree of contamination varied, with elevated concentrations of a number of solutes. The high PO_4^{3-} concentrations present in the waters would be due to the weathering of monazite and apatite in both the tailings and the ore pile. The PO_4^{3-} concentrations of the waters is highly dependent on the presence or absence of Fe. Iron is a strong adsorbent of PO_4^{3-}. The presence of Fe in the system significantly decreases the PO_4^{3-} concentration of the water. Similarly, the concentration of SO_4^{2-} is to some extent dependent on Fe. This is not as obvious as that of PO_4^{3-} due to the much larger concentrations of SO_4^{2-} in the system.

Fluoride is present in extremely high concentrations, and is probably present due to the large concentration of fluoride bearing minerals (fluorite and fluorapatite) associated with the ore body and surrounding country rocks and later exposed on the rock pile and tailings.

The high concentration of chalcophile elements (Cu, Fe, Co, Ni, Pb, Zn, As and Cd) would have been derived from the weathering of the sulphide minerals (pyrite, chalcopyrite and galena) as well as from the weathering of the oxide minerals (magnetite, ilmenite and Zn-bearing hercynite). The dominant cation in all surface water samples is Cu (giving rise to the deep blue colour). Copper is present in the unweathered ore body in concentrations of approximately 1.1 %.

The remaining metals (Al, Cr, Mn and Si) would be present in many of the minerals associated with the ore body and surrounding country rocks. The very high Al concentrations have resulted due to the high concentration of Al in the ore body and very low pH resulting in increased dissolution, solubility and mobility.

Phosphate, Th and REE proved to be the most useful solutes in identifying contamination. Uranium was found to be present in measurable concentrations in some of the background samples. This is presumed to be from U released during the weathering of the country rock.

The REE present in the ground waters have developed a similar chondrite-normalized REE pattern to that of monazite. This was expected to occur due to the fact that monazite would control the distribution of REE in the local mineralogy. The monazite-normalized REE patterns for the selected borehole waters show a marked fractionation between LREE and HREE, with the HREE strongly enriched in the aqueous phase. Read et al. (1987) found the HREE to show a greater tendency for complexation and a greater affinity for mineral surfaces. Colloids were identified in three of the boreholes, with all three boreholes having high U, Th and REE. It is, therefore, likely that colloidal transport of these elements is likely to be the dominant mechanism of transport.

The calculated speciation of U, Th and REE was consistent with that of the literature. Speciation has important implications regarding the ability of adsorption to colloidal particles and therefore mobility of the elements within the groundwaters.

Chapter 5

Soil chemistry

5.1. Introduction

As the knowledge of detrimental environmental effects from previous nuclear disposal methods has increased, the need to identify and quantify mechanisms controlling geochemical processes governing transport of these contaminants has intensified (Batson et al., 1996). The objective of the study of the soil chemistry was to determine the extent of element and ion transport away from the mine, as well as to study the effects of soil acidification resulting from the oxidation of sulphide minerals within the tailings and ore body. The impact on the soils from mining activity at Steenkampskraal has not been studied before, with the present investigation serving as a pilot study laying a foundation for further work.

5.2. Saturated paste extract analyses

Soils and sediments are the most favourable sink for heavy metals in environments polluted by mining and milling activities and readily attenuate contaminants owing to their high sorption capacity (Prusty et al., 1994). Sediments have often been used as an index to assess the water quality where no significant fluctuations in pH occur (Aston et al., 1974). Metal contamination of soils in dry arid regions as a result of mining and milling is unusual, with most studies concentrating on areas in which permanent surface water and saturated sediments are present (Prusty et al., 1994; Batson et al., 1996; Vivian and Massie, 1977; and Cabrera et al., 1984). The saturated paste extracts from ten soil samples along both soil transects have been analyzed in an attempt to determine the extent of the surface pollution as a result of mining activity. Saturated paste extracts are prepared to determine the proportion of inorganic solutes able to be dissolved in solution. The ratio of the element or metal in solution to the total element or metal concentration can give an indication to the dominant mechanism of transport. The position of the soil samples is plotted in Figure 5.1, and a perspective of the area is given in Figure 5.2.

5.2.1. Transect 1

The chemistry of the saturated paste extracts of the soils along soil transect 1 (Table 5.1) is similar to the road water and slimes dam water samples at the top of the transect near the tailings, with a general decrease in dissolved ion concentration and increase in pH away from the tailings, sample 1/2A to 1/8. Two horizons, were evident close to the tailings, with the "A horizon" being recognized by the lower degree of compaction than the "B horizon". Differences in dissolved ion concentrations were also found between the A and B horizons of samples 1/2 and 1/4, with notable decreases in the B horizon in all elements with the exception of Na, K and Si. The dominant element in both the A and B horizon of sample 1/2 is Cu. The Cu concentrations decrease rapidly with increasing distance from the tailings, resulting in the dominance of basic cations, Si and the bicarbonate (HCO_3^-) anion in sample 1/8.

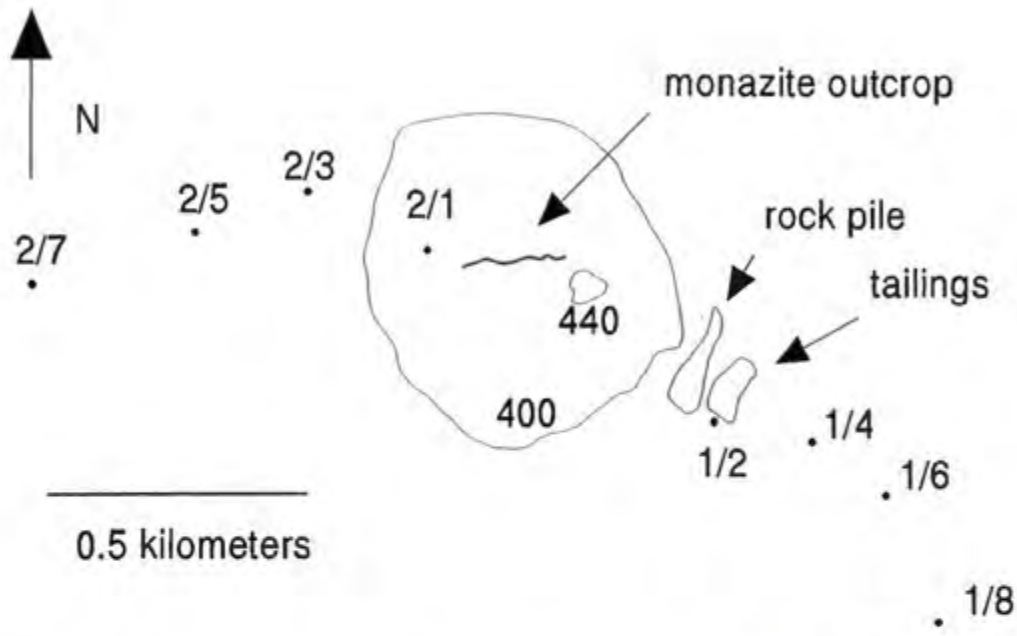

Figure 5.1. Locality map of selected soil samples along transects 1 and 2. The 400 and 440 m contours are shown.

Figure 5.2. Photograph from the top of the rock pile, looking over the tailings towards the south east in the general direction along which the soils from transect 1 were sampled.

Table 5.1. Analytical results of saturated paste extracts from soil transect 1.

Analyte	Samples					
	1/2A	1/2B	1/4A	1/4B	1/6	1/8
pH	3.57	3.59	4.99	5.17	4.92	7.57
EC: mS/cm	8.40	6.61	2.83	2.65	1.36	0.33
Acidity: mol/dm^3	0.072	0.079	0.0026	nd	nd	nd
Anions:*		mg/dm^3				
Cl^-	392	277	551	380	211	43
SO_4^{2-}	8983	6554	1041	1105	438	50
PO_4^{3-}	212	159	43	64	49	46
F^-	27	22	1.2	0.41	0.69	0.35
HCO_3^-	nd	nd	nd	6.9	21	255
NO_3^-	nd	nd	46	23	4.5	12
Cations:*		mg/dm^3				
Ca^{2+}	485	256	216	56	66	15
Mg^{2+}	351	328	150	64	58	19
Na^+	182	266	360	484	144	70
K^+	9.7	35	36	13	19	30
NH_4^+	6.1	4.8	bdl	bdl	5.6	1.4
Trace metals:#		mg/dm^3				
Fe	14	1.1	1.1	1.3	0.66	0.5
Al	182	103	2.1	1.8	1.7	1.6
Cu	3420	1427	84	40	54	1.0
Cr	0.48	<0.1	<0.1	<0.1	<0.1	2.0
Mn	52	31	13	9.0	6.2	0.81
Ni	97	58	7.1	3.0	4.2	6.2
Si	22	34	20	56	15	36
Co	17	10	2.1	1.3	1.5	0.78
Pb	12	8.0	1.2	<1.0	<1.0	2.1
Zn	39	27	4.1	2.1	2.8	1.7
Cd	0.86	0.47	0.08	<0.06	0.078	0.19

bdl - below detection limits ; nd - not determined ; * HPIC ; # ICP-AES

5.2.2. Transect 2

The chemistry of the saturated paste extracts along soil transect 2 (Table 5.2) is different from that of soil transect 1. The pH of the extracts along transect 2 is neutral to alkaline, with much lower concentrations of dissolved metals. There is a gradual change in the dominating anion from PO_4^{3-} at the top of the hill closest to the ore body (sample 2/1) to HCO_3^- further away (sample 2/7). Associated with this change in relative anion concentration is a general increase in pH.

Table 5.2. Analytical results for saturated paste extracts from soil transect 2.

	2/1	2/3	2/5	2/7
pH	7.68	7.97	7.70	8.51
EC (mS/cm)	0.22	0.28	0.32	0.59
Anions:*		mg/dm³		
Cl^-	31	32	29	31
SO_4^{2-}	28	36	45	23
PO_4^{3-}	82	69	64	44
F^-	0.34	0.19	0.11	0.11
HCO_3^-	5.4	61	182	446
NO_3^-	20	32	22	3.6
Cations:*		mg/dm³		
Ca^{2+}	17	15	17	38
Mg^{2+}	9.0	10	21	33
Na^{2+}	25	39	55	39
K^+	8.7	24	20	25
NH_4^+	0.6	0.91	2.0	10
Trace metals:#		mg/dm³		
Fe	nd	18	7.0	0.70
Al	nd	19	12	1.1
Cu	0.46	<0.2	<0.2	<0.2
Cr	0.48	<0.1	<0.1	0.34
Mn	0.64	<0.04	<0.04	<0.04
Ni	1.2	3.0	1.1	1.0
Si	25	21	19	22
Co	0.84	<0.1	<0.1	0.80
Pb	2.2	<1.0	<1.0	1.8
Zn	0.93	0.64	1.2	0.68
Cd	0.16	<0.06	<0.06	0.13

nd - not determined ; * HPIC ; # ICP-AES

5.2.3. Soil acidification

The soils in the Steenkampskraal area are derived mainly from the metamorphosed granitic gneiss and charnochite intrusion hosting the ore body. These rocks generally have high concentrations of basic cations such as Ca, Mg, Na and K, thus resulting in soils with a relatively high buffering capacity and neutral to alkaline pH. Salts accumulate in soils that are not subject to frequent leaching, with the source of these salts being mineral weathering. Silicate mineral hydrolysis and dissolution is the major weathering process in most soil-forming materials (McBride, 1994). The cation associated with the alkaline anion of primary silicate minerals becomes critical in limiting the severity of alkalinity in the soil solution. Magnesium and Ca carbonates are not very soluble and are therefore less likely to cause alkaline soils than soils formed from minerals rich in K and Na. Since soils in arid regions are usually alkaline, soil acidification is very unusual. Extreme soil acidification has, however, occurred in the soils on the eastern side of the ore body, considering Reuss and Johnson (1986) classify soils as being acidic with pH values less than 5.5 when measured in water.

The pH values of the extracts along transect 1 (Table 5.1) are generally more acidic than the saturated paste extracts along transect 2 (Table 5.2), with the exception of sample 1/8. The soil pH along transect 2 and of sample 1/8 is neutral to alkaline and conforms to the expected pH range for uncontaminated soils in the area. The soils along transect 1 have become acidified, most likely through the oxidation of sulphide minerals in the tailings to form sulphuric acid (SO_4^{2-} values initially 9000 mg/dm^3), and are characterized by a dramatic increase in the concentration of acidic cations such as Fe, Al and Cu. Soils of transect 1 exhibit a general increase in pH away from the tailings.

In the pH range commonly encountered in acid soils, several ions in addition to H^+ neutralize OH^- ions. At very low pH, ie., < 4, Fe^{3+} consumes base for neutralization. In pH ranges of 4.5 to 7, Al^{3+} and in the case of transect 1, Cu^{2+} are successively more involved. Each of these ions hydrolyses, binding with OH^- ions and releasing H^+ ions from water (McLean, 1982). These ions may form complexes on the interlayer surfaces of clays (Jackson, 1960). In neither form are they exchangeable, but their presence gives a lower pH to the soil solution than if all of the acidity was in the form of exchangeable H^+ ions. pH is a "master variable" controlling ion exchange, dissolution/precipitation, reduction/oxidation, adsorption and complexation reactions (McBride, 1994).

The pH of the saturated paste extracts along transect 2 shows a general trend of pH increase away from the mine. This is possibly due to the decrease in the degree of contamination away from the ore body. By comparing the concentrations of dissolved ions in the saturated paste extracts along transects 1 and 2, it can be seen that the degree of contamination and acidification of the soils as a result of mining activity is very much lower along transect 2.

This is due to the absence of tailings on the western side of the ore body, thus resulting in a smaller volume of material as well as a smaller surface area in which dissolution of minerals can occur. Associated with the smaller volumes and surface area of contaminant material on the western side of the ore body (Transect 2) is a steeper gradient, thus significantly reducing the residence time of water in soils in the vicinity of the mine on the western side.

The EC of samples 1/2A and 1/2B (Table 5.1) can be regarded as high, considering saline soils have traditionally been classified as those with an EC of greater than 4 mS/cm (Sparks, 1995). The high EC values are due to the high concentrations of contaminant elements and ions released into the soils from the tailings material as a result of the low pH. As expected, EC values along transect 1 decrease away from the tailings material. In both samples 1/2 and 1/4 the A horizon has a higher EC than the B horizon, suggesting a dominance of surface transport. Electrical conductivity could be used as an indication of element contamination, decreasing along transect 1 and being consistently lower along transect 2.

5.2.4. Ion and element solubility

The effects of mining on the soil along transect 1 has resulted in a major change in the soil chemistry in the proximity of the tailings material. The SO_4^{2-}, PO_4^{3-} and F^- ion concentrations decrease, while the HCO_3^- and to some extent the Cl^- concentrations increase away from the tailings. This is expected as SO_4^{2-}, PO_4^{3-} and F^- ions are released from the tailings material.

The decrease in alkalinity (HCO_3^-) towards the tailings occurs due to the increase in strong acids within the soil solution. From the equations (Chapter 4):

$$K_H = H_2CO_3 / P_{CO2} = 10^{-1.41} \text{ at } 25°C$$
$$K_1 = H^+ + HCO_3^- / H_2CO_3 = 10^{-6.3} \text{ at } 25°C$$

These two equations can be combined to give the equation:

$$[H^+][HCO_3^-] = K_1K_HP_{CO2}$$

The increase in H^+ ions from the added acids (H_2SO_4) must result in a decrease in HCO_3^- for any fixed CO_2 pressure in the soil (soluble Al, Fe and Cu have been ignored for simplicity) (McBride, 1994). It is necessary to conclude that $[H^+] > [HCO_3^-]$ and charge balance requires that $[H^+] = [SO_4^{2-}]$, with HCO_3^- no longer being a function of pH.

Phosphate and to a lesser degree SO_4^{2-} are generally immobile (Mott, 1981), resulting in their rapid decrease in concentration along transect 1. Chloride is a more mobile anion and has higher concentrations in sample 1/4 than in sample 1/2. This might indicate the presence of a contamination plume moving outwards from the tailings material.

Sulphate adsorption in soils occurs when soils contain positively-charged sites. Positively-charged sites on a soil surface are accounted for by the uptake of protons from solution onto suitable sites, particularly under acidic conditions, when OH^- groups are protonated (Mott, 1981). Sulphate adsorption by soils is strongly pH dependent, as the pH dependent charge sites are responsible for most of the positive charge sites present in soils. Negatively-charged sulphate anions interact with soil minerals that possess surface hydroxyl groups. Such minerals include the noncrystaline aluminosilicates, oxides of Fe, Al and Mn and the edge sites of layer silicate clays (McBride, 1994). Sulphate has been found to be highly desorbable from kaolinite. This is, however, not the case for SO_4^{2-} desorption from hydrous oxides of Fe and Al (Mott, 1981).

Precipitation of Fe and Al sulphate minerals is another important mechanism in which sulphate is retained in soils (Sposito, 1989). Precipitation is distinguished from adsorption by the development of a three-dimensional molecular structure which could also develop on a surface to form a surface precipitate (Sposito, 1989). The precipitation reactions forming Al sulphate minerals are possible in high sulphate, low pH environments, where the resultant minerals are more stable than the existing Al solids such as gibbsite and kaolinite (Fey and Guy, 1993). Low pH is necessary to ensure sufficient Al in solution to enable the precipitation reactions to proceed (Sposito, 1989).

The mineralogy of the soils was not determined. It is, therefore, not known to what extent adsorption or precipitation regulates the SO_4^{2-} content of the soil. MINTEQA2 was used in an attempt to predict which SO_4^{2-} containing phases would be present in the system (Table 5.3). The saturation indices of jurbanite and jarosite decrease with distance from the tailings. This is expected due to the increase in pH resulting in decreased solubility of Fe and Al, coupled with the decrease in SO_4^{2-} concentration within the extract. The massive decrease in SO_4^{2-} along transect 1 may be occurring as a result of dilution due to the greater distance from the contamination source. Adsorption and precipitation of SO_4^{2-} would be more pronounced closer to the tailings due to the greater number of positively-charged sites as a result of the low pH. The soils close to the tailings may be saturated with SO_4^{2-} due to the unnaturally high concentrations, thus resulting in precipitation as the dominant mechanism of SO_4^{2-} removal.

Table 5.3. Calculated saturation indices for sulphate and phosphate bearing minerals for the saturated paste extracts along transect 1 (From MINTEQA2).

Mineral	Formula	1/2A	1/4A	1/6	1/8
Jurbanite	$AlOHSO_4$	0.9	-0.006	0.001	-4.0
Basaluminite	$Al_4(OH)_{10}SO_4.5H_2O$	-4.9	1.7	2.0	2.9
Alunite	$KAl_3(SO_4)_2(OH)_6$	3.9	5.9	5.7	1.7
Jarosite H	$HFe_3(OH)_6(SO_4)_2$	5.8	4.7	3.7	-1.2
Jarosite K	$KFe_3(OH)_6(SO_4)_2$	9.0	9.3	8.0	5.8
Gypsum	$CaSO_4.H_2O$	0.5	-0.4	-1.0	-2.0
Strengite	$Fe(PO_4).2H_2O$	4.3	4.2	4.1	3.2
Cu phosphate	$Cu_3(PO_4)_2$	0.02	0.7	0.4	0.4

The concentrations of PO_4^{3-} in soils, like waters would be regulated by the presence Fe, and to some degree Al, in the system as described in chapter 4. The saturation indices of strengite along transect 1 indicates the importance of Fe in PO_4^{3-} retention (Table 5.3). The unusually high Cu concentrations in the soils associated with the tailings at Steenkampskraal has resulted in the prediction of positive saturation indices for $Cu_3(PO_4)_2$ in the saturated paste extracts along transect 1.

Chloride is termed a mobile anion due to its ability to be transported through soils without being retained to any significant degree. Since charge balance requires that the negative charge of soluble anions be balanced by positive charge of the associated soluble cations, anion mobility always implies cation mobility (McBride, 1994). The CO_3^{2-}, HCO_3^-, PO_4^{3-}, and OH^- anions are considered to be immobile anions in soils, and are not viewed as potential cation carriers. When materials such as $CaCO_3$, $CaSO_4$ and $CaCl_2$ are added to acid soils, Ca mobility is very limited. If $CaSO_4$ is added to acid soils possessing few cation exchange sites Ca^{2+} is generally mobile (unless SO_4^{2-} is adsorbed to a large degree). When $CaCl_2$ is added to acidic soils, the Cl^- adsorbs to an even lesser degree than SO_4^{2-}. Mobile anions are therefore indicators but not agents of cation mobility (McBride, 1994). The vertical movement of the various anions down the soil profile (McBride, 1994) could explain the relative mobility of the various anions along transect 1.

The effects of mining on the soil along transect 2 has resulted in a relatively minor change in the soil chemistry, due to the naturally high buffering capacity of the local soils, the steep gradient and rapid run-off and the small surface area of the contaminant material. The SO_4^{2-} ion concentrations have no general trend away from the ore body. This is associated with a relatively low concentration of chalcophile elements in the soil solutions.

Table 5.4. Calculated MINTEQA2 speciation of copper in the saturated paste extracts along transect 1. Values represent percentages of speciation complexes.

Sample	1/2A	1/4A	1/6	1/8
	59 Cu^{2+} 40 $CuSO_4(aq)$	76 Cu^{2+} 23 $CuSO_4(aq)$ 1.4 $CuCl^+$	81 Cu^{2+} 18 $CuSO_4(aq)$	3.0 Cu^{2+} 34 $CuCO_3(aq)$ 60 $Cu(OH)_2(aq)$ 2.0 $CuHCO_3^+$

The saturated pastes along transect 1 were calculated to be supersaturated with respect to both cuprousferrite and copper phosphate (Table 5.5), thus indicating precipitation as a possible mechanism of Cu removal.

Table 5.5. Calculated saturation indices for copper minerals for the saturated paste extracts along transect 1 (From MINTEQA2).

Sample	1/2A	1/4A	1/6	1/8
$Cu_3(PO_4)_2$	0.02	0.7	0.4	0.5
Cuprousferrite	7.1	12.4	11.7	18.7

Lead exists in soils principally in the Pb^{2+} oxidation state. The risk of lead movement from soils to edible plant parts is believed to be low. The major health concern with Pb-polluted soils arises from the contamination of edible plants by soil particles and subsequent ingestion by humans or grazing animals (McBride, 1994).

From the calculated speciation of Pb (Table 5.6), it can be seen that the Pb^{2+} ion and the $PbSO_4(aq)$ complex are dominant at very low pH values, (ie those samples closer to the tailings). With an increase in pH, the SO_4^{2-} complex becomes less important and the free Pb^{2+} ion more important. The carbonate complexes dominate in sample 1/8 as a result of the alkaline pH. The calculated speciation is very similar to that of Cu (Table 5.4).

Table 5.6. Calculated MINTEQA2 speciation of lead for the saturated paste extracts along transect 1. Values represent percentages of speciation complexes.

Sample	1/2A	1/4A	1/8
	29 Pb^{2+}	46 Pb^{2+}	2.6 Pb^{2+}
	3.5 $PbCl^{+}$	13 $PbCl^{+}$	1.4 $PbOH^{+}$
	54 $PbSO_4(aq)$	39 $PbSO_4(aq)$	92 $PbCO_3(aq)$
	14 $Pb(SO_4)_2^{2-}$	2.0 $Pb(SO_4)_2^{2-}$	2.5 $PbHCO_3^{+}$

The saturated pastes along transect 1 displayed a number of trends with respect to saturation indices of Pb minerals (Table 5.7). The saturation indices of the lead phosphate minerals increased with the increase in pH away from the tailings (Samples 1/2 to 1/8). Lead sulphate (anglesite) was supersaturated only at low pH within sample 2/1, and lead hydroxide is calculated as being present only in sample 1/8, at high pH.

Table 5.7. Calculated saturation indices for lead minerals for the saturated paste extracts along transect 1 (From MINTEQA2).

Sample	1/2A	1/4A	1/8
Plumbogummite $(PbAl_3(PO_4)_2(OH)_5H_2O)$	2.6	8.4	12.0
$Pb_3(PO_4)_2$	−2.2	0.6	----
Anglesite ($PbSO_4$)	0.6	−0.6	−2.4
$Pb(OH)_2$	----	----	0.2

The concentrations of some of the trace metals determined in the saturated paste extracts are highly dependent on the pH of the soil extract. By plotting log concentration of various metals against pH, an attempt was made to determine whether pH could be used to predict the concentrations of contaminant metals within the soil solution. Copper and Mn concentrations for all the saturated paste extracts have been plotted against pH (Figure 5.3). These metals were chosen due to the fact that Cu is abundant in the ore body whereas Mn is presumed to be more evenly distributed across the local terrain.

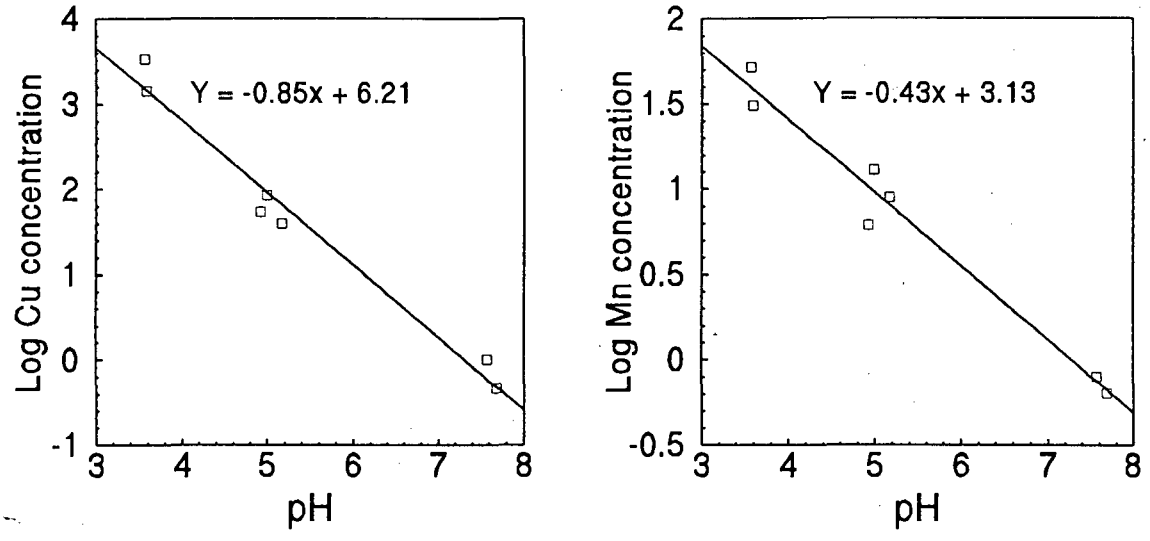

Figure 5.3. Plots of log concentration against pH for Cu and Mn for all saturated paste extracts. Concentration units in mg/dm^3.

Both Cu and Mn display strong linear relationships when the log of the concentration is plotted against pH. At very low pH values there is a sharp rise in the concentration of Cu, probably due to the abundance of Cu within the tailings associated with the very large surface area in which mineral dissolution can occur. Elevated concentrations of Mn are not expected in the ore body which has prevented the rise in Mn concentration at low pH.

Log activity against pH graphs of Cu and Mn were also plotted as the activity of the various metals would be a more accurate way of demonstrating the pH dependence. The linearity was, however, not improved when log activity was plotted against pH. Similar plots were made using other elements and ions such as Zn and PO_4^{3-}. These did not produce linear relationships from which a prediction of solution concentration could be made.

It is interesting to note that for Cu, each unit increase in pH results in a unit increase in Cu concentration, whereas for each unit increase in pH for Mn, there is only a half unit increase in the Mn concentration. The difference is likely to be due to the different valence states of the two metals, with Mn being in the tetravalent state and Cu being in the divalent state.

5.3. Organic carbon

The organic carbon content of the 10 selected soil samples is low (Table 5.8), considering soil organic matter contents range from 0.5 to 5 % in the surface horizon (Sparks, 1995). The organic carbon content of the Steenkampskraal soils is expected to be low (usually less than 0.3%) (Soil Classification Working Group, 1991), due to the very dry climate and sparse vegetation.

Table 5.8. Organic carbon from selected soil samples.

Sample	Organic C (%)
1/2A	0.44
1/2B	0.09
1/4A	0.50
1/4B	0.11
1/6	0.44
1/8	0.17
2/1	0.17
2/3	0.20
2/5	0.50
2/7	1.11

5.4. Total chemical analysis

Significant migration cannot occur, even with high solubility elements, unless there is water movement through the soil. The low annual rainfall at Steenkampskraal would limit the movement of the elements in solution. It is expected that although elemental mobility in solution does occur, the majority of the elemental transport occurs through the physical movement of material away from the tailings in short heavy storms during the rainy season, and to some extent from the movement of tailings material via wind erosion. Cabrera et al. (1984) found that high concentrations of metals were present in water and sediments originating from polymetallic sulphide deposits and old mine-spoil heaps. During heavy rains sediments were resuspended and transported downstream. Batson et al. (1996) found that between 1500 and 2800 % more U was transported during episodic storm events when compared to the same period of base flow measurements. The amount of eroded sediment depends on the intensity and duration of rainfall, and the soil susceptibility or resistance to erosion (Batson et al., 1996). The association of metals with suspended sediments is well established (Trefry, 1977). Suspended particulate matter was reported to transport more than 90 % of the metal load associated with the Mississippi river (Trefry, 1977).

Martin and Meybeck (1979) established a dissolved transport index that compared dissolved to particulate associated metal transport. The ratio showed that more than 90 % of the total U and other heavy metal load was transported by river particulates.

It was, therefore, considered important to analyze the total concentrations of contaminant elements in the soil, in an attempt to determine the extent of contamination from the mine. X-ray fluorescence spectrometry and ICP-MS were used to determine the total concentrations of the elements within the soil. All soil samples along both transects were analyzed (Figure 5.4).

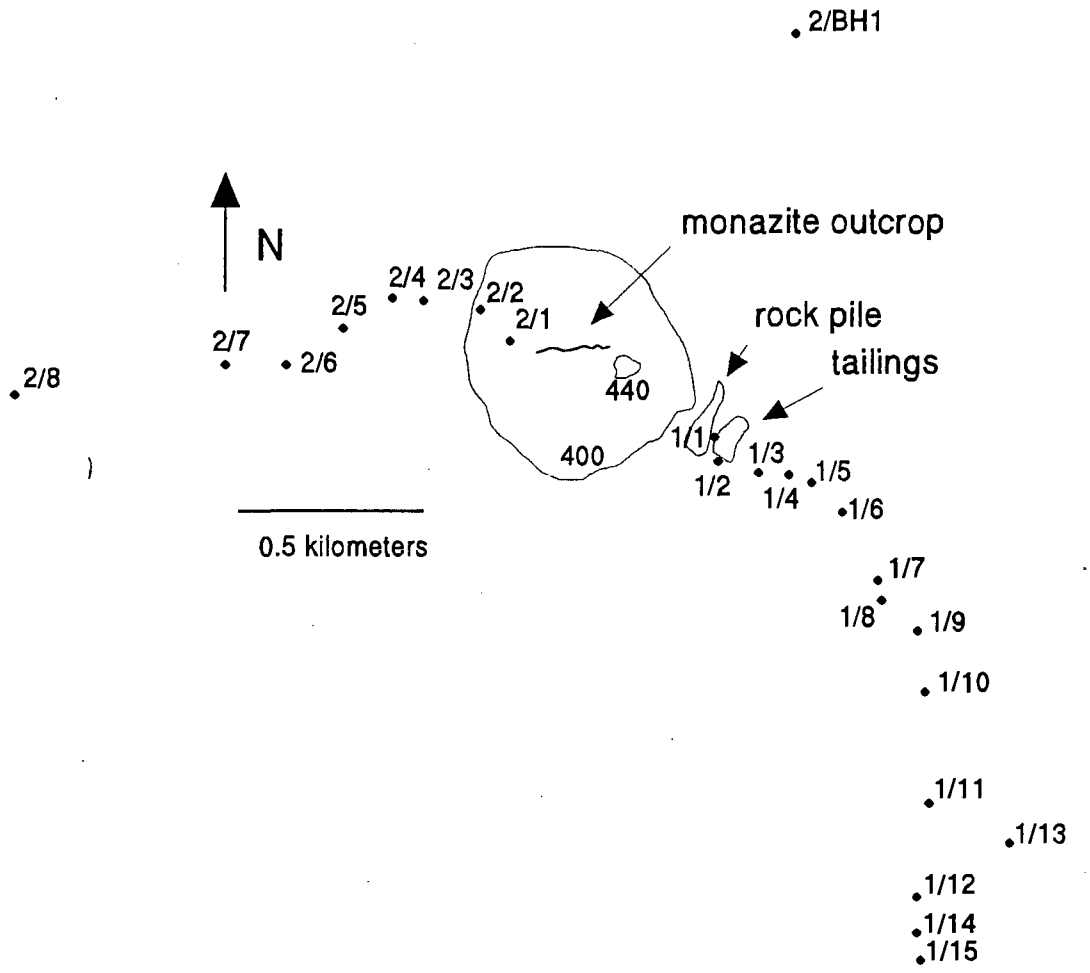

Figure 5.4. Locality map of sample positions along transects 1 and 2. Sample location of 2/9 to 2/12 are included in Figure 3.2.

The concentrations of all elements analyzed by XRF have been listed in Appendix 5. Lead, Cu, Ni, Cr, U, Th and Y have been represented graphically in this chapter. The concentrations of Zn, Co, Mn, Sr and Rb do not show obvious contamination trends with respect to relative concentrations along transect 1 or 2, and have not been represented graphically in this chapter. A semi-quantitative major element analysis has also been listed in Appendix 5. The major element analysis was done on powder briquettes and loss on ignition data was not included.

5.4.1. Subsurface dorbank

The low lying area surrounding the outcrop within the Steenkampskraal area is characterised by a siliceous dorbank below the surface soil. A dorbank (Afrikaans word for dry hard layer) is synonymous with the duripan of other classification systems (Soil Classification Working Group, 1991). The dorbank is a common feature of soil in semi-arid climates and is a hard subsurface horizon cemented by silica. Dorbanks may often contain accessory cements, mainly calcium carbonate and iron oxides (Soil Classification Working Group, 1991). The soils in the Steenkampskraal area have been classified as belonging to the Knersvlakte form, with a non-calcareous orthic A horizon overlying the dorbank (Soil Classification Working Group, 1991).

Both the trace element and major element XRF analyses of two dorbank samples, one from each transect, have been included in Table 5.9. Both are dominated by SiO_2, with Al_2O_3 and Fe_2O_3 present in high concentrations. Although CaO concentration were very low in these two samples, it is possible that the high concentration of colloidal calcite in the water from BH 6 could be due to the presence of a calcite-rich dorbank in that area. The concentrations of trace metals within the dorbank were found to be consistently lower than in the soil sampled closest to the dorbank sample (locality positions in Figure 3.1). The trace element analyses of soil samples 1/6 and 2/7 have been included in Table 5.9 for comparison.

The trace element differences between the dorbank samples and the soil samples are not as pronounced in transect 2 as in transect 1, due to the lower degree of contamination along transect 2. The dorbank sample on transect 2 was also exposed to the surface, thereby increasing the possibility of contamination. The presence of the dorbank at Steenkampskraal has probarbly resulted in little vertical movement of contaminant elements, with movement being largely restricted to the surface in a lateral direction.

Table 5.9. Trace element and major element analyses of samples 1/DOR and 2/DOR, with the associated soil samples 1/6 and 2/7.

	DOR/1	1/6	DOR/2	2/7
Trace element analysis (mg/kg)				
Pb	50	84	49	53
Cu	19	579	78	84
Ni	14	35	36	54
Cr	50	110	9	70
U	7	17	2	4
Th	33	500	27	58
Y	33	195	43	53
Major element analysis (%)				
Fe_2O_3	3.3		7.4	
TiO_2	0.39		0.53	
BaO	0.069		0.055	
CaO	0.39		0.34	
K_2O	5.0		4.2	
SO_3	0.023		0.023	
P_2O_5	0.079		0.089	
SiO_2	68		61	
Al_2O_3	13		16	
MgO	1.0		3.1	
Na_2O	1.3		0.99	

5.4.2. Transect 1

As can be seen from Figures 5.5 and 5.6 (values in Appendix 5), all 7 of the elements (Cr, Cu, Ni, Pb, U, Th and Y) have a similar relative concentration trend along transect 1. As expected, sample 1 has much lower concentrations than sample 2, due to the fact that the sampling position of sample 1 was between the rock pile and the tailings dam and it is presumed that most of the elements are released from the tailings due to both the larger surface area for dissolution and the greater susceptibility of tailings material to mass transport. The position of sample 2 was within soil which had been exposed to a high degree of contamination from tailings material.

Sample 12 is interesting in that it comes from within the Nabeep River bed upstream of the junction with the entry point of the mine spoil run-off. It was, therefore, originally thought that the higher concentrations in sample 12 were from other deposits upstream along the Nabeep River. Sample 13 was later sampled even further upstream in the Nabeep river in an attempt to confirm the origin of the high concentrations of sample 12. The concentrations of all elements believed to be high as a result of monazite mining at Steenkampskraal were found to be relatively low in sample 13. The origin of the element contamination of sample 12 is therefore not known.

The relative concentrations along transect 1 suggest the majority of the soil contamination has occurred as a result of transport of tailings material away from the tailings dump. The degree of contamination is initially very high, but drops off rapidly and reaches a fairly stable value at about sample 7, approximately 600 meters from sample position 1.

Sample positions 1/2, 1/3 and 1/4 had two distinct horizons above the dorbank. In all three samples, the B horizon was darker and more dense than the A horizon. Obvious differences in the concentration of U, Th and Y can be seen between the A and B horizons of samples 1/2, 1/3 and 1/4 (Figures 5.7). Again a similar trend can be seen between the three elements, with the difference occurring in relative concentrations. In the field, sample 1/2 was found to have the most obvious horizon differentiation, with the B horizon being much more compact than the A horizon. Samples 1/3 and 1/4 were found to have a progressively lower degree of horizon differentiation, with no differentiation occurring in sample 1/5. In Figure 5.7, smaller U, Th and Y concentration differences occur between the two horizons as the degree of horizon differentiation decreases.

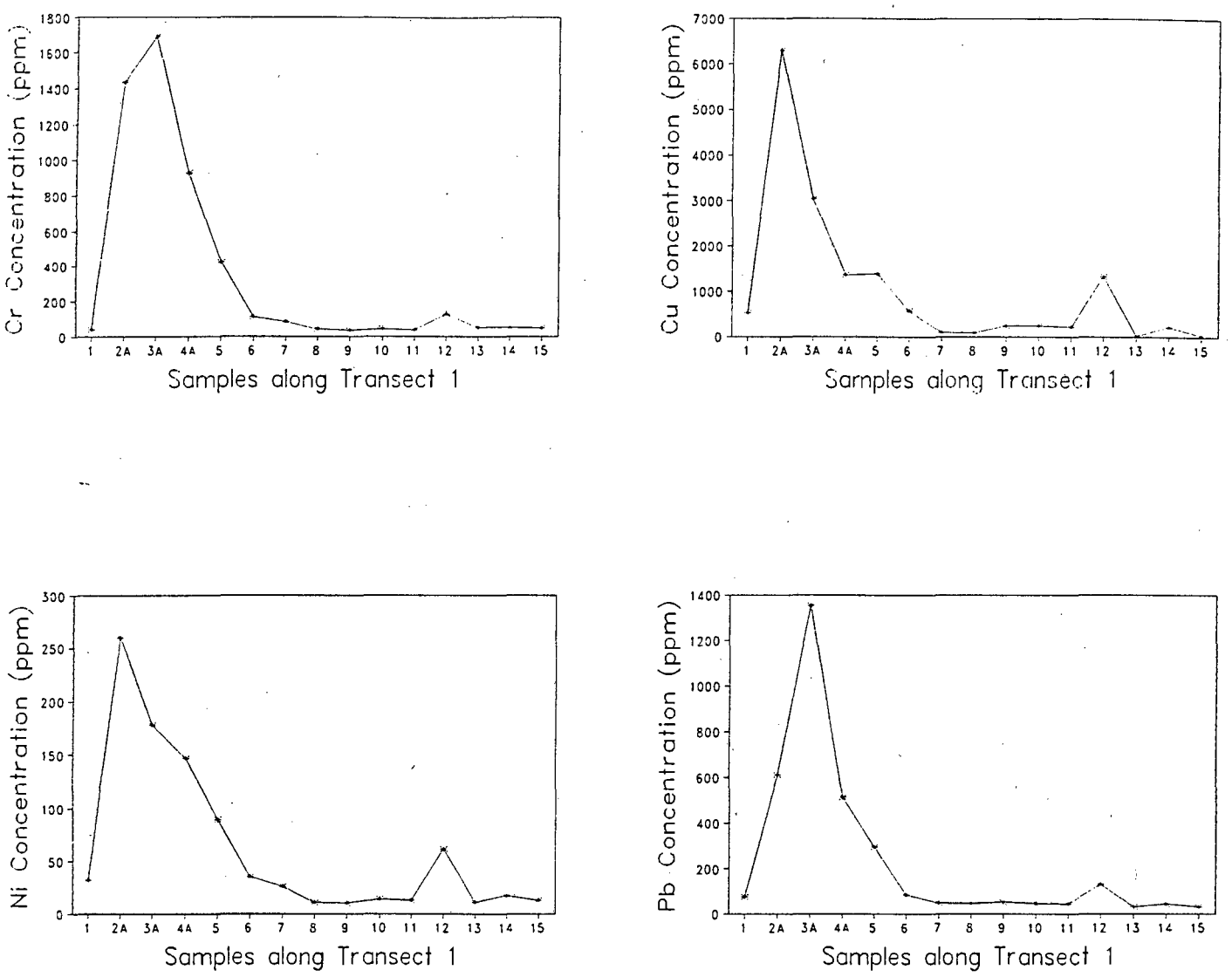

Figure 5.5. Concentrations of Cr, Cu, Ni and Pb in soils along transect 1.

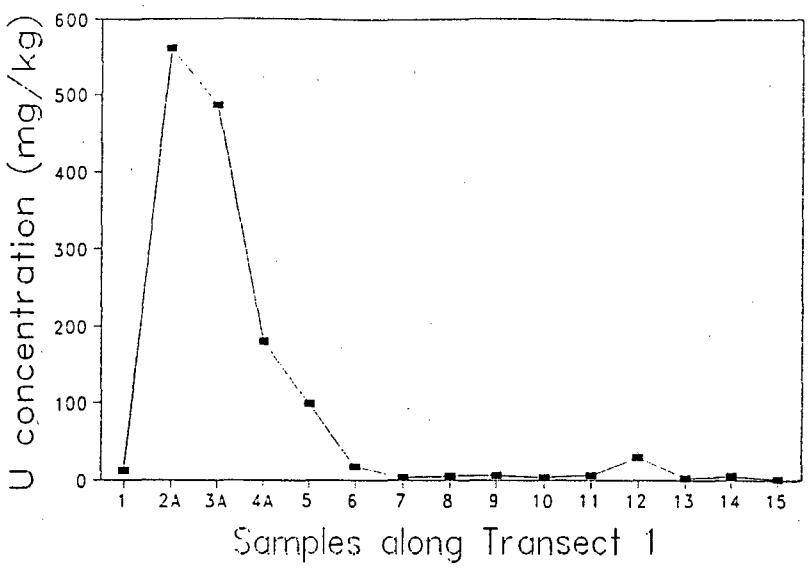

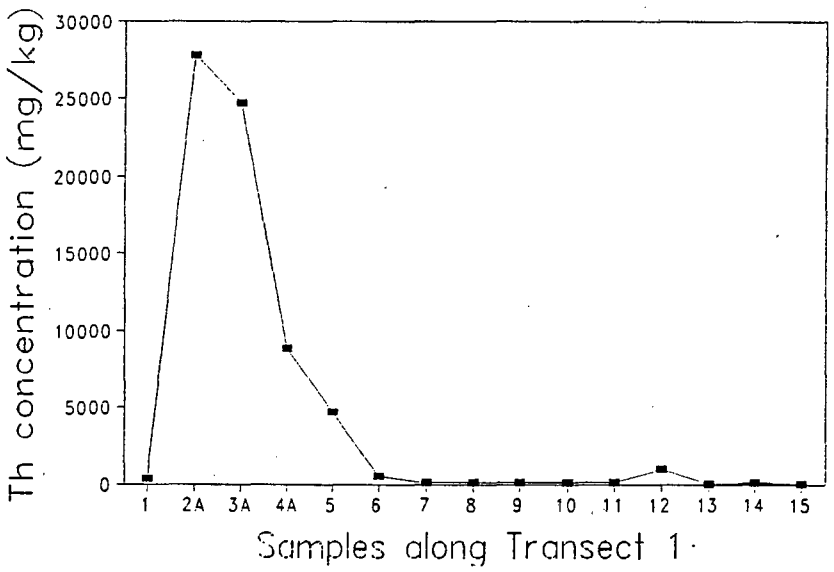

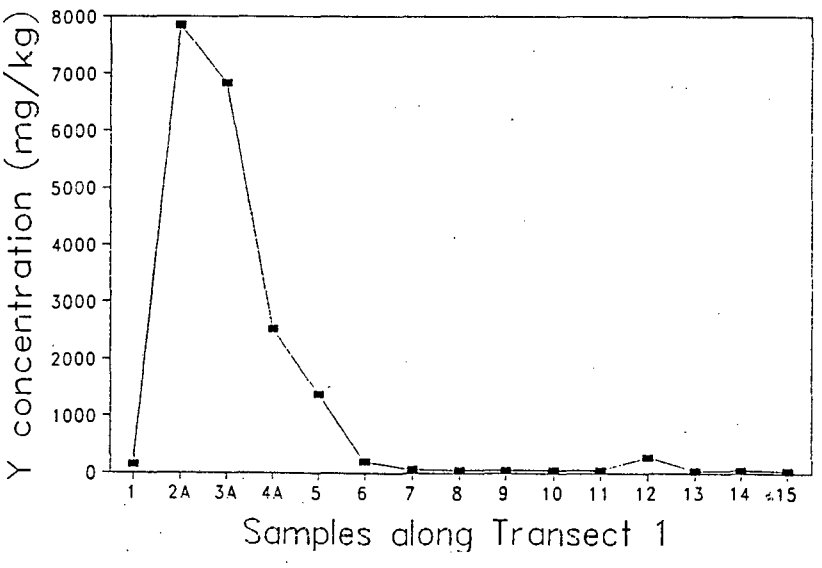

Figure 5.6. Concentrations of U, Th and Y in soils along transect 1.

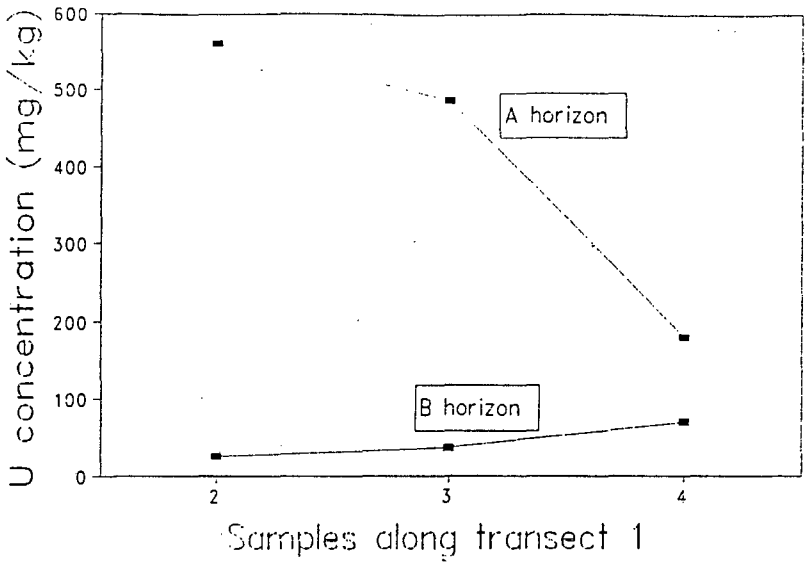

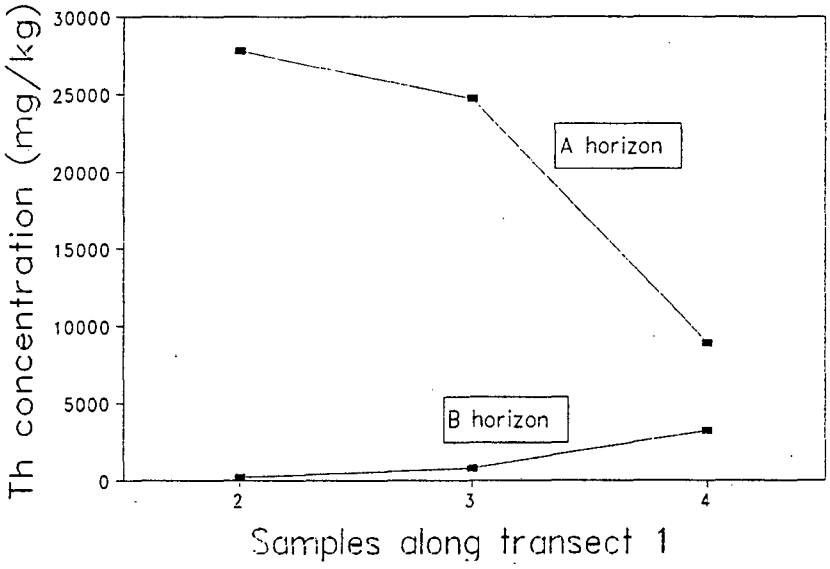

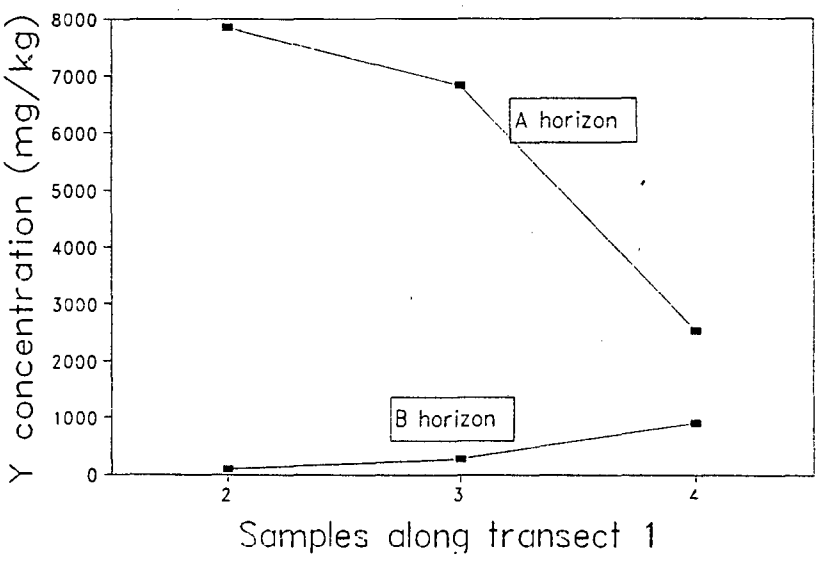

Figure 5.7. Concentrations of U, Th and Y within the different horizons of soil samples 1/2, 1/3 and 1/4.

5.4.3. Transect 2

From Figures 5.8 and 5.9 (values in Appendix 5), there are two distribution trends with the same 7 elements (Cr, Cu, Ni, Pb, U, Th and Y) along transect 2. Sample BH 1 is a background sample taken north of the mine, and is, therefore, believed to have no influence from mining activity. This is confirmed by the relatively low concentrations.

Lead and Cu along transect 2 have similar distribution trends. The highest concentrations occur closest to the ore body and decrease rapidly away from the mine. The Cr and Ni plots have a different trend, with a slight decrease away from the mine, followed by a rapid increase starting at about sample position 5 and reaching a maximum around sample position 7 before decreasing again. There is also a slight increase in the concentrations of Pb and Cu in sample position 7, which is, however, not as pronounced. The U, Th and Y trends are similar to that of Pb. There are, however, no relative increases of U, Th and Y around sample position 7.

The degree of contamination from mining operations along transect 2 is much lower than along transect 1. Transect 2 has the same general trend as transect 1, in that the concentrations of the contaminant elements are initially higher than the background concentrations, and drop off rapidly to reach a fairly stable value at about sample position 5, approximately 470 meters from sample position 1.

The increase in Cr and Ni starting at sample position 5 is likely to be due to a change in the country rock to a more mafic type. Pike (1959) found the basement to consist of a mafic rock to the west of the mine in the same vicinity of samples 2/5 outwards. The rocks were classified as the Mafic Granulite Group of the Malmesbury formation. Pike (1959) found that these rocks consist of variable proportions of plagioclase, orthoclase, hypersthene, biotite, almandine, cordierite, sillimanite, quartz, magnetite, ilmenite, pyrite, apatite and zircon. Their type occurrence is in the west of the mine, where they are associated with metaquartzites. The exact locality of the Mafic Granulite Group was not given by Pike (1959), but it is likely that the different concentration patterns and the increase in the mafic elements such as Cr and Ni is due to the presence of the Mafic Granulite group.

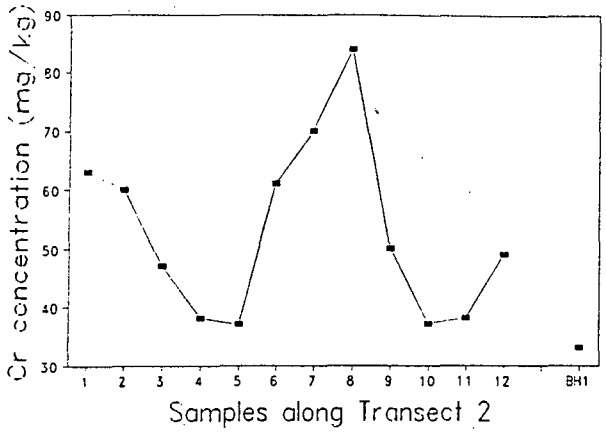

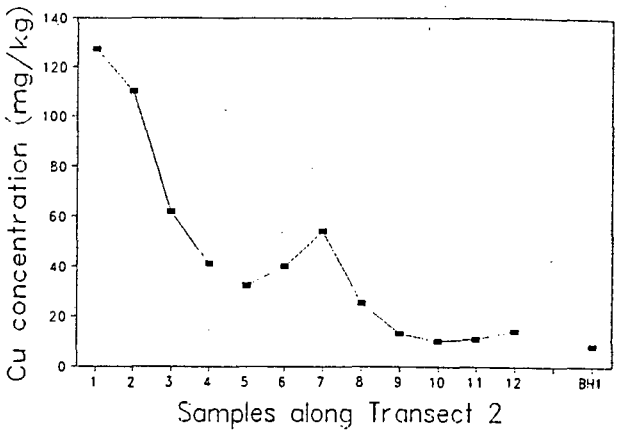

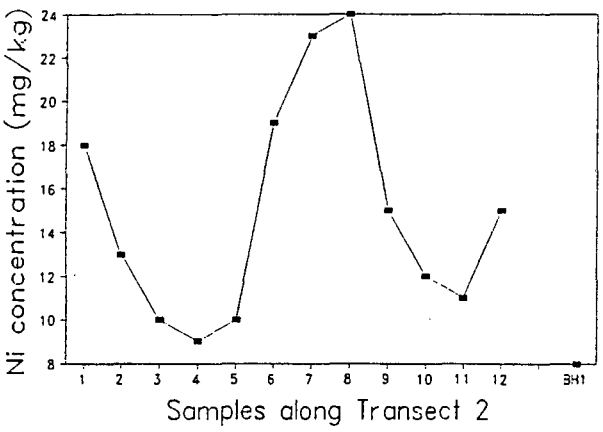

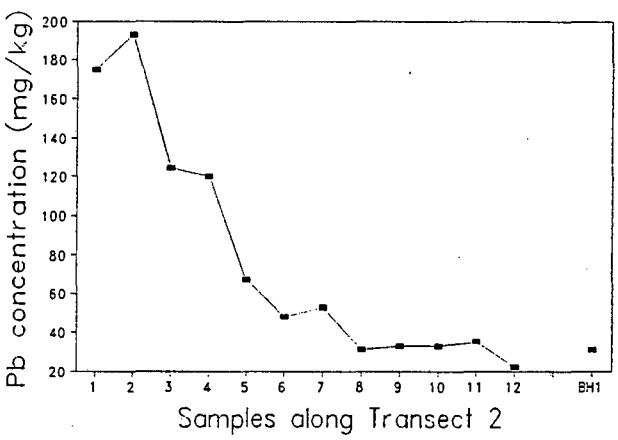

Figure 5.8. Concentrations of Cr, Cu, Ni and Pb in soils along transect 2. Sample BH 1 is included for reference as a representative background concentration and is not part of the transect.

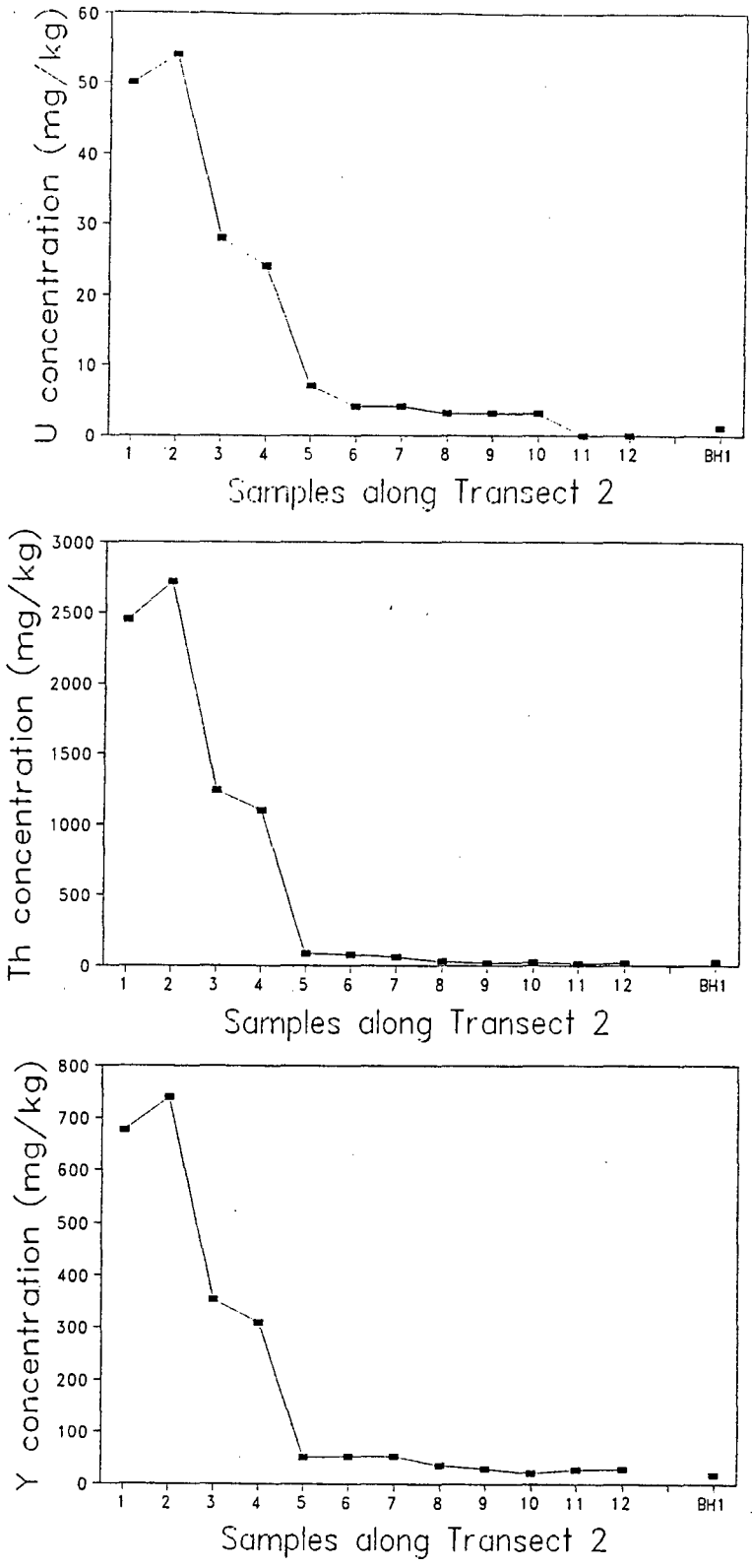

Figure 5.9. Concentrations of U, Th and Y in soils along transect 2. Sample BH 1 is included for reference as a representative background concentration and is not part of the transect.

5.4.4. Trace metal distribution with particle size

The concentrations of various trace elements in the different particle size fractions were determined in soil samples 1/4A and 2/3. A knowledge of these concentrations can give an idea as to the mechanism of elemental transport within the soil. From Figures 5.10 (values in Appendix 5) it can seen that the concentions of U, Th and Y in the size fraction analysis of sample 1/4A are highest in the finer fractions of the particle size range. Erosion has been found to remobilize contaminants associated with the clay fraction of sediments, and contribute to their concentration in the suspended sediment load in streams and rivers (Batson et al., 1996). The range between 0.5 and 0.065 mm contains the highest concentrations of the three elements. Ghadiri and Rose (1991) found that erosion was an effective process for the selective removal of fine particles (<53 μm) from sediments.

The concentrations of the U, Th and Y in the size fraction analysis of sample 3 along transect 2 (Figure 5.11) have a bimodal trend different to that of sample 4 along transect 1 (Figure 5.10). In all three plots the coarse fraction (>2 mm) contains the highest concentration of the metals. This is most likely due to the coarser nature of the soil on transect 2. The soils along transect 1 have a small proportion of coarse fraction, as most of the contamination is released from crushed tailings material. Other than the coarse fraction, the highest concentrations of all three elements are bound in the 0.5 and 0.065 mm particle size range, similar to sample 4 of transect 1. The finer fraction would be preferentially eroded, resulting in an accumulation of contaminant metals. This is similar to the results found by Ghadiri and Rose (1991).

The mass distributions for the different size fractions of both samples have been plotted in Figure 5.12. By far the most abundant size fraction in sample 1/4A is the 0.25 to 0.125 mm fraction. This is the same fraction in which the highest concentrations of U, Th and Y were present. The low percentage of coarse fraction (>2 mm) is due to the absence of the coarse fraction in the tailings. The low percentage of fine fraction (<0.125 mm) is due to the expected low clay content of the Steenkampskraal soils and lower particle size limit to which the original material was crushed.

Sample 2/3 has a more uniform mass distribution than sample 1/4. The most abundant size fraction in sample 2/3 is the 1 to 0.5 mm fraction. The coarse fraction (>2 mm) of sample 2/3 is much more abundant than the coarse fraction of 1/4A, with the coarse fraction of 2/3 being the fraction in which the highest concentrations of U, Th and Y were present. The low percentage of fine fraction (<0.065 mm) is expected due to the low clay content of the soils. The trends observed along both transects would be expected due to fact that monazite is highly resistant to weathering, therefore transport mainly occurring in the coarse fraction. The massive increase in surface area from crushed tailings material has resulted in elemental transport occurring in a finer fraction along transect 1.

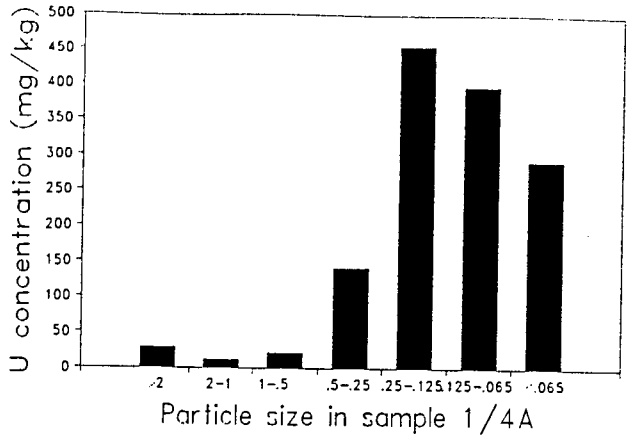

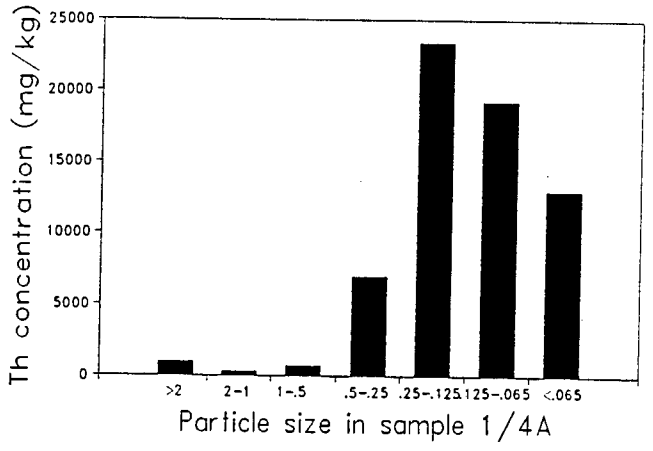

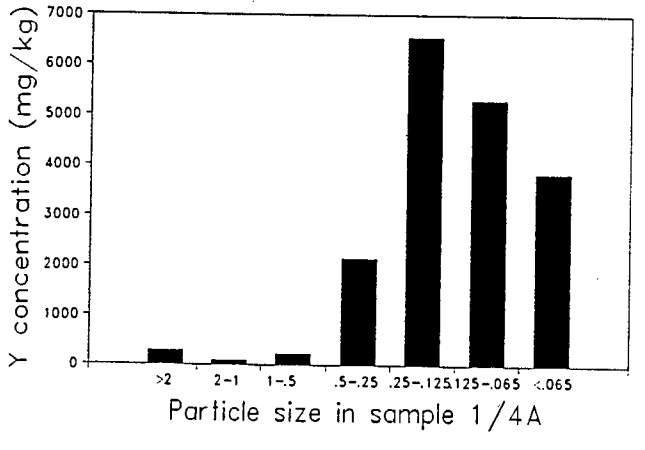

Figure 5.10. Concentrations of U, Th and Y within the different particle sizes of soil sample 1/4A (Units: mm).

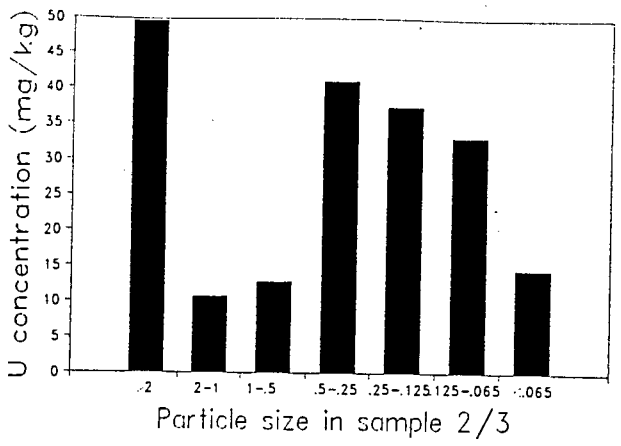

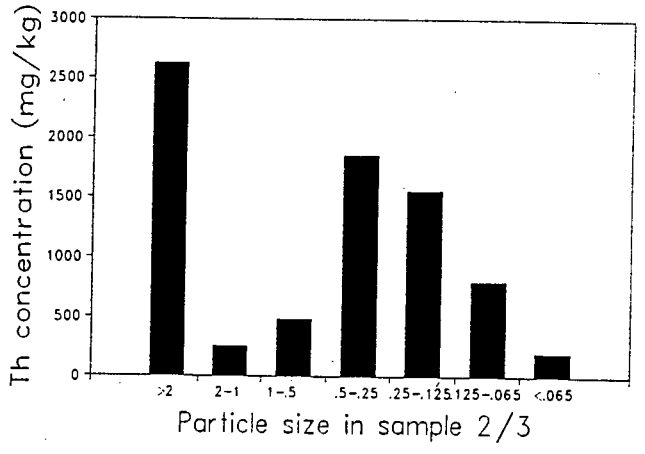

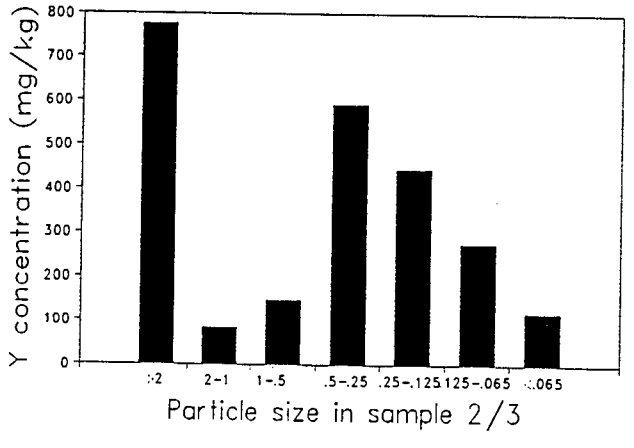

Figure 5.11. Concentrations of U, Th and Y within the different particle sizes of soil sample 2/3 (Units: mm).

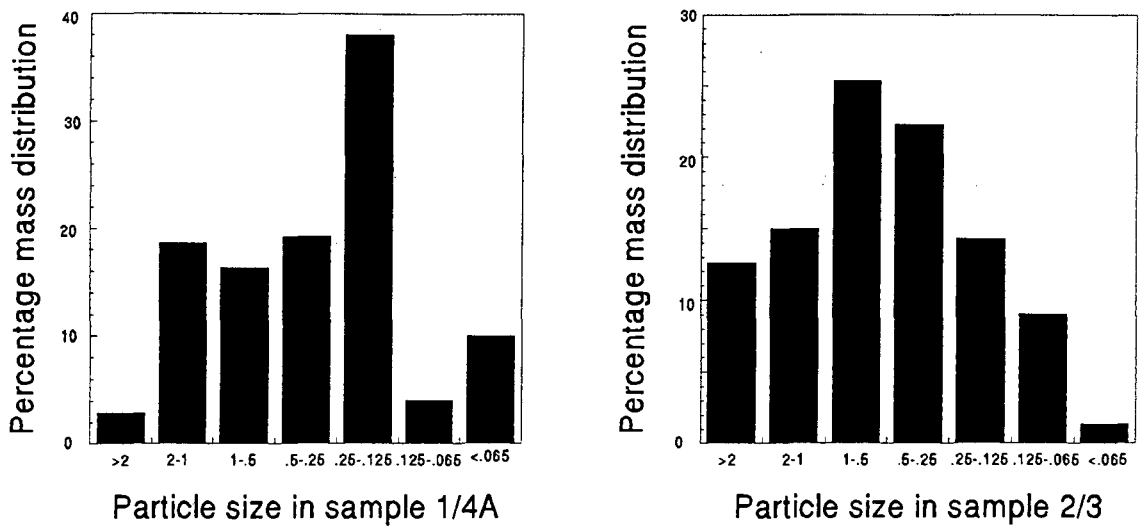

Figure 5.12. Mass distribution of the different particle sizes in soil samples 1/4A and 2/3.

5.4.5. Rare earth element distribution patterns

Most work on the behaviour of REE in soils has concentrated on the vertical movement and REE fractionation originating from the weathering of primary material (Gouveia et al., 1993; van der Weijden and van der Weijden, 1995; Mongelli, 1992; Walter et al., 1995; Marsh, 1990; and Braun and Pagel, 1994). Literature on the horizontal movement of REE away from a contaminated point source is scarce.

Fractionation of REE during the weathering of a parent rock can result in different REE patterns in different parts of the weathering profile (Duddy, 1980; van der Weijden and van der Weijden, 1995). Samples 1/2A and 1/4A (Figure 5.13) have, however, developed a similar chondrite-normalized REE pattern to that of monazite, with a well developed Eu depletion and very strong enrichment in LREE with respect to HREE. This is expected as REE in the tailings would control the chondrite-normalized REE distribution patterns of the nearby soil, and monazite would control the REE distribution in the ore body and surrounding rocks. Yunxiang (1995) found the rare earth phosphates to control the distribution trends of igneous rocks despite the fact that they were usually present only as accessory phases.

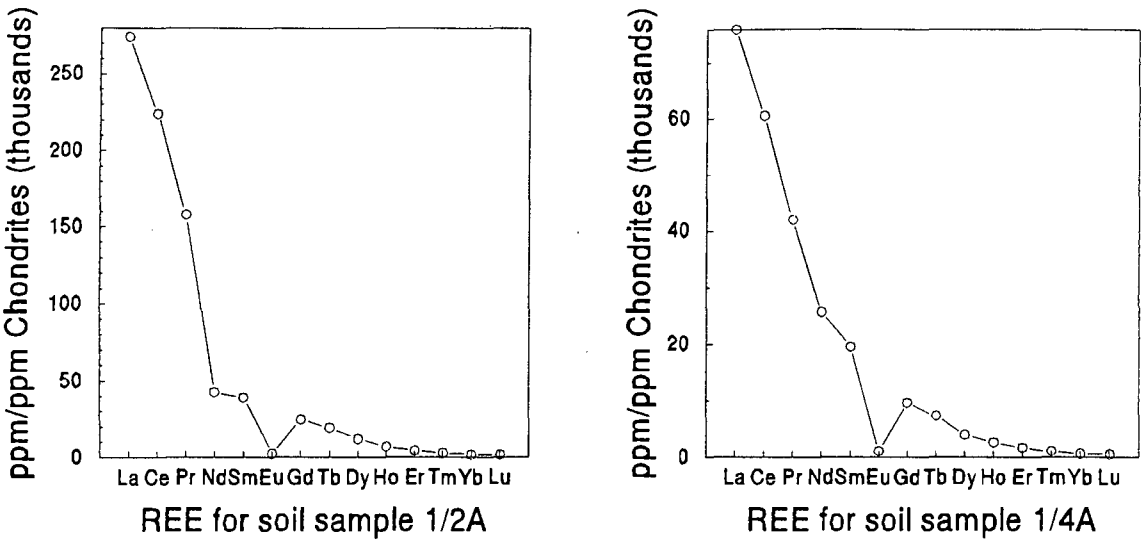

Figure 5.13. Chondrite-normalized REE data for soil samples 1/2A and 1/4A along transect 1.

The chondrite-normalized REE patterns of samples 1/11, 1/12, 1/14 and 1/15 (Figure 5.14), have a slightly different REE pattern to samples 1/2A and 1/4A, in that they have developed a distinct Ce depletion. Cerium enrichments in soils develop as a result of the oxidation of Ce^{3+} to Ce^{4+}, which is stabilized as CeO_2, while the other REE present in the more soluble ionic state are leached by circulating waters (Marsh, 1990). The absence of a Ce depletion in samples 1/2A and 1/4A (Figure 5.13) is probably due to the low pH of the soil solutions, thus inhibiting the oxidation of Ce^{3+} to Ce^{4+}. Cerium depletions in the soil are necessarily associated with Ce enrichments in other parts of the weathering profile (Marsh, 1990). Cerium has been removed during the movement of the material along the transect (Figure 5.14). It would be expected that as the pH conditions along transect 1 changed from acidic to neutral, Ce would be oxidized from Ce^{3+} to Ce^{4+} and removed from solution. This may result in a Ce enrichment following the Ce depletion along the transect as a pollution plume migrated. The large distance between samples may have been a reason for the fact that no Ce enrichments were found. The movement of material as a result of erosion would also complicate the concordance in observations with this theory since precipitated CeO_2 would also move during storm events.

As mentioned earlier, the origin of the contamination in sample 1/12 is not known. The relatively high concentrations of Cu, Pb, U, Th and REE as well as the distinct Eu depletion and LREE enrichment indicate that the source of the contamination is a monazite-sulphide rich ore body similar to Steenkampskraal. The Ce depletion would have developed after the emplacement of the material.

The chondrite-normalized REE pattern of sample 1/15 has no Eu depletion, with a Ce depletion and lower degree of LREE enrichment with respect to HREE. Sample 1/15 receives very little, if any, contaminant material from the mine due to the presence of a dam wall across the Nabeep river. The lack of the Eu anomaly could be due to the decrease in REE contribution from monazite and the increase in REE contribution from other mineral phases enriched in Eu such as plagioclase feldspar. The chondrite-normalized REE pattern of plagioclase (Figure 2.1) is enriched in LREE with respect to HREE, and has a Eu enrichment due to Eu^{2+} substitution into the feldspar structure. The actual concentrations of REE in plagioclase are very low compared to monazite, and it is not known to what extent the presence of abundant plagioclase would counterbalance a Eu depletion.

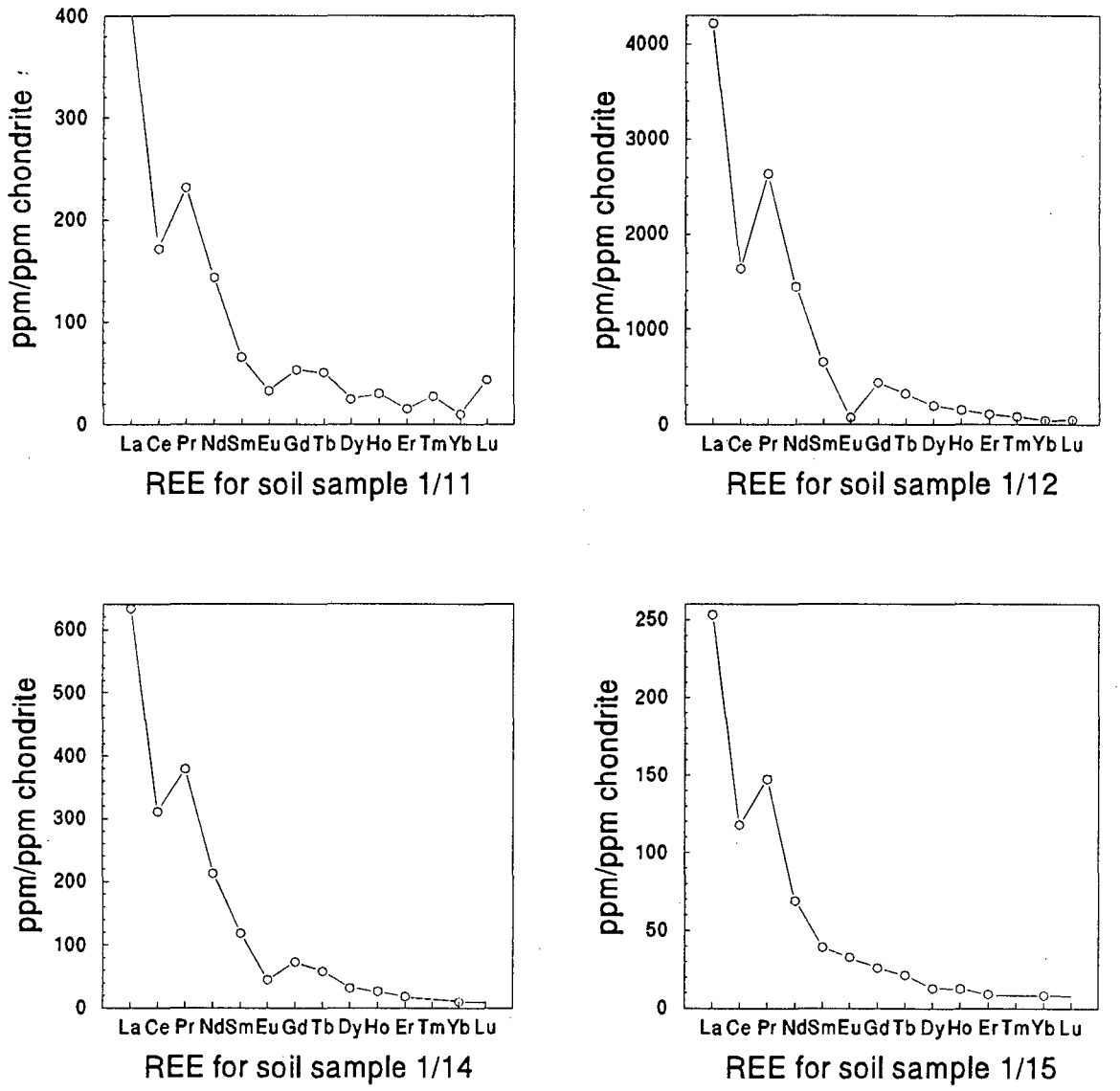

Figure 5.14. Chondrite-normalized REE data for soil samples 1/11, 1/12, 1/14 and 1/15 along transect 1.

The chondrite-normalized REE patterns of samples 2/1, 2/3, 2/5 and 2/7 (Figure 5.15) have a similar REE pattern to samples 1/11, 1/12, 1/14 and 1/15, in that they have also developed a monazite chondrite-normalized REE pattern with a distinct Ce depletion. The neutral to alkaline pH of the soil samples along transect 2 favours the oxidation of Ce^{3+} to Ce^{4+}, which is stabilized as CeO_2 (Figure 2.2). The destination of the Ce within the soil along transect 2 is not known. As in transect 1, it would be interesting to determine the destination of the Ce.

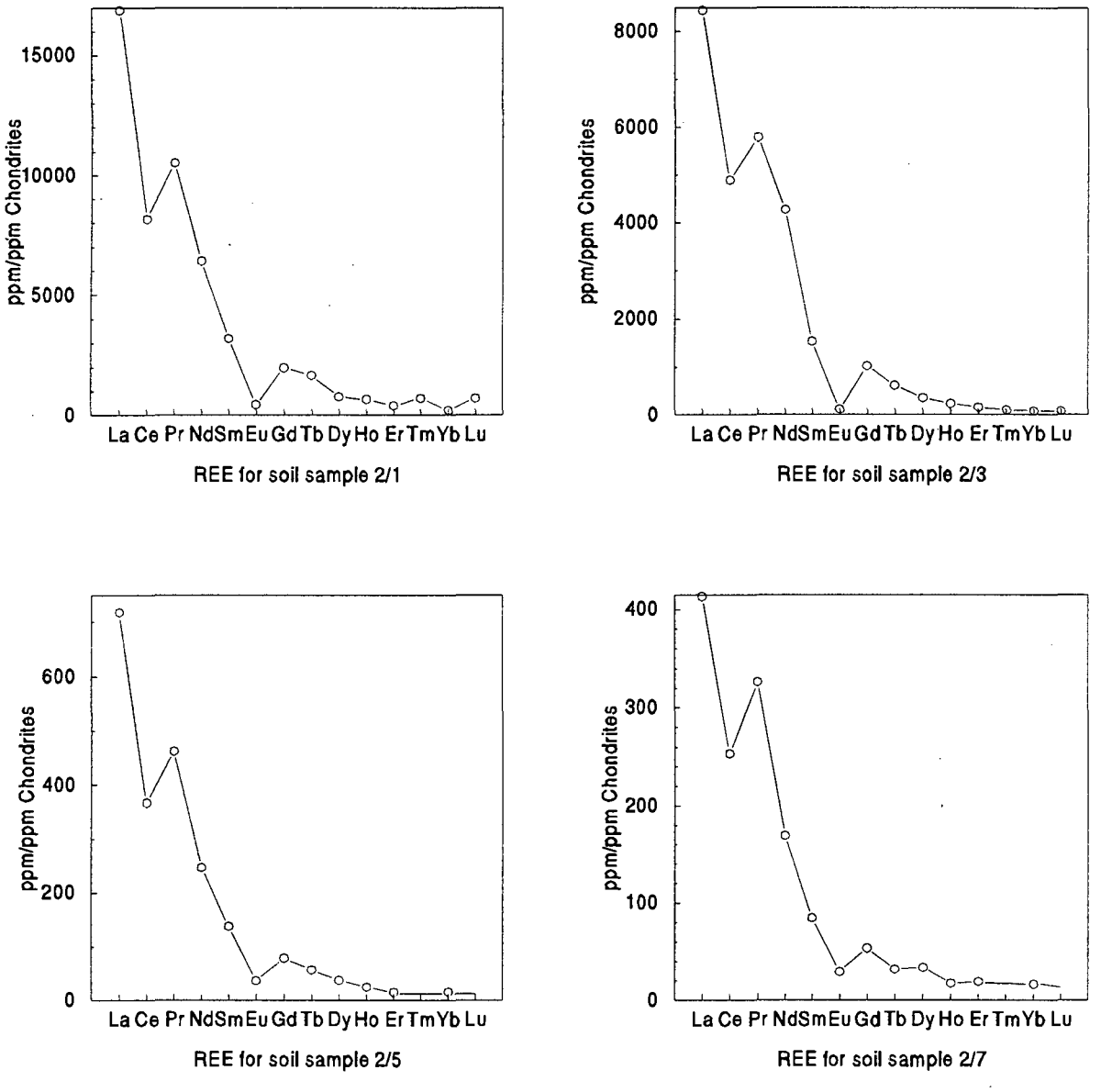

Figure 5.15. Chondrite-normalized REE data for soil samples 2/1, 2/3, 2/5 and 2/7 along transect 2.

5.5. Comparison of elemental concentrations with those of uncontaminated soils

The values obtained by XRF revealed some interesting results regarding the potential mobility and toxicity of some of the major and trace elements within the soil. The obvious decrease in concentration can be seen along transect 1 for Cr, Cu, Ni, Pb, Th, U and Y (Figures 5.5 and 5.6). Due to the dam wall between samples 1/14 and 1/15, no surface transport from the mine area occurs beyond sample 1/14. Therefore as expected, sample 1/15 has concentrations of the analyzed trace elements well within the levels of natural soils (Table 5.10). The critical concentration is the range of values above which toxicity is considered to be possible. Unfortunately no data for U, Th and Y could be found. The range of trace elements for both transects has been included in Table 5.10.

Table 5.10. Normal and critical concentrations of heavy metals in soils (after Alloway, 1995), with corresponding concentrations in sample 1/15 and the ranges found over both transects. All values in mg/kg.

Element	Normal range in soils	Critical concentration range	Sample 1/15	Range along Transect 1	Range along Transect 2
Co	0.5-65	25-50	4	bdl - 13	bdl - 13
Cr	5-1500	75-100	45	36 - 1692	9 - 84
Cu	2-250	60-125	24	11 - 6291	8 - 127
Ni	2-750	100	13	10 - 260	8 - 24
Pb	2-300	100-400	31	31 - 1352	22 - 193
Zn	1-900	70-400	29	15 - 118	18 - 63
U	0.79-11	----	1	1 - 561	1 - 54
Th	3.4-10.5	----	17	17 - 27783	18 - 2718
Y	10-150	----	24	24 - 7840	18 -740

From Table 5.10 it is evident that Cr, Cu, Pb and Ni occur in concentrations exceeding the normal range of uncontaminated soils along transect 1. These four elements greatly exceed the critical soil concentrations for at least the first 4 samples along transect 1. Vegetation along the initial section of transect 1 was found to be absent (see photo Figure 5.2). The concentrations of these same elements along transect 2, although generally higher than the background values, fall within the normal range of uncontaminated soils and below the critical soil concentration.

Uranium concentrations vary with rock type. The average crustal abundance in rocks is about 2.5 mg/kg, with sedimentary rocks rich in organic matter and phosphate rich deposits usually having high U concentrations (Alloway, 1995). Typical values in soils are of the same order as those in rocks, with the worldwide soil data summarized by Kabata-Pendias and Pendias (1984) as 0.79 - 11 mg/kg. Although the critical soil concentrations for U are not known, soil samples 1/2 to 1/6 along transect 1 and soil samples 2/1 to 2/4 along transect 2 far exceed the normal range of U in uncontaminated soils.

Worldwide mean values for Th in soils are 3.4 to 10.5 mg/kg (Kabata-Pendias and Pendias, 1984). Again, no critical soil concentrations are known. All the soil samples along both transects exceed the range of normal Th concentrations in uncontaminated soils. This includes the background sample of 2/BH 1 which has a Th concentration of 19 mg/kg. It is expected that the country rock hosting the ore body is also rich in Th thus resulting in naturally high concentrations within the soils in the area.

Yttrium is present in concentrations ranging from 28 to 50 mg/kg in sandstones and acid rocks (Kabata-Pendias and Pendias, 1984). The geochemical properties of Y are similar to those of the lanthanides. A soil survey of Y concentrations in the U.S.A. indicated a range of less than 10 to 150 mg/kg, and averaging 25 mg/kg (Kabata-Pendias and Pendias, 1984). The Y concentrations of soil samples 1/2 to 1/6 along transect 1 and soil samples 2/1 to 2/4 along transect 2 exceed the average range of Y in uncontaminated soils.

The average concentrations of REE in soils have been given in Table 5.11. The concentration of REE in most of the soil samples at Steenkampskraal were above those of uncontaminated soils given by Laul et al. (1979). The presence of isolated ore bodies similar to that of Steenkampskraal in the area and the presence of monazite in the country rock would result in naturally high concentrations of REE within the local soils.

Table 5.11. Average concentration of REE in soils (After Laul et al., 1979).

Element	mg/kg
La	30
Ce	30
Pr	7
Nd	28
Sm	5
Eu	1
Gd	5
Tb	1
Dy	----
Ho	1
Er	3
Tm	0.4
Yb	3
Lu	0.3

5.6. Conclusions

Extreme soil acidification has occurred on the eastern side of the ore body as a result of the oxidation of sulphide minerals within the tailings, associated with the massive input of acidic cations such as Fe, Al and Cu. With increasing distance from the tailings is an associated decrease in dissolved ion concentrations and increase in pH. The effects of mining on the soil along transect 1 has resulted in a major change in the soil chemistry away from the tailings material.

The SO_4^{2-}, PO_4^{3-} and F^- concentrations decrease, while the HCO_3^- and to some extent the Cl^- concentrations increase away from the tailings dam. This is expected as SO_4^{2-}, PO_4^{3-} and F^- ions are released from the tailings material. Phosphate, F^- and, to a lesser degree, SO_4^{2-} are generally immobile, resulting in their rapid decrease in concentration along the transect. Chloride is a mobile anion, that might indicate the presence of a contamination plume moving outwards away from the tailings material.

The chemistry of the saturated paste extracts along soil transect 2 indicates pH values that are neutral to alkaline, with much lower concentrations of dissolved metals than along transect 1. There is a gradual change in the dominating anion from PO_4^{3-} at the top of the hill closest to the ore body to HCO_3^- further away. The pH of the saturated paste extracts along transect 2 shows a general trend of a slight pH increase away from the mine.

By comparing the concentrations of dissolved ions in the saturated paste extracts along transects 1 and 2, it can be seen that the degree of contamination and acidification of the soils as a result of mining activity is much lower along transect 2. This is due to the absence of tailings on the western side of the ore body, thus resulting in a much smaller volume of material from which contamination can occur as well as a much smaller surface area in which mineral dissolution occurs. Associated with the smaller volumes and surface area of contaminant material on the western side of the ore body is the steeper gradient, thus significantly reducing the residence time of water in the vicinity of the mine.

The total element concentration in the soil is important, as significant migration cannot occur, even with high solubility elements, unless there is water movement through the soil. The low annual rainfall at Steenkampskraal would limit the movement of these elements in solution. It is expected that although migration in solution does occur, movement is occurring predominantly through the mass transfer of material away from the tailings in heavy storms during the rainy season, and to some extent from the movement of tailings material via wind erosion. The low lying area surrounding the outcrop within the Steenkampskraal area is characterised by a siliceous dorbank below the surface soil. The dorbank at Steenkampskraal forms a hard layer, thus inhibiting vertical movement of contaminant elements, and largely confining movement to the surface layer.

The relative concentrations of Cr, Cu, Ni, Pb, U, Th and Y along transect 1 indicate that most of the soil contamination has occurred as a result of transport of tailings material away from the tailings dump. The degree of contamination is initially very high, but drops off rapidly and reaches a fairly stable value approximately 600 meters from the tailings dump. The relative concentrations of Cu, Pb, U, Th and Y along transect 2 are highest near the ore body but decrease sharply away from the mine. The relative concentrations of Cr and Ni have a different trend, with a slight decrease away from the mine followed by a sharp increase. The increase in Cr and Ni is probably due to a change in the country rock to a more mafic type rock. Earlier work had found the basement to consist of a mafic rich rock to the west of the mine (Mafic Granulite Group of the Malmesbury formation) in the same vicinity as that in which the increases in Cr and Ni were found.

The analysis of size fraction from a soil sample selected from each transect indicated that U, Th and Y are transported in different size fractions within both transects. Uranium, Th and Y are transported in the fine fraction in transect 1 and in both the coarse and fine fraction in transect 2. This was expected as monazite is highly resistant to weathering, with transport therefore occurring in the coarse fraction in transect 2. The large decrease in surface area in crushed tailings material has resulted in U, Th and Y transport occurring in a finer fraction along transect 1.

The chondrite-normalized REE patterns along both transects are similar to that of monazite. Those soils with a neutral to alkaline pH have developed a Ce depletion, probably due to the oxidation of Ce^{3+} to Ce^{4+} and subsequent immobilization of Ce as CeO_2. Soils with acidic pH values, i.e. those close to the tailings, have no Ce depletions due posssibly to the prevention of the oxidation of Ce^{3+} to Ce^{4+} at low pH.

Chromium, Cu, Pb and Ni along transect 1 occur in concentrations exceeding the normal range of uncontaminated soils. These four elements have concentrations greatly exceeding the critical soil concentrations for at least the first 500 m along transect 1. Vegetation along the initial section of transect 1 was found to be absent. The concentrations of these same elements along transect 2, although generally higher than the background values, fall within the normal range of uncontaminated soils.

Soil samples 1/2 to 1/6 along transect 1 and soil samples 2/1 to 2/4 along transect 2 exceed the normal range of U in uncontaminated soils. All the soil samples along both transects, including the background samples, exceed the range of normal Th concentrations in uncontaminated soils. It is expected that the country rock hosting the ore body is also rich in Th thus resulting in naturally high concentrations within the local soils. The Y concentrations of soil samples 1/2 to 1/6 along transect 1 and soil samples 2/1 to 2/4 along transect 2 exceed the normal range of Y in uncontaminated soils.

It is recommended that further work should be done on determining the fraction in which metal mobility is occurring. Detailed mineralogical analysis of the soils may also prove useful.

Chapter 6

Conclusions and recommendations

6.1. Conclusions

An attempt has been made to answer the original questions laid out in chapter 1. These were:

1) What is the extent of contamination and acidification of the ground waters as a result of mining?

2) If colloidal matter is present in the groundwaters at the site, what is its role in promoting the mobilisation and movement of U, Th and REE ?

3) What is the extent of element (U, Th, Cu, and REE) transport away from the primary ore body and tailings dams under *in situ* conditions ?

Groundwater contamination by REE-bearing phosphate minerals and associated sulphide minerals has occurred at the Steenkampskraal monazite mine. This has resulted in high concentrations of REE, U and Th in all the mine waters and boreholes that extend below the local groundwater table.

Colloids were identified in three of the boreholes surrounding the mine, with all three borehole samples having high U, Th and REE in the associated groundwater. The REE present in the ground waters have a similar chondrite normalized REE pattern to that of monazite. This was expected due to the fact that monazite controls the distribution of REE in the local mineralogy. The monazite-normalized REE patterns for the selected borehole waters show a marked fractionation between LREE and HREE, with the HREE strongly enriched in the aqueous phase. Read et al. (1987) found the HREE to show a greater tendency for complexation and a greater affinity for mineral surfaces. Although the presence of colloids in these 3 boreholes does not prove that they are a vehicle for transport of REE, U, and Th, it is possible that colloidal transport of these elements is the dominant mechanism of transport and enrichment. It would be very interesting to ascertain the percentages of REE adsorbed to the colloids, verse the percentage of REE as solutes.

The presence of La data for the chondrite-normalized REE patterns of the water samples would give a better idea of the behaviour of Ce in the ground waters. Cerium depletions may be present in both slimes dam samples as well as the borehole samples, but without La data we cannot be sure.

Extreme soil acidification has occurred on the eastern side of the ore body as a result of the oxidation of sulphide minerals within the tailings, associated with the massive input of acidic cations such as Fe, Al and Cu. With increasing distance from the tailings is an associated decrease in dissolved ion concentrations and increase in pH.

The degree of contamination and acidification of the soils as a result of mining activity is much lower on the western side of the ore body. This is due to the absence of tailings material, thus resulting in a much smaller volume of material from which contamination can occur as well as a much smaller surface area in which mineral dissolution occurs. Associated with the smaller volumes and surface area of contaminant material on the western side of the ore body is the steeper gradient, thus significantly reducing the residence time of water in the vicinity of the mine.

The chondrite-normalized REE soil patterns on both the eastern and western side of the ore body are similar to that of monazite. Those soils with a neutral to alkaline pH have developed a Ce depletions due to the oxidation of Ce^{3+} to Ce^{4+} and subsequent immobilization of Ce as CeO_2. Soils with acidic pH values, i.e. those close to the tailings have no Ce depletions due to the lack of oxidation of Ce^{3+} to Ce^{4+} at low pH. The change in chondrite-normalized REE patterns along transect 1 goes from acidic soils with no Ce depletion to alkaline soils with a Ce depletion. Cerium has therefore been removed during the transition. At this stage the locality of the Ce is not known and with further work it may be interesting to determine the presence of the Ce.

6.2. Recommendations

The most obvious recommendation that must be made with regard to contamination is that the tailings material must be properly contained. Most of the contamination on the eastern side of the mine is due to the leaching and movement of tailings material away from the mine towards the south east. It is proposed that the mine is to re-open in the near future, for the recovery of REE. The high concentrations of REE in the tailings would be an incentive to reprocess the tailings material, with all new material to be stored in a appropriately designed tailings impoundment, in which seepage is controlled. The containment of the tailings material would significantly reduce the surface and to some extent the ground water (BH 6) contamination from the mine.

It is difficult to make recommendations about the ground water contamination, especially considering the most highly concentrated borehole (BH 1) lies upstream of the mine. The removal of the waters in the main shaft, main shaft extension and sump on level 3 might give an insight into the degree of mixing with the local groundwater and help in the evaluation of the extent of groundwater contamination.

References

Ahonen, L., Ervanne, H., Jakkola, T. and Blomqvist, R. Redox chemistry in Uranium-rich Groundwater of Palmottu Uranium Deposit, Finland. *Radiochimica Acta*, **66/67**(1994), 115-121.

Alloway, B.J. (ed.) *Heavy metals in Soils*, Second Edition. Blackie Academic and Professional, (1995).

Amirbahman, A. and Olson, T.M. Transport of humic matter coated hematite in packed beds. *Environ. Sci. Technol,* **27**(1993), 2807.

Anderson, N. J. B., Andreoli, M.A.G., Jarvis, N.V. and Read, D. Thorium, Uranium and Rare Earth Element Behaviour at the Steenkampskraal Monazite Mine, South Africa. *Journal of Contaminant Hydrology* (1995).

Andreoli, M.A.G., Smith, C.B., Watkeys, M., Moore, J.M., Ashwal, L.D. and Hart, R.J. The Geology of the Steenkampskraal Monazite Deposit, South Africa: Implications for REE-Th-Cu Mineralization in Charnockite-Granulite Terranes. *Economic Geology*, **89**(1994), 994-1016.

Aston, S.R., Thornton, I., Webb, J.S. and Purves, J.B. Stream sediment composition, an aid to water quality assessment. *Water, Air, Soil Pollution.* **3**(1974), 321-325.

Batson, V.L., Bertsch, P.M., and Herbert, B.E. Soil Processes and Chemical Transport, Transport of Anthropogenic Uranium from Sediments to Surface waters During Episodic Storm Events. *Journal of Environmental Quality* **25**(1995), 1129-1137.

Bigham, J.M. Schwertmann, U. Carlson, L. and Murad, E. A poorly crystallized oxyhydroxysulfate of iron formed by bacterial oxidation of Fe(II) in acid mine waters. *Geochim. Cosmochim. Acta* **54**(1990), 2743-2758.

Bigham, J.M. Schwertmann, U. and Carlson, L. Mineralogy of precipitates formed by the Biogeochemical Oxidation of Fe(II) in Mine Drainage. In: Skinner H.C.W. and Fitzpatrick, R.W. (eds.) *Biomineralization: Processes of Iron and Manganese. Catena* supplement **21**(1992).

Bigham, J.M. Mineralogy of Ochre Deposits Formed by Sulphide Oxidation. In: Jambor, J.L. and Blowes D.W. (eds.) *Environmental Geochemistry of Sulphide Mine Wastes.* Mineralogical Association of Canada, **22**(1994).

Bigham, J.M. Schwertmann, U. Traina, R.L. Winland, R.L. and Wolf, M. Schwertmannite and the chemical modelling of iron in sulfate waters. *Geochimica et Cosmochimica Acta*, **60**(1996), 2111-2122.

Birch, G.F. The Karbonat-Bombe: a precise, rapid and cheap instrument for determining calcium carbonate in sediments and rocks. *Trans. Geolical Society Southern Africa*, **84**(1981), 199-203.

Bondeitti, E.A. Adsorption of U(4+) and Th(6+) by soil colloids. *Agronomy Abstracts,* (1974).

Borggaard, O.K. The influence of iron oxides on phosphate adsorption by soil. *Journal Soil Science,* **34**(1983), 333-341.

Bourg, A.C.M. Physiochemical speciation of trace elements in oxygenated estuarine waters. In: West, T.S., (Ed) *The determination of trace elements in natural waters.* Blackwell scientific publications, London (1988).

Brady, K.S. Bigham, J.M. Jayes, W.F. and Logan, T.J. Influence of sulphate on Fe-oxide formation: Comparisons with a stream receiving acid mine drainage. *Clays Clay Minerals*, **34**(1986), 266-274. Cited by Bigham, J.M. (1994).

Braun J.J., Pagel, M., Muller, J.P., Bilong, P., Michard, A. and Guillet, B. Cerium anomalies in lateritic profiles. *Geochimica et Cosmochimica Acta,* **54**(1990), 781-796.

Braun J.J., Pagel, M., Herbillon, A. and Rosin, C. Mobilization and redistribution of REEs and thorium in a syenitic lateritic profile: A mass balance study. *Geochimica et Cosmochimica Acta,* **57**(1993), 4419-4434.

Braun, J.J. and Pagel, M. Geochemical and Mineralogical behaviour of REE, Th and U in the Akongo lateritic profile (SW Cameroon). *Catena*, **21**(1994), 173-177.

Bricker, T.M. and Houk, R.S. Speciation of Selenium in Human Serum by Size Exclusion Chromatography and Inductively Coupled Plasma Mass Spectrometry. In Andrews, D.L. and Davies, A.M.C. (Eds.) *Frontiers in Analytical Spectroscopy*. Royal Society of Chemistry (1995).

Brookins, D.G. Eh-pH diagrams for the rare earth elements at 25^{0}c and one Bar Pressure. *Geochemical Journal,* **17**(1983), 223-229.

Byrne, R.H. and Kim, K.-H. Rare earth precipitation and coprecipitation behaviour; The limiting role of PO_4^{3-} on dissolved rare earth concentrations in seawater. *Geochimica et Cosmochimica Acta,* **57**(1996), 519-526.

Byrne, R.H. Xuewu, Liu., Schijf, J. The influence of phosphate coprecipitation on rare earth distributions in natural waters. *Geochimica et Cosmochimica Acta,* **60**(1996), 3341-3346.

Cabrera, F. Toca, C.G., Diaz, E. and de Arambarri, P. Acid mine-water and agricultural pollution in a river skirting the Doñana national park (Guadiamar river, south west Spain). *Water Research,* **18**(1984), 1469-1482.

Cantrell, K.J. and Byrne, R.H. Rare earth element complexation by carbonate and oxalate ions. *Geochimica et Cosmochimica Acta,* **51**(1987), 597-605.

Chapman, N.A. McKinley, I.G., Penna Franca, E. Shea, M.J. and Smellie, J.A.T. The Poçosde Caldas project: An introduction and summary of its implications for radioactive waste disposal. *Journal Geochemical Exploration,* **45**(1992), 1-24.

Dallas, H.F. and Day, J.A. *The effect of water quality variables on riverine ecosystems*: A review. Water Research Commission, South Africa (1993).

Daux, V., Crovisier, J.L., Hemond, C., and Petit, J.C. Geochemical evolution of basaltic rocks subjected to weathering: Fate of the major elements, rare earth elements, and thorium. *Geochimica et Cosmochimica Acta,* **58**(1994), 4941-4954.

Degueldre, C. Pfeiffer, H-R. Alexander, W. Wernli, B. and Breutsch, R. Colloid properties in granitic groundwater systems. I: Sampling and characterisation. *Applied Geochemistry,* **11(5)**(1996), 677-695.

Diamond, R.E. and Harris, C. Oxygen and hydrogen isotope composition of Western cape meteoric water. Unpublished (1996).

Doner, H.E. and Lynn, W.C. Carbonate, halide, sulphate and sulphide minerals. In Minerals in Soil Environments (Dixon, J.B. and Weed, S.B. eds.) *Soil Science Society of America*, Madison, Wisconsin, 279-330, (1989).

Dongarra, G. and Langmuir, D. The stability of UO_2OH^+ and $UO_2[HPO_4]_2^{2-}$ complexes at 25°C. *Geochimica et Cosmochimica Acta,* **44**(1980), 1747-1751.

Dran , C.J., Della Mea, G., Moulin, V., Petit, J.C. and Rigato, V. Interaction of Pseudocolloids with Mineral Surfaces: The Fate of the Scavenged Cation. *Radiochimica Acta*, **66/67**(1994), 221-227.

Drever, J.I. *The Geochemistry of Natural Waters* (second edition) Prentice Hall, New Jersey (1988).

Duddy, I.R. Redistribution and fractionation of rare earth and other elements in a weathering profile. *Chemical Geology*, **30**(1980), 363-382.

DWAF, Department of Water Affairs and Forestry, RSA. *South African Water Quality Guide lines for Domestic use* (volume 1), (1996).

DWAF, Department of Water Affairs and Forestry, RSA. *South African Water Quality Guide lines for Agricultural and Irrigation use* (volume 5), (1996).

Erten, H.N., Mohammed, A.K. and Choppin, G.R. Variation of stability Constants of Thorium and Uranium Oxalate Complexes with Ionic Strength. *Radiochimica Acta*, **66/67**(1994), 123-128.

Fairhurst, A.J., Warwick, P. and Richardson, S. The Effect of pH on Europium-Mineral Interactions in the Presence of Humic Acid. *Radiochimica Acta*, **69**(1995), 103-111.

Fey, M.V. and Guy, S.A. *The capacity of soils of the Vaal Dam catchment to retain sulphate from atmospheric pollution.* Report to the Water Research Commission by the Department of Agronomy, University of Natal, Pietermaritzburg. WRC Report No 414/1/93.

Geckeis, H. Bernotat, W. Degering, D. *Analysis of monazite sand and groundwater samples from Steenkampskraal mine (South Africa) - considerations on the mobility of thorium, uranium and rare earth elements.* Institut fur Nukleare Entsorgungstechnik, Forschungszentrum Karlsruhe, Germany (1996).

Ghadiri, H and Rose, C.W. Sorbed chemical transport in overland flow: Enrichment ratio variation with erosion processes. *Journal Environmental Quality*, **20**(1991), 634-641.

Gouveia, M.A., Prudencio, M.I., Figueiredo, M.O., Waerenborgh, L.C.G., Morgado, I., Pena, T. and Lopes, A. Behaviour of REE and other trace and major elements during weathering of granitic rocks, Evora, Portugal. *Chemical Geology*, **107**(1993), 293-296.

Hardy, C.J. and Duerden, P. Progress in the Alligators Rivers analogue project. In: Come, B. and Chapman, N.A. (Eds). CEC Rep. Eur 11725(1989). In: Anderson et al. (1995).

Harshman, E.N. Geology and Uranium deposits, Shirley Basin area, Wyoming. 1972). *U.S. Geological Survey Prof. Paper*, **745**(1972).

Hounsome, R.S. The geochemistry and phosphorous sorption characteristics of Mgeni catchment sediments. Unpublished Msc theseis (1994), Universit of Cape Town.

Hunter, K.A., Hawke, D.J. and Choo, L.K. Equilibrium adsorption of thorium by metal oxides in marine electrolytes. *Geochimica et Cosmochimica Acta,* **52**(1988), 627-636.

I.A.E.A. (International Atomic Energy Agency) Statistical treatment of environmental isotope data in precipitation. Int. At. Energy Agency, Vienna, Tech. Rep. Ser. No. 206 (1981). In: Mazor, E. and Verhagen, B.Th. Dissolved Ions and Radioactive Isotopes and Noble Gases in Thermal waters of South Africa. *Journal of Hydrology*, **63**(1983).

Ivanovich, M. and Harmon, R.S. *Uranium series Disequilibrium; Applications to Earth, Marine, and Environmental Sciences.* Oxford Sciences Publication, Oxford (1992).

Jackson, M.L. Structural role of hydronium in layer silicates during soil genesis. *International Congress Soil Science*, Trans 7th (Madison, Wis.)II (1960) 445-455.

Jackson, M.L. *Soil chemical analysis-advanced course* (2nd ed). Deptartment of Soils, University of Wisconsin, Madison, (1969).

Jackson, M.L. Lim, C.H. and Zealany, L.W. Oxides, Hydroxides, and Aluminosilicates. **In** Klute A (ed.), *Methods of Soil Analysis*, Part 1. Physical and Mineralogical Methods- Agronomy Monograph no 9.(Second Edition), (1986).

Jambor, J.L. Mineralogy of sulphide-rich Tailings and Their Oxidation Products. In: Jambor, J.L. and Blowes D.W. (eds.) *Environmental Geochemistry of Sulphide Mine Wastes*, Mineralogical Association of Canada, vol.22 (1994).

Jarvis, N. Andreoli, M.A.G. Anderson, N.J.B. Walton, D. Hambleton-Jones, B.B. Fouché, F. Bernotat, W. Geckeis, H. *Investigation of the Steenkampskraal Monazite Mine as an Actinide natural System*, Progress report 2, Atomic Energy Corporation (1996).

JCPDS, *Mineral Powder Diffraction File*, Search manual (1980).

Johnson, C.A. and Thornton, I. Hydrological and chemical factors controlling the concentrations of Fe, Cu, Zn and As in a river system contaminated by acid mine drainage. *Water research*, **21**(1987), 359-365.

Jonasson, R.G., Bancroft, G.M., and Nesbitt, H.W. Solubilities of some hydrous REE phosphates with implications for diagenesis and seawater concentrations. *Geochimica et Cosmochimica Acta*, **49**(1985), 2133-2139.

Kabata-Pendius, A. and Pendius, H. *Trace Elements in Soils and Plants*. CRC Press, Inc. (1984).

Kim, J.I., Zeh, P. and Delakowitz, B. Chemical Interactions of actinide ion with groundwater colloids in Gorleben aquifer system. *Radiochimica Acta*, **58/59**(1994), 147-154.

Kim, J.I., Delakowitz, B., Zeh, P., Probst, T., Lin, X., Ehrlicher, U., Schauer, C., Ivanovich, M., Longworth, G., Hasler, S.E., Gardiner, M., Fritz, P., Klotz, D., Wolf, M., Geyer, S., Alexander, J., Read, D. and Thomas, J. *Colloid Migration in groundwaters: Geochemical interactions of radionuclides with natural colloids*. Final Progress Report CEE Contract F12W0084 (1995).

Krauskopf, K.B. Thorium and rare-earth metals as analogues for actinide elements. *Chemical Geology*, **55**(1986), 323-335.

Kremers, H.E. Rare earth's. *Engineering and Mining Journal*, **159**(1958). In: Landström, O. and Tullborg, E.L. The Influence of Fracture Mineral/ Groundwater Interaction on the Mobility of U, Th, REE and other Trace Elements. SKB Technical Report 90-37, Swedish Nuclear Fuel and waste management Co. (SKB), Stockholm, Sweden, (1990).

Landström, O. and Tullborg, E.L. The Influence of Fracture Mineral/ Groundwater Interaction on the Mobility of U, Th, REE and other Trace Elements. SKB Technical Report 90-37, Swedish Nuclear Fuel and waste management Co. (SKB), Stockholm, Sweden, (1990).

Langmuir, D. Uranium Solution-Mineral Equilibria at Low Temperatures with Applications to Sedimentary Ore Deposits. *Geochimica et Cosmochimica Acta*, **42**(1978), 547-569.

Langmuir, D. and Hermann, J.S. The mobility of thorium in natural waters at low temperatures. *Geochimica et Cosmochimica Acta*, **44**(1980), 1753-1766.

Laul, J.C. Weimer, W.C. and Rancitelli, L.A. Biogeochemical distribution of rare earths and other trace elements in plants and soils, in *Origin and Distribution of the elements*, Vol 11, Ahrens, L.H. (ed.) Pergamon Press, Oxford (1979). In: Kabata-Pendias and Pendius (1984).

Lazaroff, N. Sulfate requirement for iron oxidation by Thiobacillus ferrooxidans. *Journal of bacteriology* **85**(1963), 78-83. Cited by Bigham et al. (1992).

Lazaroff, N. Lewis, E. Santora, N. and Pueschal, C. Scanning electron microscopy and infrared spectroscopy of iron sediments formed by Thiobacillus ferrooxidans. *Geomicrobiology Journal,* **4**(1985), 231-268.

Lei, W., Linsalata, P., Penna, F.E. and Eisenbud, M. Distribution and mobilization of cerium, lanthanum, and neodynium in the Morro do Ferro basin, Brazil. *Chemical Geology*, **55**(1986), 313-322.

Marsh, J.S. REE fractionation and Ce anomalies in weathered Karoo dolerite. *Chemical Geology*, **90**(1990), 189-194.

McBride, M.B. *Environmental Chemistry of Soils*, Oxford University Press, (1994).

McCarthy, J.F. and Zacchara, J.M. Subsurface transport of contaminants. *Environmental Science and Technology*, **23**(1989), 496-502.

McLean, E.O. Soil pH and Lime Requirements. **In:** *Methods of Soil Analysis*, Part 2. Chemical and Microbial Properties- Agronomy Monograph no 9.(Second Edition), (1982).

Middelburg, J.J . van der Weijen, C.H. and Woittiez, J.R.W. Chemical processes affecting the mobility of major, minor and trace elements during weathering of granitic rocks. *Chemical Geology*, **68**(1988), 253-273.

MINTEQA2/PRODEFA2, A Geochemical Assessment Model for Environmental Systems: Version 3.0 User's Manual.

Mongelli, G. REE and other trace elements in a granitic weathering profile from "Serre", southern Italy. *Chemical Geology*, **103**(1993), 17-25.

Mott, C.J.B. Anion and ligand exchange (chapter 5) (1981). In: Greenland, D.J. and Hayes, M.H.B. (eds.) The chemistry of soil processes. John Wiley and Sons Ltd.

Mott, C.J.B. Surface chemistry of soil particles (1989). In wild, A. (ed.) Russel's soil conditions and plant growth (11th edition), Longman Scientific and Technical, Essex, 239-281.

Murphy, J. and Riley, J.P. A modified single solution method for determination of phosphate in natural waters. *Analitical Chimica Acta.* **27**(1962), 31-36.

Murray, K. and Wade, P. Checking anion-cation charge balance of water quality analyses: Limitations of the traditional method for non-potable waters, *Water SA* **22**(1996), 27-32.

Nesbitt, R.W., Mastins, H., Stolz, G.W. and Bruce, D.R. Matrix corrections in trace element analysis by X-ray fluoresscence: an extention of the Compton-scattering technique to long wavelengths. *Chemical Geology*, **18**(1976), 203. In Willis and Duncan, (1996).

Nesbitt, H.W. Mobility and fractionation of rare earth elements during weathering of a granodiorite. *Nature*, **279**(1979), 206-210.

Nesbitt, H.W., Marcovics, G. and Price, R.C. Chemical processes affecting alkalis and alkaline earths during continental weathering. *Geochimica et Cosmochimica Acta,* **44**(1980), 1659-1666.

Nordstrom, D.K. Aqueous pyrite oxidation and the consequent formation of secondary iron minerals. In: Kitrick, J.A. Fanning, D.S. and Hossner L.R. (eds.) Acid sulphate weathering. *Soil science society of America,* (1982), 37-56. Cited by Bigham et al., (1992).

Östhols, E. Thorium Sorption on amorphous silica. *Geochimica et Cosmochimica Acta*, **59**(1995), 1235-1249.

Persson, P. and Lövgren, L. Potentiometric and spectroscopic studies of sulfate complexation at the goethite-water interface, *Geochemica et Cosmochimica Acta.* **60**(1996), 2789-2799

Pike, D.R. The monazite deposits of the Van Rhynsdorp Division, cape Province: Unpublished M.Sc. Dissertation, Pretoria, University of Pretoria (1958).

Potts, P.J. *A Handbook of Silicate Rock Analysis*, Blackie and Son (1992).

Potts, P.J. Rare Earth Elements in Chondrites as normalising factors in Geochemistry. *Analytical Proceedings of the Analytical Division of the Chemistry Society*, **13**(1976), 118-120.

Prusty, B.G., Sahu, K.C. and Godgul, G. Metal contamination due to mining and milling activities at the Zawar zinc mine, Rajasthan, India, 1. Contamination of stream sediments. *Chemical geology,* **112**(1994), 275-291.

Rauret, G. Rubio, R. López-Sánchez J.F. and Casassas, E. Determination and Speciation of copper and lead in sediments of a mediterranean river (river Tenes, Catalonia, Spain). *Water Research,* **22**(1987), 449-455.

Read, D., Swanton, S.W., Thomas, J.B., Bennett, D.G., Russell, P.J. and Ivanovich, M. Transport of thorium-bearing colloids through siliceous matrices. *Radiochimica Acta*, **58/59**(1994), 683-689.

Read, D., Cooper, D.C. and McArthur, J.M. The composition and distribution of nodular monazite in the Lower Palaeozoic rocks of Great Britain. *Mineral Magazine*, (1987), 271-280.

Reitemeier, R.F. Effect of moisture content on the dissolved and exchangeable ions of soils in arid regions. *Soil Science,* **61**(1946), 195-214.

Reuss, J.O. and Johnson, D.W. *Acid Deposition and the Acidification of Soils and Waters.* Springer-Verlag, (1986).

Rhoades, J.D. Soluble Salts. **In** *Methods of Soil Analysis*, Part 2. Chemical and Microbial Properties - Agronomy Monograph no 9.(Second Edition), (1982).

Salomons, W. and Forstner, U. Trace metal analysis on polluted sediments. Part 2. Evaluation of environmental impact. *Environment Technology Letters,* **1**(1980), 506-517. In: Rauret, et al. (1987).

Santschi, P. Particle flux and trace metal residence time in natural waters. *Limnology Oceanography*, **29**(1994), 1100-1108.

Sahu, K.C., Prusty, B.G. and Godgul, G. Metal contamination due to mining and milling activities at the Zawar zinc mine, Rajasthan, India, 2. Dispersion in floodplain soils of stream. *Chemical geology*, **112**(1994), 293-307.

Schindler, P.W., Fürst, B., Dick, R. and Wolf, P.U. Ligand Properties of Surface Silonal Groups 1. Surface complex formation with Fe^{2+}, Cu^{2+}, Cd^{2+}, and Pb^{2+}. *Journal Colloidal Interface Science*, **55(2)**(1975), 469-475.

Short, S.A., Lowson, R.T., Ellis, J. and Price; D. Thorium- uranium disequilibrium dating of late Quaternary ferruginous concretions and rinds. *Geochimica et Cosmochimica Acta*, **53**(1989), 1379-1389.

Smedley, P.L. The geochemistry of rare earth elements in groundwater from the Carnmenellis area, southwest England. *Geochimica et Cosmochimica Acta*, **55**(1991), 2767-2780.

Singer, P.C. and Stumm, W. Acidic mine drainage: the rate determining step. *Science*, **167**(1970), 1121-1123. Cited by Bigham et al. (1992).

Socki, R.A., Karlsson, H.R. and Gibson, E.K. Extraction technique for the determination of oxygen-18 in water using preevacuated glass vials. *Analytical Chemistry*, **64**(1992), 829-831.

Soil Classification Working Group. *Soil Classification, A Taxonomic System for South Africa*, Dept. Agric. Development, Republic of South Africa, (1991).

Sparks, D.L. *Environmental soil chemistry*. Academic Press, San Diago (1995).

Sposito, G. *The Chemistry of Soils*. Oxford Univ. Press, Inc, (1989).

Stanier, R.Y. Ingraham, M.L. Wheelis, M.L. and Painter, P.R. *General microbiology* (5th ed.) MacMillan Education Ltd, London (1986). In: Fey, M.V and Dodds, H.A. Decontaminating Nitrate-Polluted soil, Deptartment of Geological Sciences, University of Cape town (1995).

Standard Methods for the Examination of Water and Waste Water, Sixteenth Edition. Port City Press, Baltimore, (1985).

Stumm, W. and Morgan, J.J. *Aquatic Chemistry*, 2nd ed. Wiley-Interscience, New York (1981).

Sun, S.-s. and McDonough, W.F. Chemical and isotopic systematics of oceanic basalts: implications for mantle composition and processes. In: Saunders, A.D. and Norry. M.J. (eds), *Magmatism in the Ocean Basins*, Geological Society Special Publication No 42,(1989), 313-345.

Taylor, S.R. and McLennan, S.M. *The Continental Crust: its composition and evolution*. Blackwell Scientific Publications, (1985).

Tipping, E. and Cooke, D. The effect of adsorbed humic substances on the surface charge of goethite (α-FeOOH) in fresh waters. *Geochimica et Cosmochimica Acta*, **46**(1982), 75-78.

Tisdale, S.L., Nelson, W.L. and Beaton, J.D. *Soil Fertility and Fertilizers*. Forth Edition, (1985).

Trefry, J. The transport of heavy metals by the Mississippi River and their fate in the Gulf of Mexico. Ph.D. Diss. Texas A and M Univ. Press (1977). In: Batson, V.L., Bertsch, P.M., and Herbert, B.E. Soil Processes and Chemical Transport, Transport of Anthropogenic Uranium from Sediments to Surface waters During Episodic Storm Events. *Journal of Environmental Quality*, **25**(1995), 1129-1137.

van der Weijen, C.H. and van der Weijen, R.D. Mobility of major, minor and some redox-sensitive trace elements and rare-earth elements during weathering of four granitoids in central portugal. *Chemical Geology*, **125**(1995), 149-167.

van der Weijen, C.H., van der Weijen, R.D. and Peters, A.F. Experiments on the leaching of uranium from granitic rocks and implications for geochemical exploration. *Uranium*, **2**(1985), 37-52.

Van Grieken, R. and Xhoffer, C. Microanalysis of individual environmental particles. *J. Analytical Atomic Spectrometry*, **7**(1991).

van Olphen, H. *An Introduction to Clay Colloid Chemistry* (Second Edition). Wiley-Interscience, New York, (1977).

Vieillard, P. and Tardy, Y. *Thermochemical properties of phosphates* (Chapter 4). In Nriagu, J.O. and Moore, P.B. (eds.) Phosphate Minerals, Springer-Verlag (1984).

Vivian, C.M.G. and Massie, K.S. Trace metals in water and sediments of the river Tawe, South Wales, in relation to local sources. *Environmental Pollution*, **14**(1977), 47-61.

Wadepohl, K.H. (Editor), *Handbook of Geochemistry*. Springer, New York , N.Y. 1978

Walkley, A. An examination of methods for determining organic carbon and nitrogen in soils. *Journal Agricultural Sciience*, **25**(1935), 598-609.

Walter, A.-V. Nahon, D. Flicoteaux, R. Girard, J.P, Melfi, A. Behaviour of major and trace elements and fractionation of REE under tropical weathering of a typical apatite-rich carbonatite from Brazil. *Earth and Planetary Science Letters,* 136(1995), 591-602.

Wetzel, R.G. *Limnology.* (3rd edition). Saunders College Publishing, Fort Worth (1996).

Whittig, L.D. and Allardice, W.R. X-Ray Diffraction Techniques. **In** Klute A (ed.), *Methods of Soil Analysis*, Part 1. Physical and Mineralogical Methods - Agronomy Monograph no 9.(Second Edition), (1986).

Wild, A. Plant nutrients in soil: Phosphate (1988). In Wild, A. (ed.) *Russel's soil conditions and plant growth* (11th edition), Longman Scientific and Technical, Essex, 695-742.

Willis, J.P. High Performance Ion Chromatography (HPIC). Unpublished, (1996).

Willis, J.P. Instunental parameters and data quality for routinemajr and trace element determinations by WDXRFS. Informationcircular No.14. Department of Geological Sciences, University of Cape Town, (1995).

Willis, J.P. and Duncan, A.R. Course on theory and practise of XRF spectrometry, Laboratory exercises. Department of Geological Sciences, (1996).

Wood, S.A. The aqueous geochemistry of the rare-earth elements and yttrium. 1. Review of available low-temperature data for inorganic complexes and the inorganic REE speciation of natural waters. *Chemical Geology*, **82**(1990), 159-186.

Yarif, S. and Cross, H. *Geochemistry of Colloid Systems*, Springer Verlag, Berlin, (1979).

Yunxiang, Ni., Hughes, J.M. and Mariano, A.N. Crystal chemistry of the monazite and xenotime structures. *American Mineralogist*, **80**(1995), 21-26.

Appendices

Appendix 1. Brief sample descriptions and co-ordinates of all samples

Table A1.1. Co-ordinate and sample descriptions of all borehole and surface water samples. No co-ordinate data is available for the underground samples.

SAMPLE	Latitude and Longitude Co-ordinates	X-Y Co-ordinates	Sampling date	Description
BH 1	S 30°58'05.4" E 18°38'00.9"	-34949.45 -3427212.03	08/08U 09/18P	Vertical, DTW: 48.6m
BH 2 (SKP35)	S 30°58'38.5" E 18°37'28.0"	-35819.11 -3428234.33	08/08U 09/18P	Vertical, DTW: 77.2m. Strong smell believed to be from dead termites.
BH 3 (SKP37)	S 30°58'30.1" E 18°37'29.6"	-35777.53 -3427970.38	08/08U 09/18P	Inclined (60°), DTW: 98.2 m, VD: 49.1 m
BH 4 (SKP34)	S 30°58'35.0" E 18°38'20.7"	-34421.04 -3428121.92	08/15	Vertical; water believed to be stagnant rain water.
BH 5 (BPK1)	S 30°58'32.5" E 18°36'55.4"	-36684.81 -3428041.98	08/17U 09/18P	Vertical; DTW: 44.5 m Farm: Brandewynskraal
BH 6 (STK25)	S 30°58'34.4" E 18°37'54.7"	-35111.03 -3428100.55	08/17U 09/18P	Inclined (45°); DTW: 84 m, VD: 59.4 m Yellow green colour.
MOS 1	S 30°59'56.7" E 18°37'55.2"	-35089.38 -3430640.28	08/09	Windpump on Farm: Nabeep
MOS 2	S 31°00'02.8" E 18°34'42.3"	-40206.24 -3430846.31	08/09	Windpump on Farm: Nabeep
MOS 3	S 31°01'49.4" E 18°35'18.6"	-39231.08 -3434125.74	08/09	Windpump on Farm: Nabeep
MOS 4	S 31°02'04.4" E 18°32'21.6"	-43923.39 -3434606.12	08/09	Windpump on Farm: Nabeep
BRAND 1	S 30°59'17.3" E 18°33'26.6"	-42220.07 -3429452.82	08/16	Windpump on Farm: Brandewynskraal
SD 1 and 2	S 30°58'38.4" E 18°37'51.8"	-35165.58 -3428264.14	08/08 (SD1) 08/16 (SD2)	Slimes dam samples. Blue colour.
Road water	-----	-----	09/18	Water sampled from the road below the tailings.
Stream water	S 30°59'02.3" E 18°33'16.6"	-34527.10 -3428991.91	08/16	Water in stream along transect 1.

DTW: Depth to water; VD: Vertical depth, if inclined; U: Unpurged; P: Purged.
SKP, BPK and STK: original names of boreholes.

Table A1-2. Co-ordinate and descriptions of all soil samples along transect 1.

SAMPLE	Lat-long co-ordinates	X-Y co-ordinates	Sample date	Description
1/1	S 30°58'39.7" E 18°37'53.1"	-35170.95 -3428260.06	08/08	Between rock pile and slimes dam. Sample depth: 0-25 cm.
1/2A and B	S 30°58'41.1" E 18°37'53.2"	-35150.15 -3428312.17	08/08	Sample depth: A: 0-6 cm. B: 6-11 cm, consolidated layer above dorbank.
1/3A and B	S 30°58'42.1" E 18°37'56.9"	-35051.87 -3428342.64	08/08	Sample depth: A: 0-2 cm, rich in heavy minerals. B: 2-7 cm, consolidated layer above dorbank.
1/4A and B	S 30°58'46.2" E 18°38'00.8"	-34947.97 -3428350.57	08/08	Sample depth: A: 0-3 cm, rich in heavy minerals. B: 3-4 cm, consolidated layer.
1/5	S 30°58'43.0" E 18°38'02.5"	-34903.18 -3428369.87	08/08	Sample depth: 0-10 cm. Only one horizon above dorbank, red colour.
1/6	S 30°58'45.6" E 18°38'06.0"	-34810.04 -3428449.64	08/08	Sample depth: 0-16 cm. Only one horizon above dorbank, red colour.
1/7	S 30°58'52.2" E 18°38'09.3"	-34721.81 -3428652.62	08/08	Sample depth: 0-10 cm. Only one horizon above dorbank, red colour.
1/8	S 30°58'53.5" E 18°38'10.3"	-34695.15 -3428692.57	08/08	Sample taken upstream of 1/9.
1/9	S 30°58'56.2" E 18°38'13.3"	-34615.27 -3428775.46	08/08	Sample taken in stream.
1/10	S 30°59'01.6" E 18°38'14.3"	-34588.20 -3428941.68	08/16	Sample taken downstream of 1/9.
1/11	S 30°59'11.5" E 18°38'14.8"	-34573.94 -3429246.53	08/16	Sample taken downstream of 1/10.
1/12	S 30°59'20.1" E 18°38'13.7"	-34602.26 -3429511.48	08/16	Sample taken downstream of 1/11 in the Nabeep river.
1/13	-----	-34350.00 -3429350.00	09/18	Sample taken upstream of 1/11.
1/14	-----	-34600.00 -3429600.00	09/18	Sample taken from corn field in Nabeep river.
1/15	-----	-34590.00 -3429680.00	09/18	Sample taken below dam wall in the Nabeep river.
2/DOR	S 30°58'46.6" E 18°38'03.1"	-34886.89 -3428480.69	08/16	Siliceous dorbank between 1/5 and 1/6.

Table A1-3. Co-ordinate and descriptions of all soil samples along transect 2.

SAMPLE	Latitude and longitude co-ordinates	X-Y co-ordinates	Sample date	Description
2/1	S 30°58'30.9" E 18°37'31.6"	-35724.37 -3427999.95	08/08	Sample depth: 0-5 cm, above bedrock. On slope below main shaft
2/2	S 30°58'28.5" E 18°37'28.0"	-35820.15 -3427926.36	08/08	Sample depth: 0-11 cm, above bedrock. On slope below 2/1.
2/3	S 30°58'27.4" E 18°37'22.4"	-35968.87 -3427892.98	08/08	Sample depth: 0-20 cm, above bedrock. On slope below 2/2.
2/4	S 30°58'27.3" E 18°37'18.7"	-36067.07 -3427890.24	08/08	Sample depth: 0-20 cm, above bedrock. On slope below 2/3.
2/5	S 30°58'29.7" E 18°37'13.9"	-36194.19 -3427964.58	08/08	Sample depth: 0-18 cm, above dorbank. On flat at base of hill.
2/6	S 30°58'33.7" E 18°38'07.6"	-36360.95 -3428083.01	08/08	Sample depth: 0-7 cm, above dorbank.
2/7	S 30°58'33.4" E 18°38'02.1'	-36506.93 -3428074.25	08/16	Sample depth: 0-8 cm, above dorbank.
2/8	S 30°58'36.2" E 18°36'39.6"	-37103.69 -3428167.91	08/16	Sample depth: 0-8 cm, above dorbank.
2/9	S 30°38'40.4" E 18°36'07.4"	-38089.15 -3428250.27	08/16	Sample taken 200 m from Klein-Rietrivier.
2/10	S 30°58'43.4" E 18°35'26.3"	-39047.95 -3428396.63	08/16	Sample taken in the Klein-Rietrivier.
2/11	S 30°59'24.1" E 18°34'44.8"	-40144.42 -3429654.19	08/16	Sample taken downstream of 2/10 in the Klein-Rietrivier.
2/12	S 31°02'04.4" E 18°32'21.6"	-43923.39 -3434606.12	08/16	Sample taken downstream of 2/11 in the Klein-Rietrivier near MOS 4 borehole.
2/BH1	-----	-34975.00 -3427150.00	09/18	Background sample taken from the Klein-Rietrivier, near BH 1.
2/DOR	S 30°58'34.5" E 18°37'03.0"	-36482.93 -3428113.40	08/16	Siliceous dorbank between 2/6 and 2/7.

Appendix 2. Analytical Methods

A2.1. pH

pH measurement is the determination of the activity of the hydrogen ions by potentiometric measurement using a standard hydrogen electrode and a reference electrode.

Precision and Accuracy: Under normal conditions ± 0.1 pH units was found to be the limit of accuracy for the measurement of pH in water. The limit of precision was ± 0.05 pH units.

A2.2. Electrical conductivity

Precision and Accuracy: It was found that the use of a conductivity meter had a relative standard error of approximately 8 %.

A2.3. Alkalinity

Apparatus/reagents:
Hydrochloric acid (HCl), 0.1 *N*.
Sodium carbonate (Na_2CO_3), 0.05 *N*.
Automatic potentiometric titrator.

Procedure:
HCl is added to a known volume of sample until an end point of pH 4.5 is obtained.

A2.4. Acidity

Aim: The determination of active acidity.

Apparatus/reagents:
Sodium hydroxide (NaOH), 0.01 *M*.
Automatic potentiometric titrator.

Procedure: 10 ml of sample was used in the titration using 0.01 *M* NaOH as the titrant (endpoint pH: 8.3).

A2.5. High Performance Ion Chromatography

HPIC is used for the separation and determination of a variety of cations and anions. This is achieved by measuring the conductivity of the solution, or by measuring the intensity of colour complexes formed by the ions to be measured (Willis, 1996). Ions in a solution are separated using a stationary phase ion exchange resin contained in a column. In-line detection of the ions of interest is carried out. Detection, of the common anions and cations was by conductivity with auto- suppression of the eluent. The analysis was carried out by means of a Dionex conductivity DX300 series suppressed IC system coupled to the AI-450 chromatography software package.

A Dionex AG4A guard column was used with a Dionex AS4A-SC separator column for anion determination, while a Dionex CG12A guard column was used with a Dionex CS12A separator column for cation determination.

Ions are moved through an ion exchange column within a mobile phase or eluent. The eluent used to determine anions was a 1.7 mM $NaHCO_3$/1.8 mM Na_2CO_3 solution. This prevents the determination of carbonate. A value for HCO_3^- is therefore calculated from the alkalinity titration. The running time was approximately 15 minutes at a flow rate of 1 ml/min for cations and 8 minutes for anions at a flow rate of 2 ml/min.

A number of ions were determined using HPIC. These include the cations Na^+, K^+, Mg^{2+}, Ca^{2+} and NH_4^+ and the anions of F^-, Cl^-, Br^-, NO_3^- and SO_4^{2-}. HPIC analyses were done on all the water samples and saturated paste extracts.

Sample preparation:

1) Filter samples through 0.2 μm filter paper using Millipore apparatus.
2) Dilute samples until conductivity is less than 100 μS/cm.

Precision:

Table A2.1. Precision of HPIC anion analyses. All values in mg/dm^3.

Repeat No.	F^-	Cl^-	NO_3^-	SO_4^{2-}	Date
1	0.25	0.90	0.43	0.84	01/09
2	0.25	0.93	0.49	0.85	01/09
3	0.23	0.94	0.46	1.19	03/09
4	0.23	0.94	0.48	0.96	03/09
5	0.22	0.90	0.47	0.95	03/09
6	0.24	0.93	0.49	0.96	04/09
7	0.23	0.90	0.58	0.93	04/09
8	0.22	0.91	0.57	0.97	04/09
9	0.23	0.91	0.48	0.96	04/09
10	0.24	0.94	0.50	0.96	04/09
Mean	0.235	0.92	0.493	0.956	
s.d.	0.010	0.017	0.044	0.091	
RSD (%)	4.1	1.8	8.9	9.5	

A2.6. Inductively Coupled Plasma - Atomic Emission Spectroscopy

The analyses were done using a Jobin Yvon 70C(JY70C) inductively coupled plasma atomic emission spectrometer.

Instrument settings
Power: 1 kW
Pressure - Ar gas: 3.4 bar
R.F.: 27.12 MHz
Flow rate: 2.0 ml/min
Aerosol gas flow: 0.4/min and 0.8/min (Na and K)
Plasma gas flow: 0.1 ml/min
Coolant gas flow: 16 ml/min

Table A2.2. Lower limits of detection for ICP-AES.

Element	Lower limits of detection (mg/dm^3)
Ca	0.05
Mg	0.03
Na	1.0
K	5.0
Fe	0.1
Al	0.5
Cu	0.2
Cr	0.1
Mn	0.04
Ni	0.2
Si	0.09
Co	0.1
Pb	1.0
Zn	0.1
As	0.5
Hg	0.5
Cd	0.06

A2.7. Inductively Coupled Plasma - Mass Spectroscopy

The sample is introduced into the ICP unit as an aerosol through the central tube in a flow of argon. The temperature of the ICP is in the range of 6000 to 8000 K. The high temperature allows the introduced sample to be vaporized, atomized and ionized. Due to the atmospheric pressure conditions in the plasma, the ions must be extracted into a vacuum system before mass analysis (Bricker and Houk, 1995).

For most ICP-MS experiments a conventional pneumatic nebulizer is used to introduce the liquid sample into the plasma. The liquid sample is introduced through a narrow tube and shattered into droplets at the end by interaction with a flow of Ar gas .

The samples were fused using Li_5BO_4 and HNO_3. 0.2 mg/dm^3 indium was used as an internal standard to determine matrix effects. The detection limits supplied by the Anglo American Research Laboratories was 0.005 mg/dm^3 for all REE and U and Th.

A2.8. Phosphate determination: the Ascorbic Acid Method

Principles: Ammonium molybdate and potassium antimonyl tartrate react in acid medium with orthophosphate to form a heteropoly acid, phosphomolybdic acid, that is reduced to intensely coloured molybdenum blue by ascorbic acid.

Apparatus: Spectrophotometer (for use at 880 nm).

Reagents:

a) potassium antimonyl tartrate solution: 1.3715 g $K(SbO)C_4H_4O.1/2H_2O$ was dissolved in 400 ml distilled water in a 500-ml volumetric flask and diluted to volume.
b) ammonium molybdate solution: 20 g $(NH_4)_6Mo_6O_{24}.4H_2O$ was dissolved in 500 ml distilled water.
c) ascorbic acid: 0.01 *M*: 1.76 g ascorbic acid was dissolved in 100 ml distilled water.
d) sulphuric acid, 5 *N*: 70 ml concentrated H_2SO_4 was diluted with 500 ml distilled water.
e) combined reagent: 50 ml sulphuric acid, 5 ml potassium antimonyl tartrate, 15 ml ammonium molybdate solution and 30 ml ascorbic acid solution were mixed together in the order given.
f) stock phosphate solution.
g) standard phosphate solution: 50.0 ml stock phosphate solution was diluted to 1000 ml with distilled water, 1.00 ml = 2.50 μg P.

Procedure: *Sample treatment:* 50.0 ml sample was pipetted into a dry, clean test tube. 8.0 ml mixed reagent was added and the resultant solution was mixed thoroughly. After 15 minutes the absorbance of each sample/standard was measured, using reagent blank as the reference solution at a wavelength of 880nm.

Calibration curve preparation: a series of six standards were used to prepare a calibration curve: absorbance was plotted against phosphate concentration to give a straight line passing through the origin.

The equation for the standard curve was given as:

$$ABS = 0.624\ (STD\ P) + 0.004$$

Calculation: mg P/L = (mg P (final volume)*1000) / ml sample

Precision and Accuracy:
This method gives a relative standard deviation of 2.6 % and a relative error of 2.5 %.

A2.9. Fluoride by ion selective electrode

A Corning ion analyzer coupled with a fluoride ion selective electrode and a Calomel reference electrode 255 was used for the determination of F^-. Fluoride was decomplexed by 1,2 cyclohexylenediaminetetraacetic acid (CDTA).

Precision and Accuracy:
The ion selective electrode gives a relative standard deviation of 3.6 % and a relative error of 0.7 %

A2.10. Stable isotopes of oxygen and hydrogen ($^{18}O/^{16}O$ and D/H)

A2.10.1. Oxygen preparation

The method used in oxygen preparation was taken from Socki et al. (1992). A 7 ml vacutainer test tube was placed onto a hypodermic needle and then evacuated. Approximately 0.5 atm of CO_2 was loaded into the vacutainer from a cylinder of medical grade CO_2. The vacutainer was removed and injected with ±2 ml of sample water. The vacutainer was then fixed to an automatic shaker and submerged in a 25°C bath for at least 1.5 hours.

The vacutainer was placed onto the sample preparation line with the hypodermic needle just piercing the rubber seal and not the contents. The oxygen line was then evacuated. A small portion of the line was closed off and the vacutainer was pushed over the mouth of the needle, allowing an aliquot of the vacutainer gas contents to enter the closed off portion of the line. Within 4 to 5 seconds, the vacutainer must be closed to the line to prevent excess water vapour getting into the line and degassing CO_2, or producing kinetic fractionation of the CO_2. This aliquot method gives exactly the same results as the freezing method originally advocated by Socki et al (1992).

The aliquot was allowed into the line and frozen into a cold finger with liquid nitrogen. The non-condensibles were then pumped out. The liquid nitrogen was removed from the cold finger and immediately replaced with a slush of nearly frozen isopropyl alcohol. The CO_2 was allowed to warm up and expand into the line, only to be frozen into a second cold finger attached to a pressure transducer. The second cold finger was shut off from the sample preparation line and heated to room temperature in order to measure the voltage which can be used to calculate the quantity of CO_2 and hence the yield.

The yield was required to estimate whether or not there had been any leakage of CO_2 from the vacutainer. Assuming approximately the same amount of CO_2 had been let into the vacutainer, the yields should all be similar. The second cold finger was opened to the line and liquid nitrogen was placed around a break-seal tube in order to freeze out the CO_2. The break-seal tube was then shut off from the line and seal with an oxygen-propane torch.

A2.10.2. Hydrogen preparation

Break-seal tubes were loaded with 5 or 6 grains of zinc, weighing about 10 mg, and left to dry in a 100°C oven. A break-seal tube was then placed onto the line and evacuated. 1μl of sample water was micropipetted into a short glass tube which was placed onto the line and immediately immersed in liquid nitrogen. Once the water had frozen, the short glass tube was evacuated. The liquid nitrogen was then removed and placed over the break-seal tube while the short glass tube was heated with a hot air gun. Any non-condensibles were then pumped out and the break-seal tube was shut off from the line and burnt off with an oxygen-propane torch. Prior to analysis, the break-seal tube was put in a furnace at 450°C for 30 minutes.

Certain samples with high concentrations of dissolved solutes were purified by distillation so as to prevent the reaction of some of hydrogen gas with other ions/elements in the water such as F^-.

A2.11. Saturated paste extract

Procedure: Weigh out 200 to 400 g of air-dried soil of known water content into a plastic container. Weigh the container plus contents. Add distilled water to the soil with stirring until it is nearly saturated. allow the mixture to stand covered for several hours to permit the soil to imbibe the water, and then add more water to achieve a uniformly saturated soil-water paste.

After mixing, allow the sample to stand (preferably overnight, but at least 4 hours), then recheck the criteria for saturation. Free water should not collect on the surface, nor should the paste stiffen markedly or lose its glisten. If the paste is too wet, add additional dry soil to the paste mixture. Upon attainment of saturation, reweigh the container plus contents. Record the increase in weight and calculate the saturation water percentage from the weight of oven dry soil and the sum of the weights of water added and that initially present in the air-dry sample.

Transfer the paste to a Buchner and Richards filter funnel fitted with highly retentive filter paper. Apply vacuum, and collect the filtrate in a test tube or bottle. If the initial filtrate is turbid, refilter. Terminate the filtration when air begins to pass through the filter.

The filtrate was used for various analyses, including pH, EC, HPIC, ICP-AES and ICP-MS.

A2.12. X-ray Fluorescence Spectrometry

Characteristic X-ray spectra are produced by irradiation of a sample with a beam of sufficiently short wavelength X-rays. Interaction of the primary electrons with atoms of the sample causes excitation of the atom with ejection orbital electrons. During the subsequent electronic rearrangement by which the atoms de-excite to the ground state, fluorescence X-rays of energy characteristic of that element are emitted. The emission intensity of the characteristic radiation is measured with a suitable X-ray spectrometer and compared with that from a standard sample (Potts, 1992).

A Philips X'Unique II (PW 1480) wavelength dispersive XRF spectrometer was used in the analyses. Samples were prepared by first being air dried and then milled for approximately three minutes in a carbon steel Siebtechnik swing mill, reducing grain size to below 50μm diameter. 6 g of the powdered sample was then mixed with 4% mowiol solution using a mortar and pestle, before being mechanically pressed into briquette form under a pressure of approximately 10 t. The resulting briquettes were then placed under vacuum for 1 hour in order to desiccate them and to prevent fracture from occurring in the XRF machine (under vacuum conditions). Instrument parameters and data quality are given in Willis, (1995).

A2.13. Organic Carbon: Walkley-Black Method

Principle: Organic matter in soil may be oxidised by treatment with a hot mixture of $K_2Cr_2O_7$ and sulphuric acid, according to the equation:

$$2Cr_2O_7^{2-} + 3C + 16H^+ = 4Cr_3^+ + 3CO_2 + 8H_2O$$

After completion of this reaction, the excess dichromate is titrated with iron (II) ammonium sulphate hexahydrate. The reduced dichromate is assumed to be equivalent to the organic C present in the sample, assuming that soil organic matter has an average valence of zero.

Apparatus/Reagents: Balance, Erlemeyer flasks (500 cm^3); burette, pipettes; potassium dichromate 0.167 mol/dm^3; concentrated sulphuric acid; concentrated ortho-phosphoric acid; iron (II) ammonium sulphate (0.5 mol/dm^3); indicator: barium diphenylamine sulphonate.

Method: The soil was ground to pass a 0.35 mm sieve, using a porcelain mortar and pestle. 0.5 g air dried soil was transferred to a 500 cm^3 Erleneyer flask. To this 10 cm^3 $K_2Cr_2O_7$ solution was added (by pipette), and the flask was then swirled to disperse the soil in suspension.
20 cm^3 concentrated sulphuric acid was rapidly added, and the flask was again swirled until the soil and reagents were mixed. The flask was allowed to cool on a protected surface for ± 30 minutes before 150 cm^3 de-ionised water and 10 cm^3 concentrated ortho-phosphoric acid was added to it. 1 cm^3 indicator was then added and the excess dichromate titrated with iron (II) ammonium sulphate solution. The colour change involved at the end-point was dark violet to green.

Calculations:
Concentration of $Fe(NH_4)_2(SO_4)_2$ mol dm^{-3} = (10 cm^3 $K_2Cr_2O_7$ x 0.167 x 6) / (cm^3 $Fe(NH_4)_2(SO_4)_2$)

Organic carbon % = ([cm^3 $Fe(NH_4)_2(SO_4)_2$ blank - cm^3 $Fe(NH_4)_2(SO_4)_2$ sample] x M x 0.3 x f) / soil mass

where f = 1.3 and M = concentration of $Fe(NH_4)_2(SO_4)_2$ in mol dm^{-3}

A2.14. Preparation of clay samples for mineralogical analysis

Aim: To identify the mineralogy of the colloidal fraction from selected boreholes (BH 1, BH 2 and BH 6) in the Steenkampskraal area.

A2.14.3. Separation of clay fraction from total colloidal fraction

Apparatus/Reagents:
a) Sodium hydroxide (NaOH), 1 M.
b) Sodium carbonate (Na_2CO_3).
c) Hydrochloric acid (HCl), 1 M.
d) Sodium chloride (NaCl).
e) Silver nitrate ($AgNO_3$), 0.1 M.

Procedure: The colloidal fraction was transferred to a plastic bottle, where distilled water was added to form a slurry; a few drops of 1 *M* NaOH were added to the slurry and it was shaken. pH was measured and the procedure repeated until the pH stabilized at ± 9. The bottle was capped and shaken for four hours. The contents were then transferred into a 1 L measuring cylinder which was then filled with pH 10 Na_2CO_3 solution. The suspension was stirred, covered and allowed to stand for 16 hours. The supernatant suspension was then siphoned off to a depth of 18 cm (values and times worked out using Stokes' law).

The procedure was repeated with further addition of pH 10 Na_2CO_3 solution; the decanted solution was accumulated in a large bucket to which 1*M* HCl was added dropwise to restore the pH to $5 < pH < 7$. NaCl was added to promote flocculation. The clear supernatant was siphoned off and discarded. Once this procedure had been repeated four times, the clay concentrate was transferred into a number of centrifuge tubes for centrifugation: the supernatant was again discarded.

The clay was then dialysed by adding a limited volume of water to it, shaking it thoroughly and pouring it into dialysis tubing. The clay was equilibrated with tap water (running) overnight and then with deionised water for two nights. The washing procedure was terminated once it was determined that the chloride had been removed (using silver nitrate). Ideally the clay fraction should have been saturated with Mg so as to ensure that the expandable phyllosilicates as a result of hydration will be uniform within all crystals of a species. There was, however, only one sample (BH 6) with enough clay sized fraction to analyze. The clay fraction was pippeted onto a glass slide at a concentration of approximately 20 mg/ml. The glass slide was allowed to air dry before it was analyzed using XRD.

A2.15. Dissolution of noncrystalline hydrous oxides by acid ammonium oxalate in the dark

Principles: Numerous authors have shown that acid ammonium oxalate when allowed to react with minerals in darkness for 2 h is an effective reagent for the dissolution of noncrystalline materials (Jackson et al., 1986).

Reagents:
a) Ammonium oxalate [$(NH_4)_2C_2O_4 \cdot H_2O$], 0.2 M at pH 3: dissolve 28.4 g of reagent-grade ammonium oxalate monohydrate in 900 ml of distilled water, adjust to pH 3.0 using HCl.
b) Ammonium carbonate [$(NH_4)_2CO_3$], 0.5 M: dissolve 47.0 g of reagent-grade ammonium carbonate in 1 l of distilled water.

Procedure: Approximately 250 mg of the Main shaft precipitate in the form of a powder was weighed and placed in a centrifuge tube. Fifty ml of 0.2 M ammonium oxalate solution adjusted to pH 3.0 was added to the sample.

The centrifuge tube containing the sample was immediately wrapped in aluminium foil to eliminate light, and shaken for 2 hours on a reciprocal shaker. After the designated time, the sample was centrifuged, with the supernatant decanted. The sample was oven dried at 110°C and analyzed by powder x-ray diffraction.

A2.16. X-Ray Diffraction

Principles: When a given crystalline substance is irradiated by monochromatic X-rays, a pattern is obtained which is characteristic for that material. In this way any crystalline compound may be identified. The sample usually consists of small crystallites (ground solids or particles in suspension), whose random orientation ensures that every possible reflection plane is presented parallel to the surface by some crystallites.

The Bragg equation, ie. $n\lambda=2d\sin\theta$, is utilised in this technique.

Method: Scanning was done over a two theta range of 4-80 degrees using a CoKα (λ=0.790 Å) x-ray tube (25 mA, 40 kV). The step size was 0.05°, at a counting time of 1 second.

A2.17. Carbonate content (Karbonat-bombe, Birch (1962))

Method:

a) Determination of calibration curve
   1. One gram of $CaCO_3$ was weighed out (2 dec places) into a plexiglass cylinder of the karbonat-bombe.
   2. 5 ml concentrated HCl was placed into the small plastic bucket and lowered carefully into the plexiglass cylinder without spilling.
   3. The lid was tightly screwed onto the gasket, and the pressure release screw was closed securely. The sample was immersed in the acid by tipping the plexiglass cylinder and shaking gently to ensure all the powder came in contact with the acid.
   4. The manometer was read when effervescence has ceased.
   5. An aliquot of 0.5 g was used to provide a second point on the calibration curve.

b) Steps 1 to 4 are repeated with an accurately weighed sample of dried and crushed powder.

Precision and Accuracy:
The precision has been found to be 2% for $CaCO_3$ values >5% and less than 4% for lower concentrations. The accuracy is 2% for all values >10% and 3% for lower $CaCO_3$ concentrations.

A2.18. Scanning electron microscope (SEM)

The SEM provides an electron beam that is focused to a nanometre-sized probe and used to excite various signals, which can rapidly provide information about composition and surface topography in small areas of the specimen (Van Grieken and Xhoffer, 1991). Secondary electrons are mostly used for imaging and electron micrographs. Backscattered electrons give rise to two types of images: a topographical image, which shows the roughness of the sample, and a compositional image, which is a visualization of the variation in atomic number with location in the sample.

Both the backscattered and secondary electron signals can thus be used in morphological studies (Van Grieken and Xhoffer, 1991).

The signals detected are transformed into electronic pulses and, after amplification, stored in a multichannel device according to the corresponding energy. Characteristic X-rays are superimposed on a rather intense Brems strahlung continuum background, which is the result of non-characteristic emissions from incident electrons interacting with the electrostatic field of the atomic nuclei and inner electron shells (Van Grieken and Xhoffer, 1991).

A Leica Stereoscan 440 instrument, with a lanthanum hexaboride (LaB_6) electron gun, was used for the analyses of the precipitate found on the main shaft water surface. The instrument was run at 20 kV. The combination of the LaB_6 gun and the 20 kV results in a 6-10 times more efficient brightness and a higher resolution, when compared to a tungsten filament gun.

Before the sample was analyzed by the SEM it was coated with carbon. The carbon acts as a conductor thus preventing any charge build up at the point of analysis.

Appendix 3. Analytical appraisal

A3.1. Charge balance

The cation-anion charge balance (both unspeciated and speciated) for the water and saturated paste extract samples have been inserted in Tables A3.1 and A3.2 respectively. Charge balance is an excellent test of the quality of data as all aqueous systems cannot carry a charge imbalance. Every positively charged ion in solution must be balanced by a negatively charged ion. The anion-cation balance check is based on a percentage difference between the total positive charge and the total negative charge, defined as:

$$\% \text{ difference} = 100(\Sigma\text{anions}-\Sigma\text{cations})/(\Sigma\text{anions}+\Sigma\text{cations})$$

All negative percentages therefore indicate excess cationic charge and all positive percentages indicating excess negative charge. The speciated charge balance has been inserted as the best way of establishing the charge on each component that is predicted to be present in the system under the specific pH conditions. Speciation allows one to establish the charges on the predominant forms of each component (Murray and Wade, 1996). All calculations were done using the software package MINTEQA2. An example of a MINTEQA2 output file has been inserted in Appendix 4. Charge balance differences of less than 10% have been considered acceptable, especially considering the generally high EC's of the samples.

Table A3.1. Unspeciated and speciated charge balance for all water samples sampled in the Steenkampskraal area.

	Unspeciated charge balance	Speciated charge balance
BH 1	-7.0	-0.003
BH 1P	-9.1	-1.7
BH 2	-5.0	-12
BH 2P	-4.6	-6.3
BH 3	-5.6	-8.6
BH 3P	-4.2	-5.7
BH 4	+2.3	+1.2
BH 5	+0.66	+4.5
BH 5P	+7.6	+1.1
BH 6	+8.6	+0.82
BH 6P	+20	+7.6
MOS 1	-2.7	-4.0
MOS 2	+0.23	-0.49
MOS 3	-2.2	-2.9
MOS 4	-1.2	-3.6
BRAND 1	-1.1	-3.7
SD 1	+13	+14
SD 2	+7.4	-0.63
Road water	+6.7	+7.7
Stream water	-5.4	-6.4
Main shaft	-4.2	-4.0
Main shaft extension	-6.4	-5.4
Inclined shaft	-8.6	-8.6
Sump on level 3	+5.9	+8.9

The charge balance of sample 1/2A is on the high side of the acceptable limit. This is most likely due to the high EC of the sample, especially the high Cu concentration, which has been known to cause matrix effects which were not corrected during the ICP-AES analyses (Willis, pers comm, 1996).

Table A3.2. Unspeciated and speciated charge balance for the saturated paste extracts along both transect 1 and transect 2.

	Unspeciated charge balance	Speciated charge balance
1/2A	-9.0	-18
1/2B	+4.2	+4.5
1/4A	-5.2	-7.0
1/4B	+6.8	+5.4
1/6	-1.6	-6.4
1/8	+9.5	-9.0
2/1	+18	+5.6
2/3	-14	+9.0
2/5	-1.6	-4.4
2/7	+14	-8.0

A3.2. Correlation between ICP data and HPIC data

Calcium, Mg, Na and K for all water and saturated paste extract samples were analyzed by both HPIC and ICP-AES. An r^2 value for all four elements has been inserted within each of the four graphs (A3.1 to A3.4). Good correlations occur between ICP and HPIC for Ca, Mg and Na. The correlation between ICP and HPIC for K was however not very good. Potassium is not usually accurately determined by ICP-AES (Hanforth, 1996, pers comm). All modelling using MINTEQA2 was performed using Ca, Mg, Na and K data from HPIC.

Table A3.3. Calcium, Mg, Na and K data by ICP-AES (mg/kg).

Sample	Ca	Mg	Na	K
MOS 1	75	58	946	26
MOS 2	215	162	1220	28
MOS 3	233	182	1111	44
MOS 4	101	70	796	28
BRAND 1	152	120	783	32
BH 1	64	109	530	20
BH 1P	63	51	528	22
BH 2	143	98	483	33
BH 2P	162	111	485	35
BH 3	35	74	188	11
BH 3P	35	53	160	8.1
BH 4	91	60	686	28
BH 5	125	91	1055	40
BH 5P	155	104	950	42
BH 6	77	70	1138	54
BH 6P	74	69	1070	63
Main shaft	592	276	1430	106
Main shaft extension	402	284	1500	109
Sump on level 3	607	513	1040	62
Inclined shaft	129	127	915	33
Slimes dam 1	438	230	161	65
Slimes dam 2	311	164	161	48
Road water	308	143	173	5
Stream water	54	28	101	11

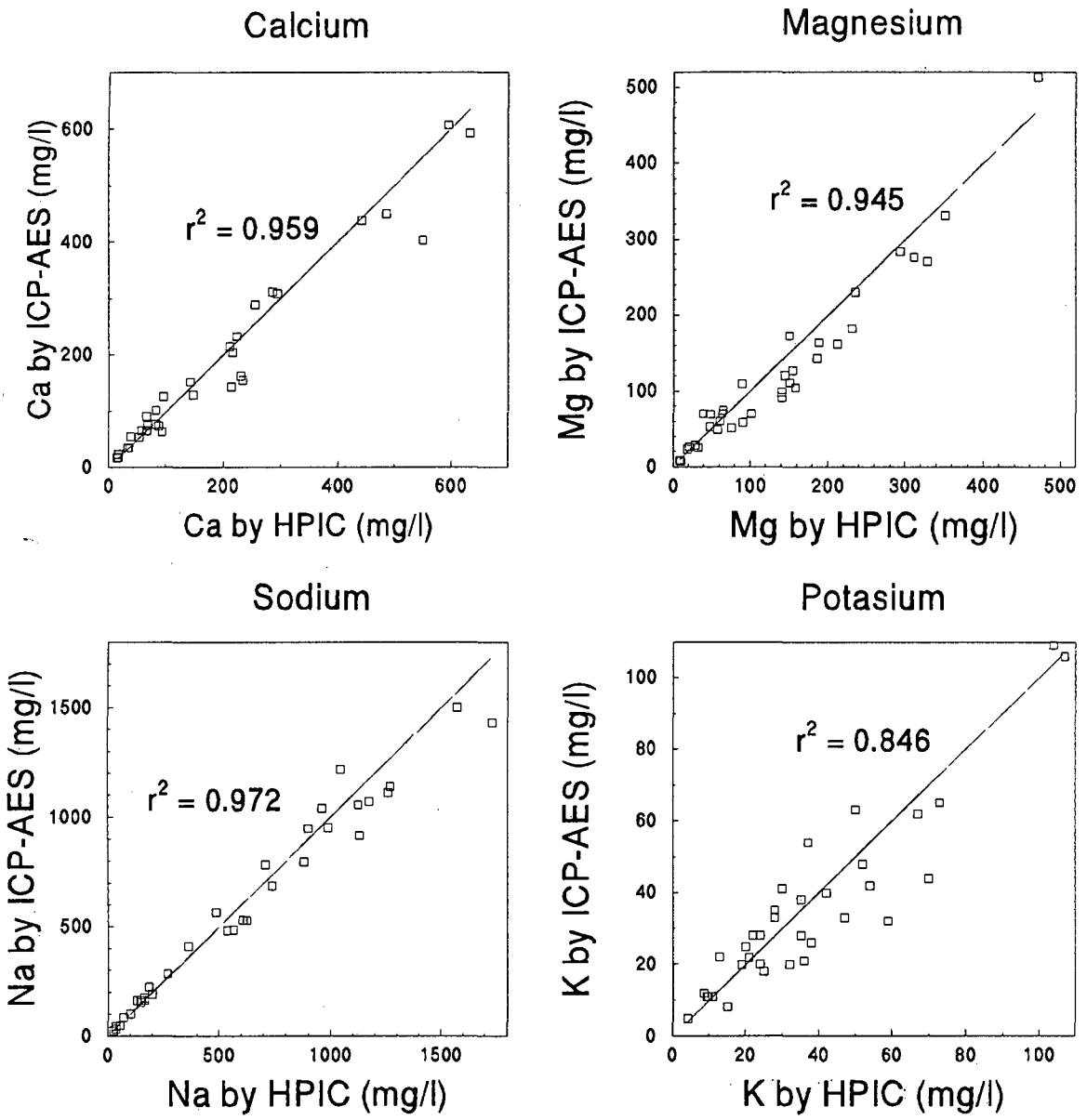

Figures A3.1. Plots of HPIC against ICP-AES data for Ca, Mg, Na and K. The straight line represents a 1:1 plot.

Table A4.1. Analytical results for the unpurged water sample from BH 1, 2, 3, 5 and 6.

	BH 1	BH 2	BH 3	BH 5	BH 6
pH	4.59	7.22	7.13	7.19	7.59
EC: mS/cm	4.11	4.04	1.34	6.19	6.02
Acidity: mol/dm^3	0.0089	nd	nd	nd	nd
Anions:		mg/dm^3			
Cl^-	1456	1051	259	1749	1510
SO_4^{2-}	77	113	261	277	545
PO_4^{3-}	1.2	89	21	31	10
HCO_3^-	nd	453	54	657	876
F^-	0.66	2.0	0.61	1.6	3.8
NO_3^-	bdl	bdl	9.1	bdl	bdl
Cations:*		mg/dm^3			
Ca	65	214	35	95	80
Mg	89	140	65	140	40
Na	607	534	196	1122	1269
K	32	28	9.5	42	37
NH_4	bdl	11	bdl	bdl	bdl
Trace metals:#		mg/dm^3			
Fe	199	0.56	1.4	0.59	0.65
Al	0.98	0.13	0.58	0.11	0.12
Cu	4.0	<0.2	<0.2	<0.2	<0.2
Cr	0.35	<0.1	0.030	<0.1	<0.1
Mn	9.7	1.4	<0.04	1.7	1.2
Ni	1.0	0.31	0.30	0.31	0.30
Si	4.6	16	27	11	11
Co	0.83	0.64	0.63	0.64	0.64
Pb	1.9	<1.0	<1.0	<1.0	<1.0
Zn	2.4	0.70	0.73	0.63	0.91
Cd$^\$$	0.23	<0.06	<0.06	<0.06	<0.06
Th	<0.005	<0.005	<0.005	<0.005	<0.005
U	<0.005	0.06	0.02	<0.005	0.18

bdl-below detection limits / nd-not determined /* HPIC / # ICP-AES / $ ICP-MS

Appendix 5. Soil XRF data

Table A5.1. Lead, Cu, Ni, Cr, U, Th and Y XRF data (mg/kg), for all soil samples along transect 1.

Sample	Pb	Cu	Ni	Cr	U	Th	Y
1/1	75	529	32	39	12	314	137
1/2A	611	6291	260	1434	561	27783	7840
1/3A	1352	3032	178	1692	487	24667	6830
1/4	512	1357	147	926	179	8865	2528
1/5	293	1387	89	420	99	4711	1375
1/6	84	579	35	110	17	500	195
1/7	48	87	26	85	4	77	54
1/8	46	83	10	39	5	69	41
1/9	51	237	10	31	5	95	48
1/10	45	235	14	41	4	65	40
1/11	43	204	13	36	6	68	38
1/12	129	1325	61	129	29	942	273
1/13	31	11	10	46	2	23	30
1/14	43	216	17	49	4	106	46
1/15	31	24	13	45	1	17	24
1/2B	61	1788	35	60	26	161	94
1/3B	97	1815	38	87	36	798	275
1/4B	215	1295	63	292	70	3168	909

Table A5.2. Zinc, Co, Mn, Sr and Rb XRF data (mg/kg) for all soil samples along transect 1.

Sample	Zn	Co	Mn	Sr	Rb
1/1	51	9	330	102	281
1/2A	102	<13	467	129	115
1/3A	118	<12	726	136	136
1/4A	92	<6.2	329	107	210
1/5	66	<4.6	295	102	235
1/6	34	3	161	100	256
1/7	78	11	526	103	206
1/8	18	3	180	77	234
1/9	15	3	129	77	236
1/10	17	3	146	76	224
1/11	15	3	122	69	215
1/12	58	12	393	109	190
1/13	22	<2.6	288	108	174
1/14	23	4	191	112	182
1/15	29	4	159	96	173
1/2B	56	13	241	101	247
1/3B	74	13	244	95	259
1/4B	74	8	318	101	245
1/Dor	41	5	177	90	245

Table A5.5. Uranium, Th and Y XRF data (mg/kg), for the different size fractions within samples 1/4A and 2/3.

	U	Th	Y
Sample 1/4A			
>2 mm	29	935	286
2-1 mm	12	309	99
1-0.5 mm	21	724	230
0.5-0.25 mm	140	6951	2144
0.25-0.125 mm	455	23373	6539
0.125-0.065 mm	397	19222	5298
<0.065 mm	293	12954	3827
Sample 2/3			
>2 mm	50	2627	776
2-1 mm	11	253	84
1-0.5 mm	13	481	146
0.5-0.25 mm	41	1856	592
0.25-0.125 mm	37	1553	445
0.125-0.065 mm	33	801	275
<0.065 mm	15	193	118

Table A5.6. Lead, Zn, Cu, Ni, Co, Mn and Cr XRF data (mg/kg), for the different size fractions within samples 1/4A and 2/3.

	Pb	Zn	Cu	Ni	Co	Mn	Cr
Sample 1/4A							
>2 mm	144	33	1295	46	7	167	88
2-1 mm	70	16	359	20	<2.5	95	51
1-0.5 mm	116	24	592	36	7	180	106
0.5-0.25 mm	443	91	1812	189	7	424	360
0.25-0.125 mm	1227	181	1890	249	<12	638	2214
.0.125-0.065 mm	1068	350	2440	382	<12	716	5254
<.065 mm	889	260	4959	390	23	633	4271
Sample 2/3							
>2 mm	213	29	86	20	<3	166	95
2-1 mm	68	19	52	11	3	122	40
1-0.5 mm	88	24	49	13	3	177	42
0.5-0.25 mm	176	39	74	12	<3	378	61
0.25-0.125 mm	144	51	74	13	<3	518	64
0.125-0.165 mm	95	62	85	18	4	550	78
<0.065 mm	63	67	109	14	6	375	74

Table A5.7. Major element analysis on briquettes by XRF for both soil transects (percentage).

	Fe_2O_3	TiO_2	BaO	CaO	K_2O	Cl	SO_3	P_2O_5	SiO_2	Al_2O_3	MgO	Na_2O	Y_2O_3	ThO_2	Ce_2O_3	Nd_2O_3	La_2O_3	Total
2/1	2.4	0.26	0.052	0.58	5.1	0	0.048	0.63	67	10	0.23	1.6	0.073	0.24	0.76	0.25	0.34	89
2/2	2.7	0.53	0.056	0.54	5.3	0	0.015	0.68	68	11	0.23	1.7	0.063	0.18	0.78	0.25	0.346	93
2/3	2.7	0.65	0.068	0.62	5.4	0	0.018	0.34	70	11	0.34	1.8	0.038	0.098	0.37	0.12	0.16	94
2/4	2.3	0.58	0.063	0.52	5.3	0	0.010	0.30	72	11	0.30	1.7	0.033	0.084	0.31	0.10	0.14	94
2/5	2.2	0.39	0.069	0.59	5.2	0	0.023	0.099	72	11	0.61	1.6	0.011	0.009	0.023	0.008	0.015	94
2/6	3.7	0.66	0.071	0.58	4.2	0	0.028	0.13	68	12	1.4	1.3	0.010	0.008	0.028	0.009	0.013	93
2/7	4.9	0.76	0.062	0.79	3.8	0	0.033	0.14	65	14	1.9	1.2	0.010	0.007	0.025	0.009	0.010	93
2/8	5.6	0.87	0.062	0.53	3.7	2.6	0.16	0.14	64	13	2.1	4.4	0.010	0.003	0.006	0.002	0.006	97
2/9	3.2	0.54	0.085	0.62	4.5	0	0.025	0.080	69	11	1.5	1.1	0.010	0.002	0.013	0.005	0.005	92
2/10	2.0	0.28	0.071	0.30	4.2	0	0.008	0.057	76	9.1	0.81	1.2	0.010	0.002	0.008	0.003	0.003	94
2/11	2.4	0.32	0.085	0.81	5.1	0	0.015	0.11	71	11	1.2	1.3	0.010	0.001	0.008	0.003	0.003	93
2/12	3.2	0.46	0.063	0.46	3.2	0	0.015	0.14	75	9.7	1.4	1.3	0.010	0.002	0.009	0.003	0.004	95
2/BH1	1.7	0.25	0.072	0.35	4.3	0	0.013	0.044	77	8.4	0.41	1.2	0.010	0.002	0.006	0.001	0.004	94
2/DOR	7.4	0.53	0.055	0.34	4.2	0	0.023	0.089	61	16	3.1	0.99	0.010	0.003	0.010	0.003	0.006	94

Table A5.7 continued.

	Fe_2O_3	TiO_2	BaO	CaO	K_2O	Cl	SO_3	P_2O_5	SiO_2	Al_2O_3	MgO	Na_2O	Y_2O_3	ThO_2	Ce_2O_3	Nd_2O_3	La_2O_3	Total
1/1	3.09	0.55	0.060	0.84	5.1	0	0.43	0.23	66	13	0.50	1.9	0.020	0.04	0.090	0.030	0.044	92
1/2A	6.4	0.66	0.053	1.8	1.6	0	2.3	5.8	25	5.4	0.28	0.66	0.56	1.93	9.2	3.0	4.2	69
1/3A	7.1	1.1	0.059	1.5	1.9	0	1.0	5.3	29	6.1	0.27	0.76	0.48	1.646	8.1	2.6	3.7	70
1/4A	6.1	0.60	0.052	1.2	3.4	0	0.42	2.5	53	9.2	0.44	1.3	0.19	0.593	2.8	0.92	1.3	84
1/5	4.7	0.57	0.060	0.92	4.2	0	0.20	1.4	62	10	0.48	1.4	0.11	0.323	1.5	0.48	0.65	89
1/6	2.9	0.46	0.070	0.59	5.0	0	0.10	0.30	67	11	0.43	1.5	0.028	0.058	0.18	0.058	0.080	91
1/7	6.1	0.68	0.052	0.60	4.2	1.8	0.25	0.14	57	15	3.0	1.7	0.013	0.012	0.029	0.009	0.012	91
1/8	1.8	0.40	0.070	0.32	4.9	0	0.02	0.066	75	9.1	0.37	1.3	0.009	0.007	0.026	0.008	0.010	94
1/9	1.4	0.32	0.070	0.30	4.9	0	0.028	0.081	76	8.7	0.20	1.3	0.01	0.009	0.030	0.010	0.015	94
1/10	1.5	0.18	0.063	0.31	4.7	0	0.033	0.070	77	8.8	0.25	1.3	0.009	0.006	0.023	0.008	0.010	94
1/11	1.3	0.19	0.058	0.26	4.5	0	0.020	0.067	78	8.1	0.14	1.3	0.008	0.006	0.018	0.004	0.012	94
1/12	4.3	0.44	0.075	0.76	4.3	0	0.27	0.58	63	12	1.4	1.1	0.038	0.12	0.33	0.106	0.14	89
1/13	2.6	1.0	0.11	0.33	4.8	0	0.015	0.052	76	8.4	0.22	1.1	0.007	0.003	0.017	0.006	0.004	95
1/14	2.2	0.29	0.10	0.44	4.9	0	0.030	0.11	74	9.4	0.55	1.1	0.009	0.011	0.038	0.012	0.017	93
1/15	2.8	0.41	0.087	0.43	4.5	0.1	0.16	0.10	70	10	0.91	0.97	0.008	0.002	0.011	0.005	0.005	90
1/2B	3.8	0.61	0.063	0.57	4.7	0	0.25	0.13	64	13	1.0	1.4	0.018	0.022	0.050	0.016	0.020	90
1/3B	4.8	0.59	0.057	0.46	4.7	0	0.12	0.24	59	15	1.7	0.95	0.04	0.12	0.25	0.082	0.11	89
1/4B	4.8	0.60	0.058	0.67	4.5	0	0.14	0.82	62	13	1.3	1.3	0.083	0.24	0.97	0.31	0.43	91

Table A5.8. Major element analysis on briquettes by XRF for the different size fractions of samples 1/4A and 2/3 (percentages).

	Fe_2O_3	TiO_2	BaO	CaO	K_2O	SO_3	P_2O_5	SiO_2	Al_2O_3	MgO	Na_2O	Y_2O_3	ThO_2	Ce_2O_3	Nd_2O_3	La_2O_3	Total
Sample 1/4A																	
>2 mm	4.2	0.12	0.057	0.62	5.1	0.37	0.54	66	9.7	0.30	1.6	0.041	0.12	0.35	0.11	0.16	89
2-1 mm	1.7	0.078	0.041	0.33	4.1	0.17	0.16	79	7.3	0.090	1.3	0.014	0.027	0.095	0.033	0.045	95
1-0.5 mm	2.3	0.13	0.052	0.48	4.7	0.27	0.33	74	9.1	0.18	1.5	0.028	0.066	0.24	0.076	0.11	93
0.5-0.25	5.8	0.504	0.058	1.8	3.9	0.70	2.2	53	12	0.55	1.8	0.17	0.47	2.3	0.75	1.0	86
0.25-0.125	8.1	1.014	0.053	1.9	1.8	0.92	5.1	27	7.2	0.45	0.93	0.47	1.6	8.0	2.6	3.6	71
0.125-0.065	18	1.8	0.041	1.4	1.4	0.64	4.5	26	7.7	0.57	0.95	0.38	1.3	6.2	2.0	2.8	76
<0.065 mm	18	1.5	0.038	1.9	2.0	1.5	3.1	37	11	1.1	1.1	0.27	0.79	3.3	1.1	1.4	85
Sample 2/3																	
>2 mm	2.5	0.19	0.077	0.60	5.5	0.030	0.78	69	11	0.13	1.9	0.068	0.18	0.80	0.26	0.36	93
2-1 mm	1.7	0.15	0.053	0.41	5.1	0.0075	0.12	77	9.6	0.14	1.7	0.013	0.020	0.074	0.024	0.034	96
1-0.5 mm	1.9	0.23	0.060	0.49	5.0	0.013	0.17	74	11	0.20	1.8	0.019	0.039	0.14	0.048	0.065	95
0.5-0.25	2.9	0.57	0.072	0.63	5.7	0.020	0.55	67	12	0.31	1.918	0.058	0.17	0.66	0.21	0.30	93
0.25-0.125	3.9	1.2	0.087	0.67	5.3	0.023	0.43	68	12	0.40	1.8	0.044	0.12	0.46	0.15	0.20	94
0.125-0.065	4.7	1.6	0.069	0.90	4.1	0.025	0.28	69	12	0.56	2.1	0.027	0.058	0.23	0.076	0.097	97
<0.065 mm	4.0	1.3	0.055	1.0	2.9	0.028	0.142	64	12	0.93	1.7	0.020	0.030	0.056	0.020	0.027	88

Table A5.9. Concentrations of REE within the soil samples along transect 1 and 2 (mg/kg).

	La	Ce	Pr	Nd	Sm	Eu	Gd	Tb	Dy	Ho	Er	Tm	Yb	Lu
1/1	nd	nd	nd	420	69	2.6	60	8.5	31	55.7	11	1.8	8.2	1.5
1/2A	65000	137000	15000	20000	6000	145	5000	710	3000	385	720	71	270	39
1/2B	nd	nd	nd	465	86	3.4	74	9.4	43	6	12	1.4	7.2	1.2
1/3A	36000	77000	8000	18000	5000	125	5000	610	2000	320	595	61	225	32
1/3B	nd	nd	nd	20000	4000	630	3000	275	1000	190	345	79	165	160
1/4A	18000	37000	4000	12000	3000	59	2000	275	1000	145	275	28	105	15
1/4B	nd	nd	nd	5000	700	16	620	80	280	43	78	8.1	31	4.9
1/5	nd	nd	nd	6000	980	24	620	110	400	59	110	12	43	6.5
1/11	95	105	22	67	10	1.9	11	1.9	6.2	1.7	2.5	0.7	1.7	1.1
1/12	1000	1000	250	675	100	4.1	89	12	50	8.4	17	2.1	7.6	1.2
1/13	61	69	17	41	5.8	1.7	5.4	1.2	3.2	0.7	1.7	<0.5	1.6	<0.5
1/14	150	190	36	99	18	2.6	15	2.2	7.9	1.5	2.9	<0.5	1.6	<0.5
1/15	60	72	14	32	6	1.9	5.3	0.8	3.2	0.7	1.5	<0.5	1.4	<0.5

Table 5.9. Continued.

	La	Ce	Pr	Nd	Sm	Eu	Gd	Tb	Dy	Ho	Er	Tm	Yb	Lu
2/1	4000	5000	1000	3000	490	26	410	63	195	38	64	18	34	18
2/2	5000	5000	1000	3000	515	15	460	53	205	30	61	6.7	27	4.2
2/3	2000	3000	550	2000	235	6.5	210	23	90	13	26	2.7	13	2
2/4	2000	2000	475	1000	200	6.4	175	21	79	12	23	2.6	11	1.4
2/5	170	225	44	115	21	2.1	16	2.1	9.4	1.4	2.5	<0.5	2.7	<0.5
2/6	130	195	34	93	17	2.8	14	1.8	9	1.4	3.7	<0.5	2.6	<0.5
2/7	98	155	31	79	13	1.7	11	1.2	8.5	1	3.1	<0.5	2.8	<0.5
2/8	47	85	16	41	8.4	2	8.3	1	4.7	0.9	2.5	<0.5	2.1	<0.5
2/9	27	38	10	nd	nd	nd	nd	nd	nd	nd	nd	nd	nd	nd
2/10	20	48	10	31	5.9	1.6	3.5	<0.5	2.4	<0.5	1.1	<0.5	0.8	<0.5
2/11	74	69	36	51	22	25	24	25	23	24	21	25	20	25

nd - no data